Analysis of Binding Events and Diffusion in Living Cells

Markus Elsner

Institute of Biomedicine
Department of Medical and Clinical Genetics
Sahlgrenska Academy
Göteborg University
2006

ISBN 978-91-628-6913-7
Markus Elsner
Institute of Biomedicine
Department of Medical and Clinical Genetics
Sahlgrenska Academy
Göteborg Univesity
Sweden
Göteborg, Sweden, 2006

Für meine Eltern

Und

Für Christiane

''The world is full of obvious things which nobody by any chance ever observes.''
Sherlock Holmes in The Hound of the Baskervilles
by Sir Arthur Conan Doyle

List of Publications

This thesis is based on the following publications, which are referred to in the text by their roman numerals:

I. Elsner, M., Hashimoto, H., Simpson, J.C., Cassel, D., Nilsson, T., and Weiss, M. (2003).
Spatiotemporal dynamics of the COPI vesicle machinery.
EMBO Rep *4*, 1000-1004.

II. Weiss M.*, Elsner, M.*, Kartberg, F., and Nilsson, T. (2004).
Anomalous subdiffusion is a measure for cytoplasmic crowding in living cells.
Biophys J *87*, 3518-3524.
* equal contribution

III. Elsner, M., Nilsson, T. and Weiss, M.
Evidence for Golgi localization by oligomerization - kin recognition revisited
In manuscript

1 Abstract

Analysis of Binding Events and Diffusion in Living Cells

Markus Elsner

Institute of Biomedicine, Department of Medical and Clinical Genetics, Sahlgrenska Academy, Göteborg University, Medicinaregatan 9A, 413 90 Göteborg

It is well known that diffusion is the main mode of transport in living cells, but the consequences of diffusion in a complex cellular environment are not generally appreciated. In this thesis, we have investigated several aspects of how diffusion properties influence the observability of cellular binding kinetics and how they can be used to obtain information about the environment of proteins and other molecules.

First, the binding kinetics of the coat protein I (COPI) vesicles machinery were investigated. Three proteins are mainly responsible for the formation of COPI vesicles; coatomer, Arf1 and ArfGAP1. From biochemical studies, it was expected that Arf1 and coatomer would show similar binding kinetics to the Golgi membranes. This was tested *in vivo* using GFP constructs in "fluorescence recovery after photobleaching" (FRAP) experiments. Surprisingly, the recovery constant of coatomer was twice that of Arf1. We could show that this did not reflect a difference in the actual binding kinetics, but difference due to a diffusion-limited exchange of coatomer between the cytosol and the membrane. For this we measured the diffusion coefficient of all three proteins with fluorescence correlation spectroscopy (FCS). We found that Arf1 and ArfGAP1 are highly mobile in the cytosol, whereas coatomer diffuses 5–10 times more slowly than expected. Using computer simulations we could show that the slow diffusion of coatomer translates into a two times slower FRAP recovery then expected for the non-diffusion limited case.

Second, the unexpectedly slow diffusion of coatomer led to the idea of investigating the diffusion properties of inert tracers in the cytosol of livings cells. Fluorescently labelled dextrans showed normal diffusion in water, but strong anomalous subdiffusion when microinjected into cells. It could be ruled out that large scale-structures like the cytoskeleton or the endoplasmic reticulum were responsible for the observed subdiffusion. Instead the emergence of subdiffusion could be attributed to macromolecular crowding using computer simulations and *in vitro* measurements in an artificially crowded solution. Anomalous diffusion caused by macromolecular crowding can be used as a measure for the extent of crowding for a given solution.

In the third part of this thesis the focus is shifted from diffusion in the cytosol to diffusion in the membrane. Previously, it had been observed in FCS experiments that Golgi resident transmembrane proteins show anomalous subdiffusion. Since no consistent explanation for this phenomenon had been provided previously, we investigated whether the formation of dynamic oligomers can explain the observed subdiffusion. We constructed a computer model for two-dimensional diffusion of particles that participate in oligomerisation reactions. It could been demonstrated that for the short time scales relevant for FCS experiments, anomalous diffusion can be observed. For long times the diffusion crossed over to normal diffusion. The extent of anomality and the crossover time depended on the equilibrium constant of the binding, the valence of the monomers and on the kinetics of the binding reaction.

Keywords: COPI, Golgi, diffusion, glycosyltransferases, sorting, molecular crowding

ISBN 978-91-628-6913-7 Göteborg, Sweden, 2006

2 Abbreviations

Arf1	ADP Ribosylation Factor 1
ArfGAP1	ARF-GTPase activating protein1
BFA	Brefeldin A
BSA	Bovine Serum Albumin
COPI	Coat Protein I
COPI)	Coat Protein II
CHO	Chinese Hamster Ovary
CTRW	Continuous Time Random Walk
DAG	Diacylglycerol
ER	Endoplasmic Reticulum
EM	Electron Microscopy
ERGIC	ER-Golgi-Intermediate-Compartment
FCS	Fluorescence Correlation Spectroscopy
FITC	fluorescein isothiocyanate
FRAP	Fluorescence Recovery after Photobleching
FRET	Fluorescence Resonance Energy Transfer
GDP	Guanidine diphosphate
GFP	Green Fluorescent Protein
GlcNAc	N-acetylglucosamine
GTP	Guanidine triphosphate
GTPγS	Guanosine 5'-(3-O-thio)triphosphate
MSD	Mean Square Displacement
MW	Molecular weight
RFP	Red Fluorescent Protein
TGN	Trans-Golgi Network
VTC	Vesicular Tubular Cluster
VSVG	Vesicular Stomatitis Virus Glycoprotein

3 Aims and Scope

In the work presented in this thesis we have investigated the nature and role of diffusion processes in cellular biochemistry and live cell experiments. It is centred on processes involved in vesicle formation and sorting in the Golgi apparatus, but the issues raised and discussed have implications for all fields of cell biology.

In two publications and one manuscript, three different aspects of diffusion in living cells have been investigated. First, the influence of slow diffusion on the analysis of binding events in “Fluorescence Recovery after Photobleaching” (FRAP) experiments is examined. Second, basic properties of the cytosol concerning the diffusion of macromolecules are explored. And last, it is shown how the formation of dynamic oligomers changes the diffusive behaviour of membrane proteins.

The thesis is divided in three parts. In the introduction I will first give an overview of the cell biology of the secretory pathway, the Golgi apparatus and the mechanism of COPI vesicle formation. This is followed by an outline of the laws governing diffusion and deviations from normal diffusion that are relevant to biology.

It is concluded with an overview of the effects of the crowded nature of cytosol and anomalous diffusion on cellular biochemistry.

In the second part, the results are summarized and discussed.

In the last part the results are presented in detail in the two publications and the manuscript.

4 Introduction

4.1 The Secretory Pathway - An Overview

The existence of an elaborate system of endomembranes is one of the hallmarks of the eukaryotic cell. While there are numerous organelles with a distinct set of proteins, the production of those proteins is centralized to the endoplasmic reticulum (ER). All proteins destined for intracellular organelles (with the exception of proteins of the mitochondria, chloroplasts and possibly peroxisomes), the plasma membrane or for the extracelluar space are synthesized by membrane-bound ribosomes attached to the rough ER. After insertion into the ER membrane or translocation into the ER lumen, the proteins are subjected to quality control before beginning their journey toward their final destination. The quality control machinery ensures that damaged or improperly folded proteins are retained in the ER or degraded[1].

Besides housing the quality control machinery, the ER is also a major site post-translational modification. For example, the enzymes mediating the formation of disulfide bridges, the hydroxylation of proline residues or the initiation of N-linked glycosylation are located in the ER. The ER also contains a large population of molecular chaperones, that assist protein folding and assembly[2,3].

Next, proteins are transported to the Golgi apparatus. Here an extensive machinery of glycosylation enzymes completes N-linked glycosylation and initiates and extends O-linked oligosaccharides[4,5]. In addition to glycosylation, the Golgi apparatus is also an major site of protein sulfation and phosporylation[6,7].

More downstream in the secretory pathway, especially in the trans-golgi network and secretory granules, most of the proteolytic processing of proteins occurs[7].

To a lesser extent the synthesis and modification of lipids is also centralized to specific organelles in the secretory pathway. The biosynthesis of cholesterol and ceramide is strictly localized to the membranes of the ER. The main site of production for sphingomyelin is the lumen of the *cis*-Golgi. The synthesis of glycosylceramide occurs on the cytosolic side of the early Golgi apparatus, while the subsequent glycolysation reactions are catalyzed by enzymes with an active site on the luminal face of the Golgi membranes[4,8,9].

For phospholipids the picture is more complex. The majority of the bulk phospolipids like phosphatidylcholin, phosphatidylethanolamine phosphonisotiol and phosphatidylserine are synthesized on the cytosolic side of the ER[10]. While the initial synthesis of those lipids is centralized, they can participate in complicated regulatory networks in other parts of the cell. A good example is the complex and dynamic role of phosphoinositol species in almost all organelles of the cell (for review see [11-13]).

4.2 Protein Transport from and to the Golgi Apparatus

The localization of protein and lipid production and modification to specialized organelles makes it necessary to have mechanisms to transport proteins and lipids between the different organelles of the cell. The transport of newly synthesised proteins and lipids can be divided in three distinct stages. First, proteins (and lipids, but I will mainly concentrate on proteins here) leave the ER and are transported to the Golgi apparatus. Then they pass through the Golgi and are sorted to their respective destinations in the *trans* Golgi network.

In the following, I will very briefly discuss ER-Golgi and Post-Golgi transport and then focus on intra-Golgi transport.

The transport of proteins from the ER to the Golgi apparatus depends on small vesicles (“COPII vesicles”) formed by the concerted action of the small GTPase Sar1p, the protein complexes Sec23/24 and Sec13/31 and the membrane-bound guanidine exchange factor Sec 12. Upon the exchange of

GDP to GTP in Sar1p by Sec12, Sar1p binds to the membrane. Sar1 first recruits the Sec23/24 complex from the cytosol to the membrane, which is followed by the binding of Sec13/31[14,15]. Sar1p has the ability to deform membranes on its own, and is essential for the final pinching off of the vesicles, but is unable to produce vesicles by itself[16]. The coat protein complexes Sec23/24 and Sec13/31 have three distinct functions. (1) They participate in cargo capture. Some cargo protein interact directly or via adaptors with the coat proteins, especially with the Sec23/24 complex[17-20]. (2) Sec23 accelerates the hydrolysis rate of Sar1p drastically, a process that is further enhanced by Sec13/31[21,22]. (3) The Sec13/31 complex has an important role in cross-linking the individual components to ensure the formation of a localised bud on the membrane[23].

The exit from the ER via COPII vesicles is restricted to special subdomains on the membrane, called ER exit sites[24,25].

After they pinched off from the donor (i.e. ER-) membrane, the vesicles uncoat when Sar1p hydrolyses GTP. The uncoated vesicles have the ability to undergo homotypic fusion and to form larger transport carriers[26]. This is thought to give rise to the ER-Golgi-Intermediate-Compartment (ERGIC) that can be seen between the *Cis*-Golgi and the ER. The ERGIC is a tubular membrane cluster that in not directly connected with either the ER or the Golgi apparatus[27-29]. So far, it is not clear if all proteins pass through the ERGIC and if and how the homotypic fusion of the COPII vesicles occurs *in vivo*. From the ERGIC, ER-resident proteins and proteins that cycle between the ER and the Golgi/ERGIC are retrieved to the ER[30,31].

The final step of the transport from the ERGIC to Golgi apparatus is controversial. The most likely sequence of events is the following: Parts of the ERGIC compartment are transported along microtubles towards the *cis*-Golgi. During the transport they fuse with vesicles from the Golgi. When the ERGIC

membranes reach the Golgi, they form a new *cis*-cisterna and drive Golgi maturation (see next chapter)[26,32,33].

For a more in depth discussion of ER exit and ER-to-Golgi transport see the following excellent review articles [34-36].

4.3 Intra Golgi Transport

The Golgi apparatus consists of stacks of flat membrane cisternae (*cf.* Figure 1). Each cisterna is about 2-3 µm long and about 100 nm thick. The number of cisternae varies from cell type to cell type, but is usually between 5 and 8. The membranes of neighbouring cisternae are in extremely close proximity. In mammalian cells the stacks align parallel to each other and form one compact juxtanuclear Golgi ribbon. Under most conditions, the cisternae within the same stacks are not interconnected while equivalent cisternae of neighbouring stacks are connected through fenestrated membrane connections. The two *trans*-most cisternae are highly fenestrated and less flat then the *medial*- and *cis*-cisternae. The surface area of all cisternae is similar, while the volume shows a variation of about 50% with *cis*-most and *trans*-most cisternae having the largest volume. Close to the rims of the cisternae, one usually detects small vesicles with a diameter of about 70 nm. All cisternae also show budding profiles. Most are located at the rim of the cisternae or on the edges of holes. Most buds appear to have a protein coat. The ER is closely associated with the Golgi at all levels, but no direct membrane connections can be found.[37-40]

The Golgi has a large population of resident proteins. Almost all of them have a least one trans-membrane domain. In contrast to the ER the Golgi has no large population of resident luminal proteins.

Interestingly, the resident proteins are not distributed evenly over the Golgi. Glycosylation enzymes for example show a gradient like distribution with a preference for one or two cisternae[39,41]. Other gradients (like a increasing cholesterol[42] content or pH[43] have been suggested to form over the Golgi).

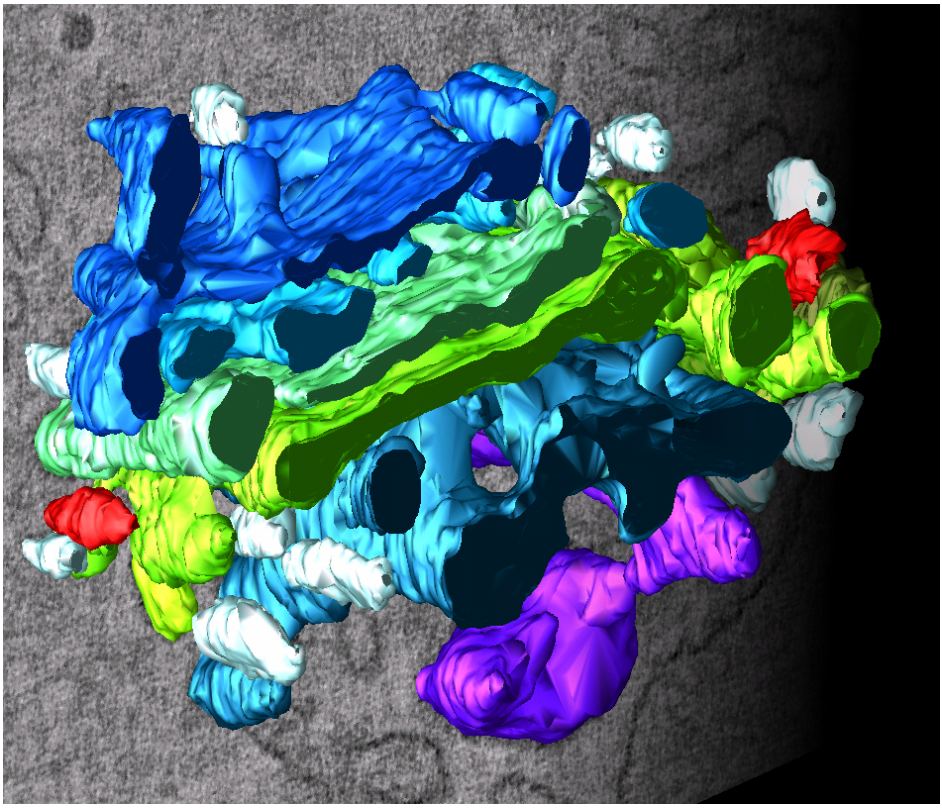

Figure 1: Three dimensional reconstruction of a single Golgi stack from EM-tomography. The individual cisternae are shown in different colours. Picture from Dr. Markus Grabenbauer, methods described in[39].

A fascinating aspect of the Golgi apparatus is its high dynamic stability. It can sustain its integrity under conditions ranging from no membrane flux at all to being flooded with a pulse of a temperature sensitive mutant of the Vesicular Stomatitis Virus Glycoprotein (VSVG)[44] and a 1000-fold over expression of resident proteins[45-47], but disintegrates within minutes upon the addition of the drug brefeldin A (BFA)[48].

Conceptually, one can imagine three different models for Golgi transport (*cf.* Figure 2) First, proteins could be shuttled between the cisternae by small transport carriers, e.g. vesicles. Second, new cisternae could form on the *cis*-

side of the Golgi, then progress through the stack as a whole and disintegrate on the *trans*-side. Third, the Golgi complex could be an interconnected network and cargo could simply diffuse from one side to the other.

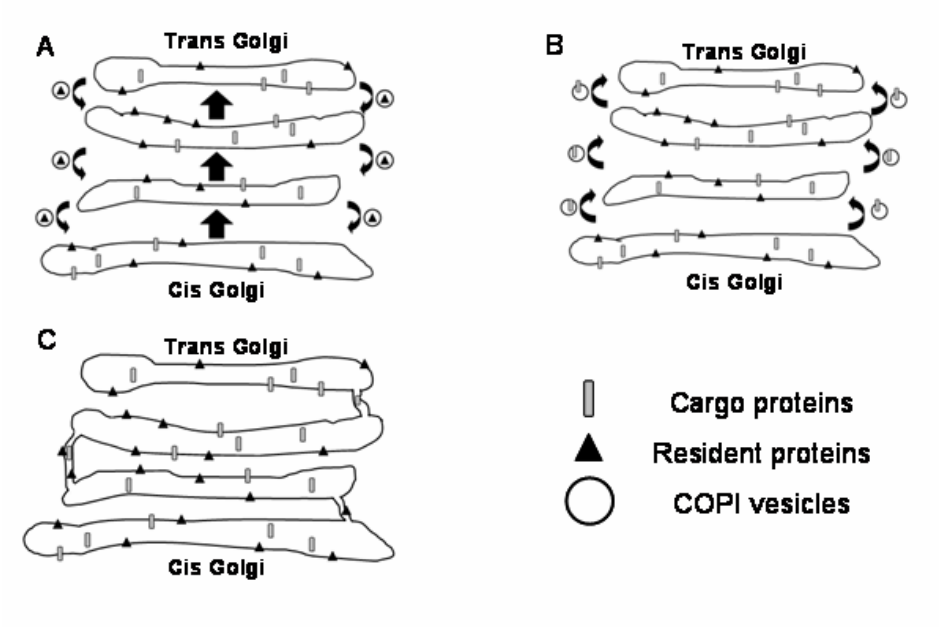

Figure 2: Models of Golgi transport (A) Cisternal maturation model, (B) Vesicular Transport model, (C) Percolation model. More details can be found in the text.

For a long time vesicular transport was regarded as the main mode of transport in the Golgi apparatus. The 'vesicular transport model' (Figure 2 A) predicts that vesicles from the ERGIC/VTC filled with anterograde cargo (i.e. proteins that move from the ER through the Golgi to their respective destinations) fuse with the *cis*-most cisterna. After the cargo has been exposed to modifying enzymes, the proteins are sorted into vesicles again and moved forward to the next cisterna. This process is repeated until the cargo reaches the *trans*-face of the Golgi apparatus and is send to the respective destinations from the TGN. In this model, the individual cisternae are viewed as stable compartments.

Several, lines of evidence led to a wide acceptance of this model. The most important was an *in vitro* system developed in the laboratory of James Rothman. In this assay the transport between isolated Golgi membranes from a wild type and a mutant Chinese hamster ovary (CHO) cell line that lacked the glycosylation enzyme N-acetylglucosamine (GlcNAc) transferase, was reconstituted. The mutant cell line was transfected with the Vesicular-Stomatitis-Virus-Glycoprotein (VSVG). As an indication for transport the incorporation of radioactive GlcNAc was measured. After careful experiments it was concluded that VSVG is transported in vesicles from the mutant to the wt-Golgi stacks[49-51]. The model received support from electron microscopy studies. Using gold labelled antibodies the presence of anterograde cargo could be detected in budding profiles and vesicles in the Golgi region[52].

In the mid-90s several groups provided data that did not fit to the simple vesicular transport model. The most striking were experiments that showed that cargo that is too big to fit into vesicles (a pro-collagen fibre) is transported within the lumen of the cisternae[53] (in fact similar experiments had been done before but where largely ignored[54,55]). This provided powerful evidence for the progression of whole cisterna from one side of the Golgi to the other. The possibility that the progression pathway is special to large cargo while small proteins are transported via vesicles was addressed in a study comparing the transport of VSVG and in the same cell[56]. It was shown that pro-collagen and VSVG showed largely the same behaviour and that very little VSVG could be detected outside the cisternae.

The role of vesicles was also revisited. It could be shown that vesicles created in an *in vitro* system in the presence of GTP[57,58] and isolated from cell culture cells[59] were enriched in Golgi residents. New immuno-EM studies showed an enrichment of retrograde cargo in fixed cells[60]. The signal in the transport assay of the Rothman laboratory could be attributed to the transport of small amounts of the glycosylation enzyme instead of the VSVG protein[61].

To account for this new data the idea of vesicular transport was combined with the progression of whole cisternae through the Golgi. In the so called “cisternal maturation model” (Figure 2 B) new cisternae are formed at the *cis*-side of the Golgi and move through the Golgi stack as a whole. During their progression retrograde vesicular transport recycles Golgi resident proteins to a more *cis*-cisterna. With computer modelling it could be shown that this model is able to explain the uneven distribution of Golgi enzymes over the stack[62,63].

Recently, cisternal maturation could be directly visualized in yeast. In *Saccharomyces cerevisiae* the individual Golgi cisternae do not form perinuclear stacks, but are dispersed throughout the cytoplasm. This allows monitoring individual cisterna with light microscopy. The groups of Benjamin Glick and Akihinko Hakano used GFP and RFP labelled Golgi resident proteins and time lapse confocal imaging to show that Golgi cisternae do not have a stable protein content. On the contrary, cisternae labelled with a *cis*-Golgi marker lost their labelling after 1.3 minutes. A rapid transition from green to red labelling of the same cisterna could be observed in yeast cells double labelled with GFP *cis*-Golgi markers and RFP *trans*-Golgi markers. The speed of maturation was shown to be consistent with the rate of secretion. Interestingly, a knock out of α-COP did not completely inhibit maturation, although slowing it down drastically[64,65].

Recently, two groups reported the dynamic appearance of tubular connections between cisterna in mammalian cells. *Marsh et al.* investigated Golgi morphology in mouse islet beta cells. They could show that upon stimulation with glucose inter-cisternal connections appeared. All connections bypassed one interceding cisterna. Both connections on the rim of the cisternae and through *fenestrae* in the cisterna where observed[66].

Luini and colleagues used the temperature sensitive mutant of VSVG and a temperature shift protocol to create pulses of cargo through the Golgi. In the temperature shift protocol cargo is accumulated in the ERGIC at 15°C. Then

the temperature is shifted to 40°C and the cargo proteins move to the Golgi. Under the conditions of the pulse they were able to observe the appearance of tubular connections between neighbouring cisternae in the same stack.[67] The use of the temperature shift protocol to study morphological changes associated with transport has been questioned by experiments showing that a temperature shift alone can lead to the formation of tubular connections[68].

In fact tubular connections between cisternae in the same stack were observed before, but since no functional framework for their function existed, their importance was not acknowledged[69-71].

Both studies suggest that high protein traffic through the Golgi can lead to the connections between the individual cisternae of a single stack. This is supported by an analysis of the kinetics of VSVG transport by the group of Jennifer-Lippincott Schwartz. They found inconsistencies of the observed kinetics with both the vesicular transport and the cisternal maturation model. This led this group to favour passive transport via tubular connections as the most probable mechanism for intra-Golgi transport (J. Lippincott-Schwartz personal communication).

So far, little is know about the mechanism of formation and the role of tubular connections in Golgi transport. The data currently available suggests a role in conditions of high protein transport activity.

4.4 The making of a COPI vesicle

While there is still debate about the exact nature of intra-Golgi transport, a major role for COPI vesicles is largely undisputed. COPI vesicles were first described as non-clathrin coated vesicles that were produced from isolated Golgi stacks in the presence of cytosol. It was observed that budding vesicles on the Golgi membranes had a distinct 18 nm thick protein coat, while free vesicles were frequently uncoated[72,73]. The uncoating of free vesicles could be inhibited by the non-hydrolysable GTP analogue GTPγS[74], which allowed for

the isolation of the coat forming proteins from vesicles accumulated in the presence of GTPγS[75,76]. The so called coatomer complex is essential for protein transport between Golgi cisternae *in vitro*[51,77] and *in vivo*[78]. Coatomer consists of 7 equimolar subunits, that form a stable cytosolic complex of approx. 570 kDa[75,79,80] (for review see [81]). Coatomer alone shows little affinity for membranes, but binds to the Golgi membranes in the presence of GTP without binding GTP itself.

The factor responsible for the GTP-dependent association of coatomer with Golgi membranes was discovered to be ADP Ribosylation Factor 1 (Arf1). Arf1 was discovered as an essential GTP-depended co-factor for ADP-ribosylation of a G-protein by cholera toxin[82]. The first hints of its cellular function came when Serafini et al. could show that Arf1 forms a stoichiometric component of the coat of COPI vesicles[83] and Taylor *et al*. identified it as a GTPγS sensitive regulator of intra-Golgi transport *in vitro*[84]. Subsequent studies showed that coatomer binding to membranes requires Arf1 and that Arf1 binds to the membrane in the absence of coatomer[85,86]. The binding is GTP dependent. The GDP-bound form of Arf1 is water soluble and binds to membranes only very weakly. After the exchange of GDP for GTP, the water solubility decreases dramatically and Arf1 binds to membranes. Arf1 is N-myristylated and in the absence of the myristylation the membrane binding is drastically decreased. The myristol moiety is supposedly hidden in the Arf1-GDP structure and only exposed to the solvent upon GDP/GTP exchange. In addition to myristol, membrane affinity is increased by a conformational change in N-terminal helix that exposes several hydrophobic residues upon GTP binding[87].

Experiments with the fungal toxin Brefeldin A suggested rapid cycling of Arf1 between the cytosol and the Golgi membranes. BFA treatment leads to a rapid loss of Arf1 from the Golgi apparatus both *in vivo* and *in vitro*[88,89]. This cycling was later directly visualized using GFP-tagged proteins and modern

microscopy techniques like FRAP[90,91] (see also 5.1 and Paper I). The dependency of the binding and unbinding cycle on the ability of Arf1 to hydrolyse GTP could be shown using an Arf1 mutant unable to catalyse GTP hydrolysis[90,92] and GTPγS[93,94]. While Arf1 is necessary for vesicle formation, it is not able to bend the membrane itself. Only in complex with coatomer deformation of membranes is obeserved[76]. In experiments with purified Arf1 and coatomer it could be shown that Arf1 and coatomer are sufficient for the formation of vesicles from artificial liposomes[95] and Golgi membranes[96,97], although the lipid composition[95] and possibly receptors on the target membrane enhanced the rate of vesicle formation[97].

From these and other observations the following model was developed for the formation of functional COPI vesicles (*cf.* Figure 3). First, cytosolic Arf1 exchanges GDP for GTP and binds to the Golgi membrane. Second, cytosolic coatomer is recruited to the membrane by Arf1-GTP and starts to deform it. A bud is formed. The growing bud finally pinches off and a free vesicle is formed. Finally, Arf1 hydrolyses GTP and coatomer and Arf1 dissociate from the vesicle.

After this model was formulated and widely accepted in the mid-90s, research concentrated on the regulation of the binding and un-binding events of the vesicle forming machinery and the sorting of proteins into vesicles.

Surprisingly, purified Arf1 is neither able to hydrolyse GTP nor to exchange GDP for GTP at significant levels[88,89,98,99].

This led to the search for co-factors that are necessary for these functions.

It has been known that Golgi membranes have an Arf1-GEF (Guanidine exchange factor) activity since 1992, when it was shown that BFA inhibits Golgi membrane catalysed GDP/GTP exchange of Arf1[88,89]. The first ARF-GEF identified were Gea1 in yeast[100] and BIG1 in mammals[101]. ARF-GEFs vary widely in size, structure and domain composition, but all share a domain homologous to the yeast protein SEC7. The SEC7 domain alone is enough to

catalyze the exchange reaction, the other domains of the proteins are responsible for localization and substrate specificity[102]. All ARF-GEFs studied so far are peripheral membrane proteins, in contrast to the GEF involved in the COPII (Sec12) vesicle machinery, which is a transmembrane protein[103].

The 15 human proteins containing Sec7 domains, can be divided in 7 families[104]. Two of them, the BIG/SEC7 and the GBF/GEA families, are important for trafficking through and from the Golgi. Namely, GBF1, BIG1 and BIG2 have been localized to the Golgi region. GBF1 binds mainly to early Golgi compartments, including the ER-to-Golgi-Intermediate-compartment[105,106], while BIG1/2 is found mainly in later Golgi compartments. BIG2 localizes to the trans-Golgi-network and is not involved in COPI trafficking[107-109].

BIG1 is found at trans-Golgi cisternae and is BFA sensitive[110]. Contrary to the initial reports, it could recently be shown that BFA inhibits GBF1 in living cells[111].

Currently, it seems likely that GBF1 is responsible for catalysing GDP/GTP exchange in the early the ERGIC and early Golgi, while BIG1 is active in later Golgi compartments. How the subcellular localisation of GBF1 and BIG1 is controlled and if and how they participate in regulatory processes during the formation of COPI vesicles is currently not known.

The first protein with an Arf1GAP (GTPase activating protein) activity was cloned in 1995[112]. ArfGAP1 is still by far the best studied Arf-GAP, although at least 24 genes with Arf-GAP domains exist in the human genome.

ArfGAP1 associates with the Golgi apparatus. The binding is Arf1 depended, since BFA treatment leads to a rapid loss of ArfGAP1 from the Golgi. Overexpression causes disintegration of the Golgi[112].

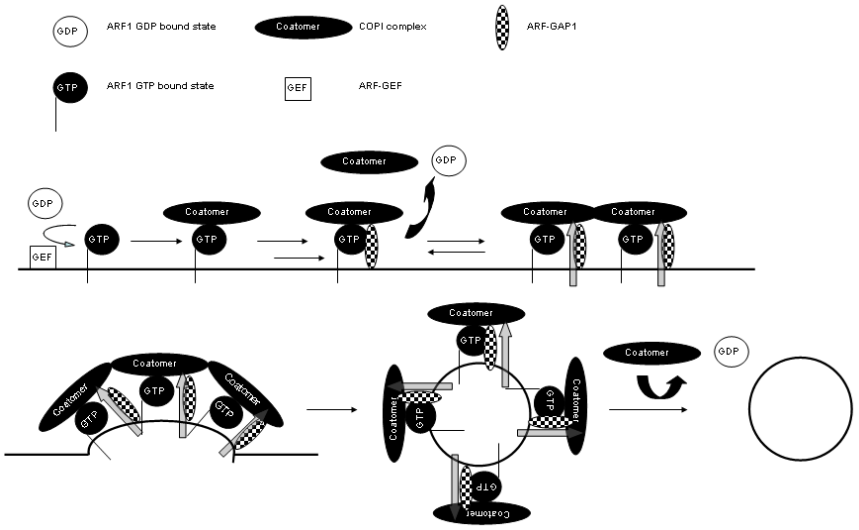

Figure 3: Current model for the formation of COPI vesicles. See main text for more details.

First, it was thought that ArfGAP1 simply counteracts vesicle formation and facilitates the uncoating of the vesicles[97,112]. More recent experiments point towards a more complex role of ArfGAP1. ArfGap1 plays an important role in the sorting of proteins into COPI vesicles. Lanoix *et al.* could show that GTP hydrolysis by Arf1 is essential for sorting events during vesicle formation[57]. This observation led to the idea that ArfGAP1 could be a target for regulation of the vesicle forming machinery by cargo molecules. Goldberg demonstrated that coatomer increases the effect of ArfGAP1 on a soluble form of Arf1 ([Δ17])Arf1. This enhancing effect could be blocked with peptides derived from the cytoplasmic tails of an abundant cis-Golgi protein family, the p24 proteins. Although coatomer does not have an effect on the hydrolysis rate of full length Arf1[113], it could be shown by Lanoix *et al* that p24 peptides have the ability to regulate sorting and GTP hydrolysis in an *in vitro* budding assay[58]. In

this study it was demonstrated that ArfGAP1 is the target of this regulatory pathway.

These studies lead to the proposition of a model for cargo sorting during the formation of COPI vesicles[58,114]. The so-called 'kinetic proof-reading mechanism' extends the sequence of events that lead to the formation of a vesicle by one regulatory step. In the absence of cargo molecules ArfGAP1 efficiently catalyses the hydrolysis of GTP by Arf1, which leads to a residence time of the Arf1/coatomer complex too short for the formation of a vesicle. If a sufficient number of cargo molecules are present ArfGAP1 is sequestered by binding to the cytoplasmic tails of those molecules and is unable to catalyse hydrolysis. This increases the residence time of the Arf1/coatomer and allows for enough time to form a vesicle (*cf.* Figure 3).

A second regulatory mechanism of ArfGAP1 seems to ensure an efficient uncoating of the budded vesicle. The group of Antonny showed in elegant experiments that the activity of ArfGAP1 depends on the curvature of the membrane[115]. ArfGAP activity increases for increasing curvature of the membrane. During vesicle formation ArfGAP1 would therefore show little activity while the membrane is flat. The formation of a vesicle increases the curvature of the membrane and therefore increases the ArfGAP1 activity. This in turn increases the GFP hydrolysis rate in Arf1 and leads to uncoating of the vesicle. The region of the ArfGAP1 protein that is responsible for sensing the curvature (called ALPS for "ArfGAP1 lipid packing sensor") forms an amphipathic helix. One side is polar but only weakly charged. The membrane insertion of this helix seems to be responsible for the changes in ArfGAP1 activity. As the name suggest it does not sense the curvature *per se*, but the tightness of the lipid packing on the surface of the membrane, which decreases when curvature increases. A similar effect to the one that curvature exerts can be observed when the content of diacylglycerol (DAG) is altered. An increasing content of the small lipid DAG decreases the lipid packing of the

bilayer and allows the ALPS helix to insert further into the membrane, which in turn increases ArfGAP1 activity[116].

In addition to its role in regulating Arf1 activity ArfGAP1 is also thought to be a structural component for the coat. COPI can bind to ArfGAP1 and the existence of a three party ArfGAP1-coatomer-Arf1-GTP complex has been suggested[117,118].

For the yeast Arf-GAP Glo3p it has been demonstrated that it binds to β´-COP and γ-COP [119,120]. At least one study suggest that the presence of ArfGAP1 is necessary for efficient vesicle formation[121].

4.5 The localisation of Golgi resident proteins

As discussed in chapter 1.3, the cisternal maturation model is the current paradigm for Golgi transport. It predicts that Golgi resident proteins are sorted into COPI vesicles backwards to counterbalance the forward flow of the cisternae.

Strangely, the most abundant class of Golgi resident proteins, the family of glycosyltransferases, have no known interaction with the COPI vesicle machinery. Yet they are enriched in COPI vesicles[58,60]. In contrast to proteins that cycle between the ER and the Golgi apparatus, they do not carry an K(X)KXX motif, that binds directly to coatomer[122]. In fact, glycosyltransferases have a very short cytoplasmic tail, devoid of recognisable sequence motifs. All glycosyltransferases have the same overall structure a single transmembrane domain with a very short N-terminal cytoplasmic sequence. On the luminal side a so-called stem region is adjacent to the TM-domain. The globular catalytic domain is located at the C-terminus.

The signal for the correct localisation was discovered to lie in the transmembrane domain and the stem region for most glycosyltransferases[45,46,123-126]. Only for α1,3-galactosyl-transferase and α1,2-fucosyltransferase an involvement of the cytoplasmic tail has been shown[127,128].

This observation raises the question how the transmembrane and part of the luminal domains of the proteins can mediate incorporation into vesicles, when all the components that are responsible for vesicle formation are soluble, cytosolic proteins. Two not necessarily exclusive models have been proposed to account for that problem. The lipid bilayer sorting model was proposed by Bretscher and Munro[129] and Masibay *et al.*[130] in 1993. It is based on four observations. First, the average length of the transmembrane domain of Golgi resident enzymes is on average shorter than of plasma membrane proteins[131]. A related observation is that the overall hydrophobicity of Golgi enzyme transmembrane domains is significantly lower than of proteins that move through the Golgi[132]. Second, it was thought that the thickness of the lipid would increase along the secretory pathway because the sphingolipid and cholesterol contend increases, as cholesterol was shown to have a strong influence on the thickness of model membranes[133]. The relevance of the results obtained from model membranes was recently challenged by studies on purified cellular membranes[134]. Third, mutational studies of the transmembrane domain failed to find specific motifs sufficient for Golgi localisation[45,135], while varying the length of the TM-domain altered the Golgi localisation. In fact, a protein with a 17 residue poly-leucine TM-domain was retained in the Golgi, while the same protein with a 23 residue Poly-L TM-domain localises to the plasma membrane[136].

From those observations, a model was constructed that predicts that Golgi resident proteins will be excluded from lipid microdomains. Vesicles would then form preferentially from cholesterol and sphingomyelin-poor domains, which in turn leads to an enrichment of Golgi resident proteins in COPI vesicles. To support this theory, it was shown that the content of cholesterol and sphingomyelin is lower in COPI vesicles then in the Golgi membranes[137] and that the membrane is thinner in COPI/II buds and vesicles[77]. Since this model was developed, however, it was shown by multiple groups that the TM-

domain does not fully account for the Golgi localization of several enzymes[124,128,138-140].

An alternative model termed ’kin recognition model’ was suggested by Nilsson *et al.* in 1993[141]. The model predicts that enzymes that are localized to the same cisterna will form homo- and/or hetero-oligomers by forming contacts with their TM- and luminal domains. For some glycosyltransferases it has been shown that their active form is a homodimer in native membranes[142]. When the model was suggested, the complexes where supposed to be too large to be incorporated into COPI vesicles in accordance with the 'vesicular transport model'. In the light of the ‘cisternal progression model’ favoured by recent evidence, such complexes would preferentially be incorporated into vesicles. How this is achieved can be elegantly explained by a kinetic proofreading mechanism for the formation of COPI buds[58,114]. The model predicts that complexes of cargo molecules inhibit the activity of ArfGAP1 by incorporating proteins that interact with the COPI machinery. This leads to an increased residence time of coatomer on the membrane and therefore to an increased rate of vesicle formation in areas containing complexes of resident proteins. Proteins without the ability to influence Arf1 activity would be in a complex with proteins that can influence the Arf1 activity directly or indirectly. The higher the concentration of Arf1 influencing proteins in the complex the more likely is an incorporation of complex into COPI vesicles. The immobilisation originally envisaged by the kin-recognition model was not observed in studies with GFP tagged glycosylation enzymes in living cells[143,144]. The formation of small dimers and oligomers has been confirmed by a number of groups for a large number of enzymes (for a review see [145] and [146]). How large this complexes are *in vivo* and if they contain proteins that are able to interact with the COPI machinery is not known so far. The question of the size of the oligomers will be addressed in this thesis in chapter 5.3 and paper III.

So far, most of the oligomers described are complexes of enzymes involved in the same glycosylation pathway. This opens the possibility that the observed oligomers are less important for localisation, but allow substrates to be shuttled between subsequent enzymes in the pathway in order to increase catalytic efficiency and specificity. One example for a multi-enzyme complex that is apparently governed by the necessity for catalytic efficiency, is the oligomer formed by at least three enzymes of the ganglioside synthesis pathway. Galactosyltransferase1 and sialyltranferase1 form stable dimers and as well as sialyltranferase2 with sialyltranferase1. The trimerization is mediated by ST1, as GalT1 and ST2 have no obvious affinity[147].

Whether an absence of kin recognition leads to mislocalisation is a question that cannot be clearly answered at the moment. While replacing the complete region responsible for kin recognition of Manosidase II by N-acetylgucosamintransferase I (NAGT I) leads to a cell surface expression of NAGT I, no thorough investigation has been performed for the possible connection between kin recognition and localisation of Mannosidase II or for point mutations that would abolished kin recognition [123]. To my knowledge the only two other studies dealing with the question whether lack of kin recognition leads to mislocalisation were done by Chen et al. [139] and Sasai *et al.* [148]. Chen *et al.* could demonstrate a clear correlation between complex formation and localisation. In the same study the interesting observation was made that the oligomerisation is strongly dependent on the pH, opening a new way to control localisation by a pH gradient over the Golgi. Sasai *et al.* investigated the role of disulphide bonds between the stem regions of N-acetylglucosaminyltransferase V in homooligomer formation and retention. The also found a clear correlation between oligomerisation and Golgi retention.

Most of the studies that have described the formation complex between Golgi enzymes so far have used either genetic or biochemical approaches. Only one study has tried to look at the problem in unperturbed living cells. Giraudo *et al.*

used fluorescence resonance energy transfer (FRET) to demonstrate that two glycosyltransferases are physically associated [147]. A big disadvantage of FRET based approaches is that they cannot distinguish between dimerisation and larger oligomers.

Taking together those observations Benjamin Glick *et al.*[62] and Matthias Weiss/Tommy Nilsson[63] have developed a scheme to explain the sub-Golgi localisation of glycosyltransferases in the Golgi. According to this model, sorting is achieved by a competition of the resident enzymes to enter COPI vesicles. The more likely a protein is to enter retrograde vesicles the more they localise to the *cis* side of the Golgi stack. Resident proteins that are not incorporated in vesicles at all are recycled from the TGN directly to the ER and show an equal distribution over all cisternae. In the original model the system proved to be quite sensitive to over-expression in computer simulations. In order to account for the remarkable stability of the Golgi localisation under conditions of high over expression[45-47], Weiss and Nilsson introduced the concept of 'triggered sorting'. It assumes that the probability to be sorted into vesicles in not only determined by intrinsic properties, but influenced by an external trigger like pH and/or membrane thickness. With this modification, the system proved to be extremely robust in simulations[63].

4.6 Diffusion and Biology

Almost all biological processes happen in solution, either in three dimensional fluids like the cytoplasm or in the two dimensional fluids of cellular membranes. In solution particles undergo random motion due to the thermal noise of the solvent molecules. This process is called diffusion or Brownian motion[149,150]. Since the diffusive movement of proteins, lipids, nucleic acids ect. is essential for the function of life it is important to understand how diffusion works and which laws govern it.

Even before the link between the thermal motion of molecules and the diffusion had been formalized by Einstein in 1905[149], Adolf Fick had already provided a mathematical framework for its description, although Fick could not derive the law from first principles or provide extensive experimental evidence. Inspired by Einstein's seminal paper in 1905, modern treatments of diffusion usually derive the diffusion equations from the model of a random walk.

For simplicity I will only consider the diffusion along one axis and show how the equation is derived for the one dimensional case[151,152]. I will mainly follow the derivation given in[152].

For the derivation we will make the following assumptions.

1. Each particle will move on step Δx with equal probability to left or to the right at each time step Δt.
2. The probability to go to the right is $p_r=1/2$, the probability to go to the left is $p_l=p_r=1/2$.
3. The movement at each time step is statistically independent from the previous time step, the process has no memory (Markov assumption).
4. All particles move independently from all other particles.

After *n* time steps each particle can be anywhere between $+n\Delta x$ and $-n\Delta x$, but clearly the probabilities for each position are different.

To get the probability *p(m,n)* that a particle reached a spot m after n time steps, we need to get the number of possible combinations of steps to right and steps to the left that lead to point m. If we call the number of steps to the right *a* and the number of steps to the left *b* we can write:

m=a-b, a+b=n,

therefore:

$$a = \frac{n+m}{2} \;,\; b = n - a \quad \textbf{Eq. 1}$$

The probability to go exactly *a* steps to right in n tries is given by the binomial distribution:

$$p(a,n) = \frac{n!}{a!(n-a)!}\frac{1}{p_r^a}\frac{1}{p_l^{n-a}} \quad \text{Eq. 2}$$

since $p_l=p_r$ and *m* is defined by *a*:

$$p(m,n) = \frac{n!}{a!(n-a)!}\frac{1}{2^n} \quad \textbf{Eq. 3}$$

For large *n*, as we usually have in diffusion problems, the binomial distribution is well approximated by the Gaussian distribution, due to the central limit theorem:

$$\mathrm{p(n,m)} = \left(\frac{2}{\pi n}\right)^{1/2} \exp\left(-\frac{m^2}{2n}\right) \quad \text{Eq. 4}$$

if we now set $m\Delta x=x$ and $n\Delta t=t$ and let $n\to\infty$, $\Delta x\to 0$ and $\Delta t\to 0$, we can transfer the result from the random walk approximation to continuous space and time.

The probability to find a particle in the interval $[x,x+\Delta x]$ is given from equation (4):

$$\frac{p(\frac{x}{\Delta x},\frac{t}{\Delta t})}{2\Delta x} = \left(\frac{\Delta t}{2\pi(\Delta x)^2}\right)^{0.5} \exp\left(-\frac{x^2}{2t}\frac{\Delta t}{(\Delta x)^2}\right) \quad \text{Eq. 5}$$

if we set:

$$\lim_{\substack{\Delta x\to 0\\ \Delta t\to 0}}\left(\frac{(\Delta x)^2}{2\Delta t}\right) = D \quad \textbf{Eq. 6}$$

with D being the diffusion coefficient, we get the diffusion equation:

$$p(x,t)dx = \left(\frac{1}{4\pi Dt}\right)^{\frac{1}{2}} \exp\left(\frac{x^2}{4Dt}\right)dx \quad \textbf{Eq. 7}$$

This equation gives the probability to find a has particle in an interval [x,x+dx] at a distance x from its origin x_0=0 at a time *t* (see Figure 4).

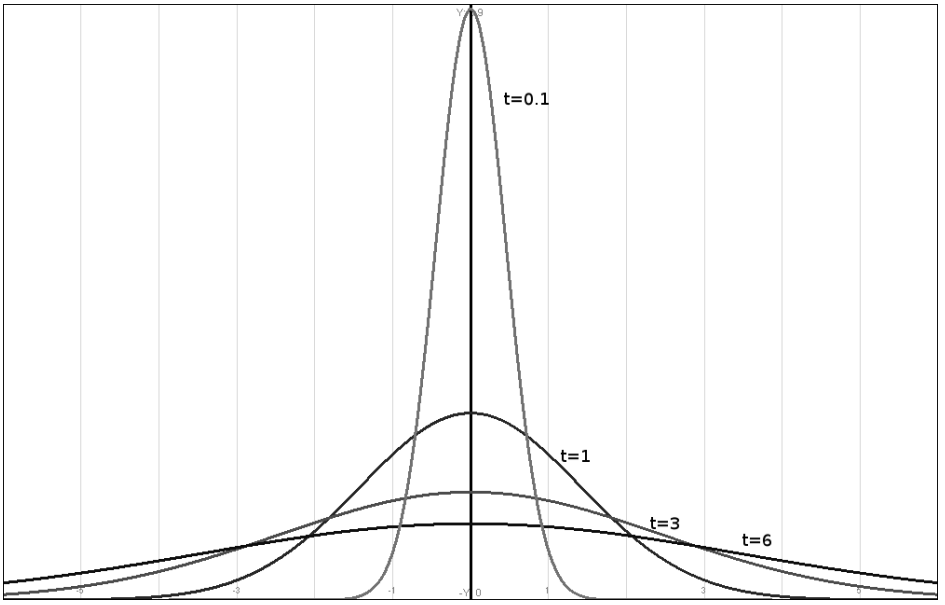

Figure 4: The solution of the diffusion equation (eq. 7) plotted for 4 different time points. All units are arbitrary.

Not incidentally, this equation is also a solution for Fick's diffusion law that relates the change of concentration at one point to the gradient of concentration at this point:

$$\frac{\partial c}{\partial t} = D\frac{\partial c^2}{\partial x^2} \quad \textbf{Eq. 8}$$

for a point source of particles at t=0

Equation 7 has some interesting properties. The mean distance a particle travelled is given by:

$$\left\langle |x| \right\rangle = 2\left(\frac{1}{4\pi \mathrm{Dt}} \right)^{\frac{1}{2}} \int_0^\infty x \exp\left(\frac{x^2}{4Dt} \right) dx = 2\left(\frac{Dt}{\pi} \right)^{\frac{1}{2}} \quad \textbf{Eq. 9}$$

The mean square displacement (MSD) is directly proportional to time:

$$\left\langle x^2 \right\rangle = 2\left(\frac{1}{4\pi \mathrm{Dt}} \right)^{\frac{1}{2}} \cdot \int_0^\infty x^2 \exp\left(\frac{x^2}{4Dt} \right) dx = 2Dt \quad \textbf{Eq. 10}$$

Another interesting result from Einstein's molecular theory of diffusion is the Einstein-Stokes equation that relates molecular properties to the diffusion coefficient:

$$D = \frac{kT}{f} \quad \textbf{Eq. 11,}$$

where k is the Boltzmann constant, T the absolute temperature, and f the frictional force between the particle and its surrounding. If f is described by Stokes' law for the friction of a sphere in a fluid equation 11 becomes:

$$D = \frac{kT}{6\pi\eta r} \quad \textbf{Eq. 12}$$

with r being the radius of the sphere and η the viscosity of the fluid.

For biological membranes the dependence of the diffusion coefficient on the size of the particle is more complicated than for the ideal objects in an ideal solvent used to drive equations 11 and 12. This was first analysed by Saffman and Delbrück in 1975[153]. They found that the diffusion coefficient of a cylindrical inclusion of the radius r in a membrane with the thickness h is given by the following equation:

$$D_T = \frac{k_B T}{4\pi\mu_{mem} h}\left(\log\left(\frac{\mu_{mem} h}{\mu_{flu} r}\right) - \gamma\right) \quad \text{Eq. 13}$$

μ_m and μ_{flu} are the viscosities of the membrane and the surrounding medium, γ is Euler's constant (0.5772). The most striking difference between equations 12 and 13 is the logarithmic dependence of the diffusion coefficient in the membrane. The Saffman-Delbrück relation was recently under scrutiny both in simulation and experimental studies. Guigas and Weiss used mesocopic simulations to confirm the Saffman-Delbrück relation for small and medium sized inclusions in the membrane. For larger inclusions they found deviations from the Saffman-Delbrück relation that lead to a scaling $D \sim 1/r^2$. If internal degrees of freedom are neglected the diffusion coefficient scales with $1/r$[154].

While earlier experimental studies confirmed the validity of Saffman-Delbrück relation[155-157], a recent study raised the possibility that the diffusion coefficient scales with 1/r for r>1 nm [158]. The conflicting results warrant a more thorough investigation of the dependence of the diffusion coefficients on molecular size and lipid bilayer properties.

In the above treatment of diffusion one makes a number of simplifications that are not necessarily applicable, especially in the environment of living cells. Three important complications will be discussed in the remainder of the chapter.

First, we assumed that all space is accessible for the diffusing particle. This is not necessarily true. In living cells there are a number of essentially immobile structures that will obstruct the diffusion of particles. How does this influence the diffusional behaviour? The influence of obstacles has been intensively studied by percolation theory. Most results have been obtained for situations close to the percolation threshold. The percolation threshold is the highest concentration of obstacles at which there is on average still an unobstructed path from each point of the medium to every other point. The diffusing particle

can go around the obstacles, but will encounter bottlenecks and be trapped in dead ends on all length scales[159-161].

At the percolation threshold the MSD changes its behaviour, and is no longer proportional to time, but to a fractional power of time:

$$\left(|x|\right)^2 \sim t^{\alpha}, \alpha < 1 \quad \text{Eq. 14}$$

For the two dimensional case α is 0.697 at the percolation threshold, in three dimensions 0.55[159]. Diffusion processes with a MSD of the form of equation 14 are called anomalous diffusion. For α<1 it is called anomalous subdiffusion, for α>1 anomalous superdiffusion.

The diffusional behaviour at obstacle concentrations less than the percolation threshold has been studied using Monte Carlo simulations[161]. For long time scales diffusion is normal, although the diffusion coefficient decreases compared to the unobstructed case. At short times the diffusion is anomalous even at concentration below the percolation threshold. The time point when anomalous diffusion crosses over to normal diffusion and the extent of the anomalous diffusion (measured by the value of the exponent α in equation (14)) are functions of the obstacle concentration. The closer the obstacle concentration approaches the percolation threshold, the longer subdiffusion persist and the lower is α [161].

A related phenomenon is molecular crowding. This will be discussed further down in this thesis (chapters 4.8 and 5.2, and paper II).

Second, we assumed that the diffusing particles are free of interaction with other particles and structures. This is usually not the case. A simple example is the diffusion of electrolytes, where the anions and cations strongly influence each other due to electrostatic forces[162].

Binding of molecules to immobile structure can also have a strong influence on diffusion. Structures that are immobile on the time scales relevant for diffusion are abundant in living cells. The cytoskeleton and the endomembrane system allow for numerous interactions of cytosolic particles with stationary objects.

In membranes the underlying cytoskeleton provides an immobile scaffold that membrane bound proteins can interact with.

How does binding to immobile structures influence diffusion? This has been studied both theoretical and using computer simulations[163,164].

If we assume thermal equilibrium and a simple binding reaction characterised by an on rate k_{on} and an off-rate k_{off} the diffusion remains normal, but the diffusion coefficient can be drastically decreased, depending on the strength of the binding and the concentration of binding partners. If binding to immobile structures is combined with obstructed diffusion, diffusion does not get more anomalous, but the cross-over time from anomalous to normal diffusion is increased due to the slower diffusion.

The picture is entirely different if the system is out of thermal equilibrium or one assumes more complicated binding kinetics.

Saxton studied how diffusional behaviour changes for different initial conditions in Monte Carlo simulations. When he used random initial conditions, he found strong anomalous diffusion that persisted for long times. This raises the possibility that active processes that drive diffusing particles out of equilibrium could lead to anomalous diffusion.

If one considers more complicated binding kinetics, diffusion can be anomalous even in thermal equilibrium. The important property is the distribution of the waiting times τ (i.e. the time that the diffusing particle stays bound to the immobile binding partner). Distributions of τ that have a significant probability for long waiting times, give raise to anomalous diffusion. An example for such a distribution is[159,165]:

$$p(\tau) = \frac{\beta}{(1+\tau)^{1+\beta}} \quad \textbf{Eq. 15}$$

For long times t the mean square displacement approaches:

$\left\langle x^2 \right\rangle \sim t^{\beta}$ **Eq. 16**

This mechanism of creating anomalous diffusion is called Continuous Time Random Walk (CTRW).

For normal on/off kinetics the waiting time τ distribution is given by a Poisson Distribution:

$p(\tau) \sim e^{-\tau}$

This does not lead to anomalous diffusion, but reduces the diffusion coefficient[164].

A third complication that can arise is the formation of polymers by the diffusing particles. I will give a short introduction here; a special case is studied further down in this thesis (chapter 5.3 and paper III).

A simple but highly instructive model for polymer motion is the self-avoiding Rouse model[166,167]. It treats the polymers as chains of beads connected by ideal springs in an ideal solvent. Hydrodynamic interactions are not taken into account. From this model some interesting predictions can be made.

The motion of the centre of mass can be shown to be normal diffusive on all time scales. This is not true for the motion of the individual monomers. For long times (longer then a critical time τ_c) the monomer motion will follow the centre of mass. For short times ($t>\tau_c$) the monomers can perform a semi-independent random walk restrained by their bonds to neighbouring particles. This leads to an anomalous diffusion with

$\left\langle (\Delta x)^2 \right\rangle \sim \sqrt{t}$ for $t< \tau_c$ in 3D **Eq. 17**

and

$\left\langle (\Delta x)^2 \right\rangle \sim t^{\frac{3}{5}}$ for $t< \tau_c$ in 2D **Eq. 18**

Polymers also show an interesting behaviour in the presence of immobile obstacles or a high concentration of other polymers. Under those conditions it moves along defects in the obstacle/polymer matrix. Movements are much more likely along the axis of the polymer then perpendicular to it. It is said that the polymer moves along a tube. The mode of movement was first investigated by de Gennes, who coined the term reptation to describe it. Reptational movement is characterized by the movement along a free tube between the obstacles. The main mode of movement will be the formation of "defects" by fluctuation of the polymer in the tube. The "defects" can be imagined as protrusions, like those that form during the movement of a caterpillar.

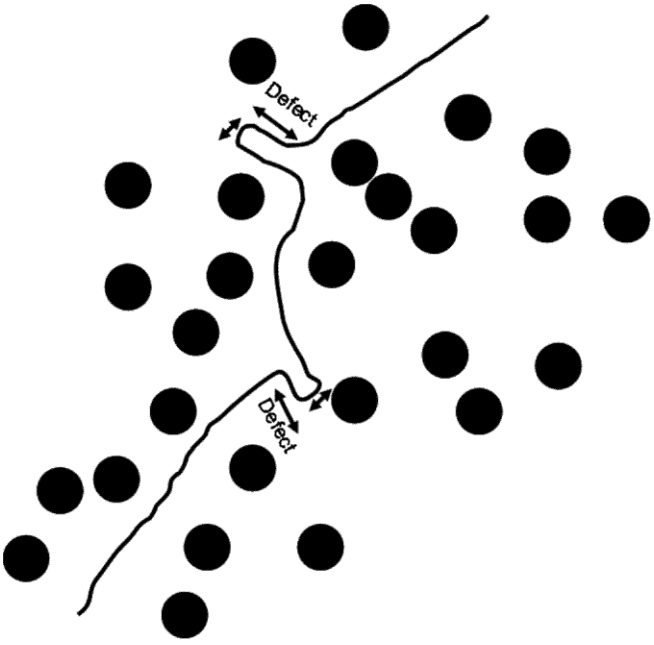

Figure 5 A polymer in a mesh of immobile obstacles. The main mode of movement will be the relaxation of defects, which will drive the polymer forward along its axis. Adopted from[166]

The extra length stored in the protrusions drives the movement of the polymer between the obstacles. A mathematical analysis of this model yields for the MSD:

$$\left\langle (\Delta x)^2 \right\rangle \sim \sqrt{t} \quad \text{for } t<\tau_{rep} \quad \textbf{Eq. 19}$$

for time less then a critical time τ_{rep}. Above that time the diffusion process will appear to be normal, i.e. MSD ~ t [166,167].

Deviations from normal diffusive behaviour can indeed be observed in living cells and model system. Anomalous subdiffusion has been described using single particle tracking for the plasma membrane[168-170], model membranes[171,172], and the cytoplasm of yeast[173] and E. coli[174], using Fluorescence Correlation Spectroscopy (see next chapter) for the nucleoplasm[175], for organelle membranes[144] and the plasma membrane[176,177].

4.7 Measuring Diffusion with Fluorescence Correlation Spectroscopy

Most standard methods of measuring diffusion coefficients are only applicable in simple in vitro systems[162]. With the exception of some NMR techniques[178,179], studies of diffusion in systems relevant to biology rely mainly on techniques based on fluorescence.

Especially since the advent of genetically encoded fluorescent markers like GFP, the dynamics of cellular processes are experimentally accessible *in vivo*.

Two techniques have been widely used for the measurement of diffusion in living cells, “Fluorescence Recovery after Photobleaching” (FRAP) and “Fluorescence Correlation Spectroscopy” (FCS).

FRAP was pioneered in the 1970s[180,181] and is mainly applicable to two dimensional systems (for further developments of the technique see[182]). FRAP measurements are based on the observation of the recovery of fluorescence in a (preferably) circular area after the fluorophores have been irreversibly bleached

by a short laser pulse. Experiments are usually done in confocal microscopes using a strong laser for bleaching.

For a circular area the shape of the recovery curve has been calculated analytically[183]:

$$I(t) = e^{-\frac{2\tau_D}{t}}\left(I_0\left(\frac{2\tau_D}{t}\right)+I_0\left(\frac{2\tau_D}{t}\right)\right) \quad \textbf{Eq. 20}$$

with $\tau_D=w^2/4D$. w^2 is the diameter of the bleach spot and D the diffusion coefficient. I_0 and I_1 are modified Bessel functions of the 1st and 2nd kind.

As a method to investigate the diffusion coefficient FRAP suffers from a number experimental and theoretical limitation that are nicely summarised and discussed in[184]. FRAP is also not very sensitive to deviations from normal diffusion[159].

FRAP can also be used to quantify binding of molecules to larger structures. This is discussed in detail in chapter 5.1 and paper I.

FCS was also invented in the 1970s[185-188], but due the difficult experimental setup it only became widely used in the late 1990s.

FCS measurements can be performed on fluorescently labelled molecules diffusing in aqueous solutions, in living cells and on membranes. FCS is based on the analysis of the fluctuations of fluorescently labelled molecules in a small volume. Today FCS is usually performed using the setup of a confocal microscope, as it was first suggested by Rigler and co-workers[189,190]. In combination with high numerical aperture lenses (NA>0.9) the confocal microscope offers a detection volume ("confocal volume") of less than 1fl. A small detection volume is essential since the fluctuations are governed by a Poisson process. The root mean square fluctuations of the number of particles N are given by:

$$\frac{\sqrt{(\partial N)^2}}{\langle N \rangle} = \frac{\sqrt{\left\langle \left(N - \langle N \rangle\right)^2 \right\rangle}}{\langle N \rangle} = \frac{1}{\sqrt{N}} \quad \textbf{Eq. 21}$$

Hence, the relative fluctuations decrease with rising numbers of particles, and are more difficult to observe. In principle very low numbers of particles are ideal for the analysis of fluctuations, as long as the signal is well over the background fluorescence, which can be a problem in living cells.

A good approximation for the shape of the confocal volume is a three dimensional Gaussian volume (Figure 6).

$$W(r) = e^{-2\frac{x^2+y^2}{r_0^2}} \cdot e^{-2\frac{z^2}{z_0^2}} \quad \textbf{Eq. 22}$$

The diameter perpendicular to the optical axis ($r_{0;}$ x and y direction) is about 0.25 μm (W(r) decayed to $1/e^2$ at r_0). Along the optical axis the volume is elongated and about 3 times longer then wide (z_0).

The fluorescence emitted from the particles in this volume is recorded photon by photon with a high temporal resolution.

The fluctuations are defined by the deviation of the signal at a given time from the average signal:

$$\partial F(t) = F(t) - \langle F(t) \rangle \quad \text{Eq. 23}$$

If the only source of fluctuations in the fluorescence signal are changes in the local fluorophore concentration in the confocal volume, the fluctuations can be expressed by integrating the fluctuations over the observation volume:

$$\partial F(t) = \int_V W(r) \eta \partial(C(r,t) dV \quad \textbf{Eq. 24}$$

η combines the information about the maximal excitation intensity I_0, the quantum yield q, the absorption cross section δ and the overall detection efficiency κ: $\eta = I_0 \cdot q \cdot \delta \cdot \kappa$ and C(r,t) is the local fluorophore concentration.

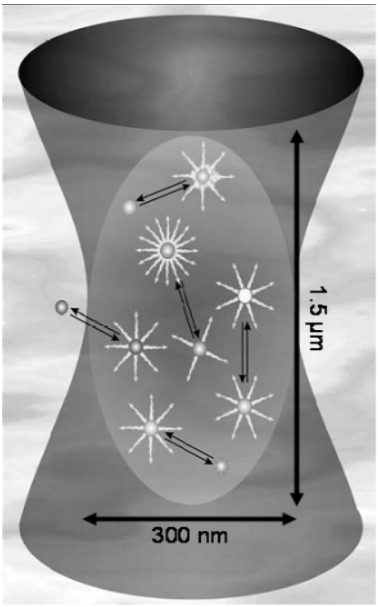

Figure 6 The observation volume in a modern confocal microscope. Modes of change in the fluorescence intensity are depicted: Transformation into a dark state, change in molecular brightness or colour, movement in and out of the volume. Reproduced from[191]

To analyse the diffusional behaviour, we measure the self-similarity of the fluctuating fluorescence signal by autocorrelation analysis.
The normalized autocorrelation function is defined by:

$$G(\tau) = \frac{\langle \partial F(t) \cdot \partial F(t+\tau) \rangle}{\langle F(t) \rangle^2} \quad \textbf{Eq. 25}$$

Using those definitions, the autocorrelation curve can be calculated for a freely diffusing particle in three dimensions (for a detailed derivation of the equations see[191]):

$$G(\tau) = \frac{1}{V_{eff}\langle C\rangle} \cdot \frac{1}{\left(1+\frac{\tau}{\tau_D}\right)} \cdot \frac{1}{\sqrt{1+\left(\frac{r_0}{z_o}\right)^2 \frac{\tau}{\tau_D}}} \quad \textbf{Eq. 26}$$

and in two dimensions:

$$G(\tau) = \frac{1}{V_{eff}\langle C\rangle} \cdot \frac{1}{\left(1+\frac{\tau}{\tau_D}\right)} \quad \textbf{Eq. 27}$$

V_{eff} is the effective measuring volume: $V_{eff}=\pi^{3/2} r_0^2 z_0$. τ_D is the average time a particle stays in the confocal volume and is related to the diffusion coefficient D:

$$\tau_D = \frac{r_0^2}{4D} \quad \textbf{Eq. 28}$$

The intercept of the curve with at $\tau=0$ is at

$$\frac{1}{V_{eff}\langle C\rangle} = \frac{1}{N} \quad \textbf{Eq. 29,}$$

which makes FCS an elegant method to measure concentrations by measuring the average number N of molecule in the confocal volume.

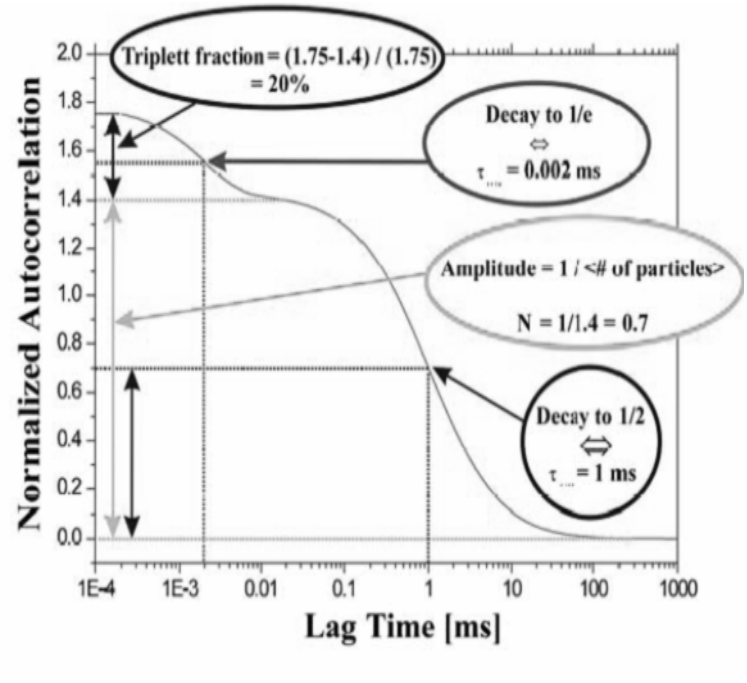

Figure 7: A plot of the FCS autocorrelation function (equation 30). The main parameters are highlighted in the graph, see the main text for more details, (Reproduced from[191])

When using real fluorophores, one usually also observes internal properties of the fluorescent molecules like the excitation of triplet states at short times τ. This will contribute an additional shoulder to the correlation curve for short times. The functions for the autocorrelation curve (equations 26 and 27) have to be amended with the expression for the decay of the triplet states:

$$G_{triplett}(\tau) = 1 - T + T \cdot e^{\frac{\tau}{\tau_{triplett}}}$$
$$G_{total}(\tau) = G_{Diffusion}(\tau) \cdot G_{triplett}(\tau) \qquad \textbf{Eq. 30}$$

FCS is quite sensitive to deviations from the normal diffusion laws. If a particle shows anomalous diffusion the autocorrelation function takes the form (in the 2D case):

$$G(\tau) = \frac{1}{V_{eff}\langle C\rangle} \cdot \frac{1}{\left(1+\left(\frac{\tau}{\tau_D}\right)^{\alpha}\right)} \quad \textbf{Eq. 31}$$

Due to the much smaller size of the confocal volume compared to the bleach area of a FRAP experiment, FCS is able to determine the behaviour on molecules on much shorter time and length scales.

The theory of FCS can be extended to allow analysis of inter-molecular interaction by dual colour cross-correlation analysis and to analyse active transport and rotational diffusion. This is discussed in detail in[176,191,192].

4.8 Biological consequences of molecular crowding and anomalous diffusion

In chapter 4.6 I briefly mentioned the term molecular crowding and introduced anomalous diffusion. In this chapter, I will discuss how these phenomena influence biological processes.

Physiological fluids contain a high concentration of macromolecules (proteins, RNA, oligosaccharides) that occupy between 7% and 40% of the total volume[193,194]. Most of those molecules will have no specific interaction with each other, but their mere presence will make space inaccessible for other molecules by a simple hard-core repulsion. This excluded volume effect can have astonishing consequences. How much volume is available to each solute depends on the shape and size of all molecules present in the environment of interest. The concept of excluded volume can be explained using a macroscopic analogy[193]. Imagine a beaker filled with 5 mm metal balls. Although the close packed balls occupy only about 65% of the volume, no additional ball can be

added to the beaker. Geometrical constraints make the 35% empty volume inaccessible to the metal balls. While it is impossible to enter more metal balls one can easily enter sand grains, but they also occupy only about 65% of the space unoccupied by the metal balls. When the beaker is filled with metal balls and sand grains about 10% of the volume is still empty, but is accessible to still smaller molecules, like water.

The thermodynamic effects can be understood when considering the effect of the excluded volume model on the activity of the individual molecule species.

The activity of a molecule can be understood as the thermodynamically relevant concentration. When you consider a simple bimolecular reaction like:

$$r_1E_1 + r_2E_2 \rightleftharpoons p_1P_1 + p_2P_2 \quad \textbf{Eq. 32}$$

The thermodynamic activity w is then defined as:

$$w = \gamma \cdot c \quad \textbf{Eq. 33}$$

with c being the real concentration and γ the activity coefficient.

The equilibrium constant K is then defined as:

$$K = \frac{\left(\gamma_{E_1} c(E_1)\right)^{r_1} \cdot \left(\gamma_{E_2} c(E_2)\right)^{r_2}}{\left(\gamma_{P_1} c(P_1)\right)^{p_1} \cdot \left(\gamma_{P_2} c(P_2)\right)^{p_2}} \quad \text{Eq. 34}$$

For dilute solutions (i.e. c→0) γ approaches 1 and we get the familiar expression for the equilibrium constant:

$$K_i = \frac{\left(c(E_1)\right)^{r_1} \cdot \left(c(E_2)\right)^{r_2}}{\left(c(P_1)\right)^{p_1} \cdot \left(c(P_2)\right)^{p_2}} \quad \textbf{Eq. 35}$$

For real cases we can separate K in an ideal factor K_i and a “non-ideal factor” Γ:

$$K = \frac{c(E_1)^{r_1} c(E_2)^{r_2}}{c(P_1)^{p1} c(P_2)^{p_2}} \cdot \frac{\gamma_{E_1}{}^{r_2} \gamma_{E_2}{}^{r_2}}{\gamma_{P_1}{}^{p_2} \gamma_{P2}{}^{p_2}} = K_i \cdot \Gamma \quad \textbf{Eq. 36}$$

Interestingly, the activity coefficients that govern the deviation from the ideal case can be expressed quite simply in the case that no other effects, but the excluded volume effect is present[193]:

$$\gamma = \frac{V_{total}}{V_{available}} \quad \textbf{Eq. 37}$$

Depending on the relative sizes of the crowding species and the particle of interests the excluded volume effect can lead to very large activity coefficients exceeding 100[193,195].

This simple theory for the thermodynamic effects of molecular crowding is surprisingly successful in some cases. It predicts for example the activity coefficient of haemoglobin in concentrated solutions, which is 10times higher at $200gl^{-1}$ and 100 times higher at $300gl^{-1}$ than in diluted solutions[196,197]. Similar studies have shown that crowding leads to large increase in activity coefficients for macromolecule in the cytosol of *E. coli* bacteria[198]. The increase of the thermodynamic activity depends strongly on the molecular weight of the molecule. While the activity is three time larger at MW 3000 Da, it is more than 100 times larger for molecular weights over 50 kDa[198].

Besides changing the thermodynamic activity, crowding also affects the equilibrium constant of the association reactions. The main effect here is that association reactions decrease the excluded volume, which in turn increases the volume accessible for other molecules, therefore decreasing the chemical potential for those molecules. This leads to a 8-40 fold higher dimerisation constant for two 40 kD proteins, for tetramerisation a 10^3-10^5 fold increase would be predicted[199]. This can indeed be observed in biological systems. For example in the T7 Replication Complex one of the members has a relatively high dissociation constant of approximately $7 \cdot 10^{-6}$ M. Upon the addition of crowding reagents (dextran or Polyethylene glycol (PEG)) the dissociation constant decreased to $3.5 \cdot 10^{-8}$ M[200]. Recently, the influence of crowding

reagents on the formation of decamers of the bovine trypsin inhibitor was investigated. In the presence of only 14 Vol% dextran the concentration of decamers increased 30-fold [201].

Other examples for the effect of molecular crowding include actin polymerisation[202], the association of the 50 s and 70 s ribosomal subunits[203], DNA polymerases[204] and the bacterial cell division protein FtsZ[205].

Molecular crowding not only influences the thermodynamics of biochemical reactions, but also has a strong effect on the kinetics and dynamics.

A well studied aspect is the influence on long range diffusion of macromolecules. Using FRAP experiments the diffusion constant of inert tracers was investigated by several groups. Early experiments suggested that the ratio between the D_{water} /$D_{cytosol}$ (i.e. increase of the viscosity compared to water) depends on the size of the tracer particle, with large particles experiencing a larger viscosity[206-208]. This was challenged by the Verkman group that could not see a dependence of the D_{water} /$D_{cytosol}$ ratio on the tracer size[209]. All groups agree that for small macromolecules with hydrodynamic radii of ~5 nm the viscosity of the cytosol is about 5 times higher than water and attribute that to molecular crowding (for a discussion of other possibilities and experimental verification of the role of molecular crowding see the excellent reviews by Luby-Phelps[210] and Verkman[211]).

The influence of crowding on diffusion at shorter distances was investigated with FCS in this thesis and will be discussed in Paper II and chapter 2.2.

Crowding is also essential to understand the role of chaperones in protein folding and the assembly of multi-protein complexes. This is nicely discussed in[199].

While the effects of crowding on cellular biochemistry have been described in some detail, much less is known about those of anomalous diffusion.

The effect of anomalous diffusion in systems where it occurs due to obstruction by immobile obstacles was investigated by Saxton[212] and by Bujan-Nunez *et*

al.[213] using Monte Carlo simulations. For reactions of the type A+B → product they found that anomalous diffusion strongly decreases the reaction rate for fast reactions, i.e. reactions where a high proportion of the inter-molecular collisions yields a product. For less likely reactions the difference between the anomalous diffusion case and the unobstructed diffusion case decreases until reactions occur slightly faster in the case of obstructed diffusion for very low reaction probabilities. From this cross-over point on, the rate of product formation is almost independent of the obstacle concentration and therefore the degree of anomalous diffusion. This can be understood if one considers the two effects that influence the rate of product formation. The first factor is the time needed for the first collision between two particles. This is decreased by anomalous diffusion. The second is the rate of re-collision after an unsuccessful collision. Since the particles will separate slower in case of anomalous subdiffusion, this rate increases.

For reactions with a low probability those effects can offset each other, making the reaction rate nearly independent of the concentration of the obstacles.

The influence of obstacles on Michaelis-Menten kinetics in 2D was investigated in Monte Carlo simulations by H. Berry[214]. He could show that even at obstacle concentrations well below the percolation limit, the Michalis-Menten equation fails to describe the reaction kinetics if both enzyme and substrate are subject to hindered diffusion in the same way. This was due to a time dependence of the effective rate of formation of the enzyme-substrate complex in the Michalis-Menten scheme ($E + S \underset{k_{-1}}{\overset{k_1}{\rightleftarrows}} ES \xrightarrow{k_2} P$).

The time dependence of the effective rate k_1 is a consequence of anomalous diffusion. The enzyme stays close to its starting point much longer than in the case of normal diffusion. It reacts with substrate molecules close to it fast in the beginning, but it takes a longer time to react in distant regions. Since k_1 decreases with time.

The influence of anomalous subdiffusion on the formation of Turing patters was investigated by M. Weiss[215]. Turing patterns arise from simple reaction-diffusion systems. They are named after the English mathematician Alan Turing who proposed them first in 1952 as a mechanism for the formation of form and shape in biological systems with an particular emphasis on embryogenesis[216].

Mechanisms related to those suggested by Turing have been proposed in several biological systems [152,217-221]. An especially well described example for dynamic self-organisation is the formation of the central division plane in *E.coli*[222-226].

A general problem with self-organisation mechanisms is the stability at low number of particles, as expected in living cells. Investigating a simple model system, M. Weiss could show that a relatively high number of particles might be necessary to get a stable pattern. In living cells and bacteria, it can be expected that only a few hundred or thousand particles participate in pattern formation. In this case anomalous diffusion was shown to stabilize the pattern formation mechanism greatly. In the Schnakenberg model patterns were only stable when much more than 5000 particles were involved. When only modest anomalous diffusion (α=0.9) was introduced, the number of molecules needed to form stable patterns decreased to less then 2000[215].

Recently subdiffusion has received some attention in the field of gene expression. For a long time researchers have been baffled by the short time transcription factors need to find their targets on the DNA. The times are much shorter than those that would be expected, if the transcription factor just randomly collides with the DNA during simple 3D diffusion. Usually it is supposed that the transcription factors bind to the DNA unspecifically and perform a 1D diffusion for significant times, which would increase the efficiency of finding the correct binding site[227-229] (for a in depth review see [230]). Anomalous diffusion could provide an alternative mechanism for effective

search. Even tough the transcription factor needs a longer time to find the DNA initially it would also stay close to it longer. It was estimated that the probability *p* of finding a target of the size *a* starting at an initial distance r is:

$$p_{capture} \approx \left(\frac{a}{r} \right)^{3-\frac{2}{\alpha}} \quad \text{Eq. 38}$$

The smaller α is the higher is the probability to find the target. As the probability of finding the target increases the rate slows down:

$$k = \frac{\Gamma^{\frac{1}{\alpha}}}{a^{\frac{2}{\alpha-3}}} \quad \text{Eq. 39}$$

Subdiffusion therefore increases the probability to find the target on the DNA at all, but decreases the overall rate in of association. For the small number of available transcription factors available in living cells the overall effect of anomalous maybe to tip the balance between the protein finding its binding site and running away to far from the DNA[174,230]. A more detailed analysis of the effect of anomalous diffusion on gene expression, taking into account the particularities of the pro- and eukaryotic systems and cellular geometries, is missing so far.

Most studies on the effects of anomalous diffusion are done *in silico*, to my knowledge no experiment study has been done so far.

5 Results and Discussion

5.1 Paper 1: Spatiotemporal dynamics of the COPI vesicle machinery

The model for the formation of COPI vesicles was mainly developed from *in vitro* studies on isolated Golgi membranes or liposomes in connection with cytosol or purified components (compare chapter 4.4). To confirm the model *in vivo*, we employed live cell imaging approaches. A crucial prediction of the current model is that coatomer and Arf1 binding to and release from the membrane are coupled events. To investigate if this is the case in living cells we used GFP tagged ε-COP, Arf1 and ArfGAP1 and measured their binding kinetics to Golgi membranes using FRAP. Surprisingly, the apparent binding kinetics of coatomer was two times slower then of ARF. As expected Arf1 and ArfGAP1 showed similar kinetics (Fig. 2[*]). Similar results for Arf1 and coatomer were obtained by the group of J. Lippincott-Schwartz[90]. While the Lippincott-Schwartz group suggested a modification of the model for coatomer action *in vivo*, we decided to take a closer look at the experimental conditions. The measurement of the binding kinetics with FRAP is based on the assumption that the diffusion from and to the membrane is not limiting to the measured binding constant. We tested this assumption using a combination of Fluorescence Correlation Spectroscopy and computer simulation. First, we measured the diffusion coefficients of ε-COP, Arf1 and ArfGAP1. All three showed a fast and a slow diffusing component. In all cases the fast diffusing component had a diffusion coefficient D of about 15 $\mu m^2/s$, while the slow

[*] The figure numbers used in this and the following chapters correspond to the figures in the papers reproduced in section 3

component had a very low diffusion coefficient of about 0.5 $\mu m^2/s$. The percentages varied greatly. For ARF the slow component comprised only 15% of the total pool. The slow ArfGAP1 component accounted for 30% and the slow component of ε-COP 26% in stably transfected Hela cells and 52% of the whole pool in stably transfected CHO cells (Fig. 1).

The slow diffusion components suggested that the GFP labelled proteins were part of a large protein complex. We theorized that ArfGAP1 could be in a complex with coatomer. To test this we increased the concentration of free coatomer by treating the cells with BFA, which releases coatomer from Golgi membranes. As predicted, the increased availability of coatomer increased the percentage of the slow ArfGAP1 component from 30% to 50%.

The slow component of ε-COP is likely to consist of ε-COP that is correctly inserted in into the coatomer complex, while the fast component is probably free ε-COP not incorporated in the complex due to overexpression. Treatment with BFA again increased the slow component. To further strengthen this argument, we knocked down β-COP using RNA interference. β-COP is essential for the correct assembly of the coatomer complex. As expected a decreased slow component was observed reflecting an absence of intact coatomer complexes (Fig. 1),

Having established that coatomer diffuses about 30 times slower in the cytoplasm than the main component of Arf1, we investigated next if this could account for the 2 times slower binding kinetics observed in the FRAP experiments.

We used a simple computer model determine the influence of diffusion on the binding kinetics. For simplicity we assumed the cell to be square shaped and overlaid it with an 11x11 grid. To account for the height of the cell we added a second 11x11 grid in top of the first. 2x6 grid points on one level were declared Golgi points. In accordance with microscopic data we assumed that the dimensions of the cell to be 33x33x3 μm. For the simulation we allowed the

particles to freely diffuse between the cytosolic sites. Binding and unbinding to the cytosolic sites was only allowed from and to adjacent cytosolic sites with specific rates (Fig. 3).

From the simulations we estimated that for a $D< 2\ \mu m^2/s$, the binding constants estimated from the FRAP data, deviated significantly from those used in the simulation (we used the binding/unbinding rates in accordance with the experimental results for Arf1). For the diffusion coefficient that was measured *in vivo*, the apparent binding rate was about twice the real binding rate used in the simulation. This showed that the slow diffusion of coatomer is sufficient to account for the slow binding rates of coatomer without the need for additional factors in the COPI machinery (Fig. 3)

Besides the fact that we found that the binding kinetics of the COPI machinery are consistent with the biochemical model, the paper raises issues important for the analysis of binding events in living cells in general. Our results show that not only the binding kinetics themselves influence the recovery in FRAP experiments, but that one has to take the diffusion of the molecules in question into account as well. An experimental measurement of the diffusion coefficient *in vivo* is essential for estimating its effect on the recovery. In our case we would have overestimated the diffusion coefficient of the coatomer complex greatly if we had used an estimation based on the molecular size of the coatomer. A more detailed analysis of possible diffusion artefacts in FRAP experiments was published by M. Weiss[184]. For the field of Golgi it is important that our experiments hinted towards an association of ArfGAP1 and coatomer in the cytosol, warranting a closer investigation of the role of this association.

5.2 Paper 2: Anomalous Subdiffusion Is a Measure for Cytoplasmic Crowding in Living Cells

The coatomer diffusion in living cells that we found in the first paper was surprisingly slow. From calibration measurements with GFP and the size of the coatomer complex, one would have expected a much higher diffusion coefficient. In the discussion of paper I we suggested that the slow diffusion of coatomer could be a consequence of binding to immobile structures in the cytosol or the formation of large protein complexes in the cytosol.

Since the there was some discussion in the literature over the size dependence of the diffusion coefficient of proteins in the cytosol (compare chapter 4.8) and no study had employed the non-invasive method of FCS, we decided to investigate if the cytosol has properties different from a simple viscous solution that can affect diffusion properties. We used fluorescently labelled, but inert tracer particles as probes and compared their diffusion in solution, in life cells and an artificial crowded environment. The results were confirmed with computer simulations. As tracer particles we used FITC labelled dextran polymers of different sizes. In PBS buffer all dextrans showed normal diffusion and the hydrodynamic radius increased proportional to $m^{0.4}$ (Fig. 2). In living cells all dextrans showed different degrees of anomalous subdiffusion (see chapter 4.6) (Fig. 3 and Table 1).

To separate properties of the cytosol from properties imposed by higher order structures like microtubules, actin and the ER, we used different drugs to disrupt these structures. In all cases subdiffusion persisted ruling out those structures a cause for the phenomenon. The major rearrangement of all cellular components in cells arrested in mitosis had also just a minor effect on the α-values (Table 2).

After ruling out higher order structures as a cause for subdiffusion we investigated if molecular crowding can cause subdiffusion.

We studied this possibility in two ways. First, we constructed a computer model for free 3D diffusion. We simulated the diffusion of tracer particles in a crowded environment of diffusing particles by solving the Langevin equation numerically. The excluded volume effect was considered by using a softcore repulsive force between the particles. Consistent with the assumption that crowding can cause subdiffusion we found a size dependent anomalous diffusion of the tracer particles. We also tested two different distributions for the sizes of the solutes. Both were inspired by the size distribution we obtained from an SDS page of purified cytosol of Hela cells. The overall effect was similar for an equal distribution of solutes ranging from 0.05 to 1 MDa and a Poisson distribution over the same range of masses. But there was a clear difference in the critical size of the probe before it became subdiffusive (Fig. 4).

Second, we studied the diffusion of labelled dextrans in a concentrated solution of a mixture of unlabeled dextrans. The dextrans showed a concentration and size dependent subdiffusion. The higher the concentration of unlabelled dextrans, the lower the observed α. Interestingly, we detected the same relation between the size of the dextran and the α-value as in living cells (Fig 5).

This puzzling non-linear relationship is likely to be an effect of the polymer properties of the dextrans. Polymers can show a phenomenon called reptation, which leads to $\alpha=0.5$ under ideal conditions of obstructed diffusion. Globular particles under the same conditions show a much higher value for α. We propose that small dextrans adopt a snake like, elongated confirmation, while larger dextrans have a more globular confirmation. Behaviour like this was, for example, reported for a close relative of dextran called fructan.

The results of the paper show that diffusion of large particles in the cytosol is more complicated than in a simple viscous solution. Large particles will diffuse much slower and in a qualitatively different way then expected from measurements in solution.

This has important consequences for the kinetics of biochemical reactions. The slow diffusion that was expected for crowded solutions, should lead too a low rate of encounter of proteins in the cell. The discovery that diffusion is not only slower, but anomalous gives an indication of how efficient biochemistry can still take place. If most biochemical reactions have a quite low probability of reaction per encounter, then it is expected that those reactions are favoured by the increased rate of re-collision in that case of anomalous diffusion[213] (see chapter 4.8). Anomalous diffusion could therefore be a prerequisite of an efficient biochemistry in the cell.

We also suggested that anomalous diffusion could be used as a measure for the crowding experienced by a particle of a certain size. A simple measure is necessary, since crowding effects on specific cellular pathway have not been well described so far. To reconstitute crowding effects *in vitro* or *in silico* one needs to be able to quantify the effect. As we have seen in chapter 4.8, the excluded volume effect can explain most effects of molecular crowding, but is very tedious to determine the excluded volume experimentally for a give experimental situation, if at all possible. The measurements of the diffusive behaviour are comparably straight forward and could be used to compare the *in vivo* with the *in vitro* situation.

Our results have been largely confirmed in a study by Banks and Fradin[231]. In addition to our paper they investigate the influence of the size of the crowding particles on the observed anomalous diffusion. For streptavidin as a tracer they find, that small crowding dextrans cause only α values close to 1, while larger dextrans cause considerable subdiffusion. They also investigated the ability of Bovine serum albumin and streptavidin to cause crowding for BSA sized particles. It was found that BSA sized proteins are weaker crowding agents than large dextrans.

In a recent study it was shown that molecular crowding also causes anomalous diffusion in bacterial cytoplasm[174].

In the light of these findings we have to revise the conclusion we drew in the first paper. A large part of the surprisingly slow diffusion of coatomer will not be due to specific interactions or protein oligomerisation, but reflects a basic property of the cytosol. Since it is likely that the shape of coatomer is far from spherical, coatomer will be affected stronger by an inhomogeneous cytoplasm than spherical proteins.

5.3 Paper 3: Evidence for Golgi localization by oligomerisation - kin recognition revisited

In chapter 4.5 we saw that oligomerisation is one mechanism suggested for the localisation of Golgi resident proteins. It is expected that oligomerisation influences the diffusion properties of the enzymes. This was studied by Weiss *et al* using EGFP tagged proteins and FCS. They found that all proteins studied show strong anomalous diffusion with α values ranging from 0.55 to 0.75.

In this publication the anomalous diffusion was explained with a continuous time random walk. For a CTRW the kinetics binding have to be rather complicated or the system has to be out of thermal equilibrium.

We therefore decided to investigate if another mechanism can explain the subdiffusion that is observed in FCS experiments. In chapter 4.6 I discussed the occurrence of anomalous diffusion in the motion of the monomers in a polymer chain for short time scales. Those results have been obtained in static polymers of a given length. In biology polymers formed by proteins are most likely dynamic.

In this manuscript we investigate if the dynamic formation of oligomers on the membrane leads to anomalous diffusion on time scales relevant to FCS.

For this we constructed a computer model for the diffusion of membrane proteins that participate in the dynamic formation of oligomers. Diffusion was simulated by solving the overdamped Langevin equation in two dimensions. In addition to the random forces in the Langevin equation, two types of

conservative forces were applied on the particles. Particles not bound to each other interacted by soft core repulsion, when their distance was lower then a critical distance r_s. Bound particles were subject to a linear restoring force, when their distance deviated from the bond length r_s.

Binding and unbinding occurred with simple on/off kinetics. Bonds could be formed with a rate k_{on}, if particles were closer then a minimum binding distance r_c and were dissolved with a rate k_{off}. Each particle had two or three binding sites.

Deviations from normal diffusion were measured by plotting the MSD versus the time.

As expected, diffusion was normal for long times. The diffusion coefficient decreased for decreasing k_{off}/k_{on}-ratios, since larger oligomers were formed.

For the short timescales relevant to FCS experiments, the MSD shows strong deviations from normal diffusion (Figure 2). The α-value decreased when the one-rate was increased and the subdiffusion persisted to longer times.

An increase of the valency from 2 to 3 gives the same picture, but the deviations from normal diffusion are stronger and persist to longer times (Figure 3).

The dependency of the α-value on the equilibrium constant (changing k_{on} while k_{off} is kept constant) has a sigmoid shape (Figure 4). In both the valency 2 and 3 case the crossover from the subdiffusive regime to the normal diffusion is smooth and covers about two orders of magnitude of the equilibrium constant. At valency 3 the particles are always more subdiffusive then in the valency 2 case. Very low α values down to 0.25 can be reached for low k_{off}/k_{on} ratios.

We could show that the dynamics of the association is as important as the k_{off}/k_{on} ratio. When we increased k_{off} + k_{on} while keeping the k_{off}/k_{on} ratio constant, α increased in a sigmoid curve. The crossover from anomalous to normal diffusion was again smooth and was spread over at least 3 orders of magnitude.

The results indicate that oligomerisation of proteins can indeed be observed in FCS measurements by measuring the anomality of the diffusion. If we assume a valency of 3, α values less then 0.6 can be reached. For the case of Golgi enzymes this is important since we observe 0.55 for one of the enzymes. This ability to explain low α make this model for anomalous subdiffusion superior to the popular model of obstructed diffusion if it come to explaining α-values below 0.69.

We can conclude that the diffusion properties that we observe for Golgi resident proteins are consistent with the model of kin-recognition and the formation of large oligomers.

The original kin recognition model envisaged an immobilisation of the kin-oligomers and an exclusion of the proteins from COPI vesicles. The model clearly has to be reformulated to reconcile it with the redefined role of COPI vesicles. Glycosyltransferases are mobile in the Golgi membrane[143,144] and are incorporated preferentially into COPI vesicles in an GTP hydrolysis depended manner[57,59,60].

The easiest way to picture the sorting of Glycosyltransferases, is to assume that kin-oligomers contain proteins that have the ability to interact with both the COPI machinery and the resident proteins. So far, no obvious candidate for this role has been suggested. The members of the p24 protein family cycle between the ER and have the ability to influence the COPI machinery[58,232-234]. Although they have been suggested to function as cargo receptors[232], no interaction with other proteins that are sorted into COPI vesicles has been reported so far. It is possible that some Glycosyltransferases might have the ability to interact with the COPI machinery as their cytoplasmic tail is important for their localisation[127,128], but this has not been investigated, yet.

The increase of α values for resident proteins from the *cis* to the *trans*-Golgi suggests that *trans*-proteins participate in the formation of larger oligomers

than *cis*-proteins. Whether this is a general trend, valid for all proteins, will have to be verified by studying more proteins.

In the simplest form, the kin-recognition/cargo-receptor model would predict that large oligomers are more efficient in recruiting the COPI machinery, because a larger number of cargo receptors would be present in the same area of the membrane. In the maturation scheme for Golgi transport, one would expect the opposite preference for sorting into COPI vesicles. *Trans*-proteins should be less competitive in the sorting reaction compared to *cis*-proteins[62,63].

A possible mechanism to ensure a reduced competitiveness of large oligomers, can be found if one considers the processes during vesicle budding.

The formation of a bud/vesicle requires a large increase in the curvature of the membrane. Due to its intrinsic stiffness the oligomers will resist this bending, and reduce the probability to make a vesicle during the time given by Arf1 hydrolysis. Large oligomers will offer more resistance to membrane bending than small ones. In addition larger and stiffer polymers will have a reduced probability to enter the highly curved rim regions of the Golgi were most of the buds are observed, especially if the large oligomers have to compete with smaller oligomers for places in the rims.

An alternative explanation is to assume that that putative cargo receptor has different affinities to proteins that are resident in different cisternae. *Cis*-oligomers would have a higher concentration of cargo receptors, and be incorporated more efficiently into COPI vesicles.

This model poses a lot of new questions that have to be addressed in future work. Our simulation results will have to be verified experimentally in systems allowing for controlled oligomerisation of tracer proteins. An oligomer-size dependence of the Golgi localisation of resident proteins will have to be shown. Proteins with the ability to bind both, to the COPI machinery and glycosyltransferases, will have to be identified.

6 Acknowledgements

mmmhhh, here comes the most difficult part. Not only because it is the most personal section, but also because this is the only section that most people will actually read.
I will begin with an apology to those people I will forget to mention. Those who know me know that this is not evil will, but ..well… just me.

I want to thank:

First, **Tommy**: I cannot believe it is more then 4 years ago that I walked into your tiny office in the corner of the EMBL lab for the first interview! Thank you for everything! (Which includes the opportunity to work in his lab, the science, the freedoms I had, the interesting discussion etc. etc.)

Then **Matthias Weiss**, for being a never ending source of inspiration and ideas and a friend!

Fredrik, Jacqui and Johan for being great lab mates and much more importantly good friends! F. and Jo. good luck with the rest of your thesis! F. and Ja. Good luck with **Nathalie!** Jo. good luck with your Hattrick team!

Maria for suffering with me through subdiffusion and FCS. For always being there for my questions and problems! Hope we will stay friends!

Lennart for all the interesting and long science discussions. I will miss them!

Je remercie **Fred2** pour avoir été mon seul compagnon pendant beaucoup des nuits entières à la paillasse et pour tous nos conférences bière et pizzas.

Marlies for being the “Gute Geist” of the lab.

Linda for being always, always there to help!

Julia for introducing us to that Spanish ham whose name I cannot remember. For lively coffee brakes and kicking the a.. of the Zeiss people to get the microscope repaired on time.

Magnus for being a valuable source of experience**.**

Cecilia for starting up the lab, when we moved and keep it running afterwards.

Gunnar Hansson for helping me with all the administrative stuff and always answering my many questions.

Martin for introducing me in the art and science of doing a disputation in Gothenburg.

Brigitta, Michael, Ulrika, Cecillia and Minette for being there when one of the many papers and forms was missing.

Sweden for being a wonderful host country.

Meinen Eltern ohne deren Hilfe und Liebe ich nie so weit gekommen wäre!

Christiane für die letzten drei, trotz

 ,

die fünf davor, mit einem dicken:

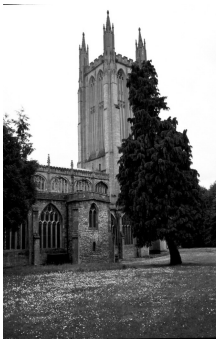

und für hoffentlich viele weitere Jahre! Beginnend mit:

7 References

1. Ellgaard L, Helenius A. Quality Control in the Endoplasmic Reticulum. Nat Rev Mol Cell Biol 2003;4(3):181-191.
2. Gaut JR, Hendershot LM. The modification and assembly of proteins in the endoplasmic reticulum. Curr Opin Cell Biol 1993;5(4):589-95.
3. van Anken E, Braakman I. Versatility of the endoplasmic reticulum protein folding factory. Crit Rev Biochem Mol Biol 2005;40(4):191-228.
4. Maccioni HJF, Giraudo CG, Daniotti JL. Understanding the Stepwise Synthesis of Glycolipids. Neurochemical Research 2002;27(7 - 8):629-636.
5. Varki A. Factors controlling the glycosylation potential of the Golgi apparatus. Trends in Cell Biology 1998;8(1):34-40.
6. Huttner WB. Tyrosine Sulfation and the Secretory Pathway. Annual Review of Physiology 1988;50(1):363-376.
7. Halban PA, Irminger JC. Sorting and processing of secretory proteins. Biochem J 1994;299 (Pt 1):1-18.
8. Jeckel D, Karrenbauer A, Burger KN, van Meer G, Wieland F. Glucosylceramide is synthesized at the cytosolic surface of various Golgi subfractions. J. Cell Biol. 1992;117(2):259-267.
9. Holthuis JC, Pomorski T, Raggers RJ, Sprong H, Van Meer G. The organizing potential of sphingolipids in intracellular membrane transport. Physiol Rev 2001;81(4):1689-723.
10. Vance JE, Vance DE. Phospholipid biosynthesis in mammalian cells. Biochem Cell Biol 2004;82(1):113-28.
11. De Matteis MA, Godi A, Corda D. Phosphoinositides and the golgi complex. Current Opinion in Cell Biology 2002;14(4):434-447.
12. Cho W, Stahelin RV. MEMBRANE-PROTEIN INTERACTIONS IN CELL SIGNALING AND MEMBRANE TRAFFICKING. Annual Review of Biophysics and Biomolecular Structure 2005;34(1):119-151.
13. Cockcroft S, De Matteis MA. Inositol Lipids as Spatial Regulators of Membrane Traffic. Journal of Membrane Biology 2001;180(3):187-194.
14. Mancias JD, Goldberg J. Exiting the Endoplasmic Reticulum. Traffic 2005;6(4):278-285.
15. Kirchhausen T. Three ways to make a vesicle. Nat Rev Mol Cell Biol 2000;1(3):187-98.
16. Lee MC, Orci L, Hamamoto S, Futai E, Ravazzola M, Schekman R. Sar1p N-terminal helix initiates membrane curvature and completes the fission of a COPII vesicle. Cell 2005;122(4):605-17.
17. Kuehn MJ, Herrmann JM, Schekman R. COPII-cargo interactions direct protein sorting into ER-derived transport vesicles. Nature 1998;391(6663):187-90.
18. Mossessova E, Bickford LC, Goldberg J. SNARE selectivity of the COPII coat. Cell 2003;114(4):483-95.

19. Aridor M, Weissman J, Bannykh S, Nuoffer C, Balch WE. Cargo selection by the COPII budding machinery during export from the ER. J Cell Biol 1998;141(1):61-70.
20. Miller EA, Beilharz TH, Malkus PN, Lee MC, Hamamoto S, Orci L, Schekman R. Multiple cargo binding sites on the COPII subunit Sec24p ensure capture of diverse membrane proteins into transport vesicles. Cell 2003;114(4):497-509.
21. Antonny B, Madden D, Hamamoto S, Orci L, Schekman R. Dynamics of the COPII coat with GTP and stable analogues. Nat Cell Biol 2001;3(6):531-7.
22. Yoshihisa T, Barlowe C, Schekman R. Requirement for a GTPase-activating protein in vesicle budding from the endoplasmic reticulum. Science 1993;259(5100):1466-8.
23. Lederkremer GZ, Cheng Y, Petre BM, Vogan E, Springer S, Schekman R, Walz T, Kirchhausen T. Structure of the Sec23p/24p and Sec13p/31p complexes of COPII. Proc Natl Acad Sci U S A 2001;98(19):10704-9.
24. Stephens DJ, Lin-Marq N, Pagano A, Pepperkok R, Paccaud JP. COPI-coated ER-to-Golgi transport complexes segregate from COPII in close proximity to ER exit sites. J Cell Sci 2000;113 (Pt 12):2177-85.
25. Orci L, Ravazzola M, Meda P, Holcomb C, Moore HP, Hicke L, Schekman R. Mammalian Sec23p homologue is restricted to the endoplasmic reticulum transitional cytoplasm. Proc Natl Acad Sci U S A 1991;88(19):8611-5.
26. Xu D, Hay JC. Reconstitution of COPII vesicle fusion to generate a pre-Golgi intermediate compartment. J. Cell Biol. %R 10.1083/jcb.200408135 2004;167(6):997-1003.
27. Schweizer A, Matter K, Ketcham CM, Hauri HP. The isolated ER-Golgi intermediate compartment exhibits properties that are different from ER and cis-Golgi. J Cell Biol 1991;113(1):45-54.
28. Martinez-Menarguez JA, Geuze HJ, Slot JW, Klumperman J. Vesicular tubular clusters between the ER and Golgi mediate concentration of soluble secretory proteins by exclusion from COPI-coated vesicles. Cell 1999;98(1):81-90.
29. Stephens DJ, Pepperkok R. Differential effects of a GTP-restricted mutant of Sar1p on segregation of cargo during export from the endoplasmic reticulum. J Cell Sci 2004;117(Pt 16):3635-44.
30. Ben-Tekaya H, Miura K, Pepperkok R, Hauri HP. Live imaging of bidirectional traffic from the ERGIC. J Cell Sci 2005;118(Pt 2):357-67.
31. Shima DT, Scales SJ, Kreis TE, Pepperkok R. Segregation of COPI-rich and anterograde-cargo-rich domains in endoplasmic-reticulum-to-Golgi transport complexes. Curr Biol 1999;9(15):821-4.
32. Presley JF, Cole NB, Schroer TA, Hirschberg K, Zaal KJ, Lippincott-Schwartz J. ER-to-Golgi transport visualized in living cells. Nature 1997;389(6646):81-5.
33. Scales SJ, Pepperkok R, Kreis TE. Visualization of ER-to-Golgi transport in living cells reveals a sequential mode of action for COPII and COPI. Cell 1997;90(6):1137-48.
34. Watson P, Stephens DJ. ER-to-Golgi transport: form and formation of vesicular and tubular carriers. Biochim Biophys Acta 2005;1744(3):304-15.

35. Tang BL, Wang Y, Ong YS, Hong W. COPII and exit from the endoplasmic reticulum. Biochim Biophys Acta 2005;1744(3):293-303.
36. Lee MC, Miller EA, Goldberg J, Orci L, Schekman R. Bi-Directional Protein Transport Between the ER and Golgi. Annu Rev Cell Dev Biol 2004.
37. Marsh BJ, Mastronarde DN, Buttle KF, Howell KE, McIntosh JR. Organellar relationships in the Golgi region of the pancreatic beta cell line, HIT-T15, visualized by high resolution electron tomography. Proc Natl Acad Sci U S A 2001;98(5):2399-406.
38. Ladinsky MS, Mastronarde DN, McIntosh JR, Howell KE, Staehelin LA. Golgi structure in three dimensions: functional insights from the normal rat kidney cell. J Cell Biol 1999;144(6):1135-49.
39. Grabenbauer M, Geerts WJC, Fernadez-Rodriguez J, Hoenger A, Koster AJ, Nilsson T. Correlative microscopy and electron tomography of GFP through photooxidation. Nat Methods 2005;2(11):857-862.
40. Marsh BJ. Lessons from tomographic studies of the mammalian Golgi. Biochim Biophys Acta 2005;1744(3):273-92.
41. Rabouille C, Hui N, Hunte F, Kieckbusch R, Berger EG, Warren G, Nilsson T. Mapping the distribution of Golgi enzymes involved in the construction of complex oligosaccharides. J Cell Sci 1995;108 (Pt 4):1617-27.
42. Moreau P, Cassagne C. Phospholipid trafficking and membrane biogenesis. Biochim Biophys Acta 1994;1197(3):257-90.
43. Paroutis P, Touret N, Grinstein S. The pH of the secretory pathway: measurement, determinants, and regulation. Physiology (Bethesda) 2004;19:207-15.
44. Presley JF, Smith C, Hirschberg K, Miller C, Cole NB, Zaal KJM, Lippincott-Schwartz J. Golgi Membrane Dynamics. Mol. Biol. Cell 1998;9(7):1617-1626.
45. Munro S. Sequences within and adjacent to the transmembrane segment of alpha-2,6-sialyltransferase specify Golgi retention. Embo J 1991;10(12):3577-88.
46. Aoki D, Lee N, Yamaguchi N, Dubois C, Fukuda MN. Golgi retention of a trans-Golgi membrane protein, galactosyltransferase, requires cysteine and histidine residues within the membrane-anchoring domain. Proc Natl Acad Sci U S A 1992;89(10):4319-23.
47. Nilsson T, Lucocq JM, Mackay D, Warren G. The membrane spanning domain of beta-1,4-galactosyltransferase specifies trans Golgi localization. Embo J 1991;10(12):3567-75.
48. Donaldson J, Lippincott-Schwartz J, Bloom G, Kreis T, Klausner R. Dissociation of a 110-kD peripheral membrane protein from the Golgi apparatus is an early event in brefeldin A action. J. Cell Biol. 1990;111(6):2295-2306.
49. Balch WE, Dunphy WG, Braell WA, Rothman JE. Reconstitution of the transport of protein between successive compartments of the Golgi measured by the coupled incorporation of N-acetylglucosamine. Cell 1984;39(2 Pt 1):405-16.
50. Orci L, Malhotra V, Amherdt M, Serafini T, Rothman JE. Dissection of a single round of vesicular transport: sequential intermediates for intercisternal movement in the Golgi stack. Cell 1989;56(3):357-68.

51. Ostermann J, Orci L, Tani K, Amherdt M, Ravazzola M, Elazar Z, Rothman JE. Stepwise assembly of functionally active transport vesicles. Cell 1993;75(5):1015-25.
52. Orci L, Amherdt M, Ravazzola M, Perrelet A, Rothman JE. Exclusion of golgi residents from transport vesicles budding from Golgi cisternae in intact cells. J Cell Biol 2000;150(6):1263-70.
53. Bonfanti L, Mironov AA, Jr., Martinez-Menarguez JA, Martella O, Fusella A, Baldassarre M, Buccione R, Geuze HJ, Mironov AA, Luini A. Procollagen traverses the Golgi stack without leaving the lumen of cisternae: evidence for cisternal maturation. Cell 1998;95(7):993-1003.
54. Brown RM, Jr. OBSERVATIONS ON THE RELATIONSHIP OF THE GOLGI APPARATUS TO WALL FORMATION IN THE MARINE CHRYSOPHYCEAN ALGA, PLEUROCHRYSIS SCHERFFELII PRINGSHEIM. J. Cell Biol. 1969;41(1):109-123.
55. Marchi F, Leblond CP. Radioautographic characterization of successive compartments along the rough endoplasmic reticulum-Golgi pathway of collagen precursors in foot pad fibroblasts of [3H]proline-injected rats. J Cell Biol 1984;98(5):1705-9.
56. Mironov AA, Beznoussenko GV, Nicoziani P, Martella O, Trucco A, Kweon HS, Di Giandomenico D, Polishchuk RS, Fusella A, Lupetti P and others. Small cargo proteins and large aggregates can traverse the Golgi by a common mechanism without leaving the lumen of cisternae. J Cell Biol 2001;155(7):1225-38.
57. Lanoix J, Ouwendijk J, Lin CC, Stark A, Love HD, Ostermann J, Nilsson T. GTP hydrolysis by arf-1 mediates sorting and concentration of Golgi resident enzymes into functional COP I vesicles. Embo J 1999;18(18):4935-48.
58. Lanoix J, Ouwendijk J, Stark A, Szafer E, Cassel D, Dejgaard K, Weiss M, Nilsson T. Sorting of Golgi resident proteins into different subpopulations of COPI vesicles: a role for ArfGAP1. J Cell Biol 2001;155(7):1199-212.
59. Love HD, Lin CC, Short CS, Ostermann J. Isolation of functional Golgi-derived vesicles with a possible role in retrograde transport. J Cell Biol 1998;140(3):541-51.
60. Martinez-Menarguez JA, Prekeris R, Oorschot VM, Scheller R, Slot JW, Geuze HJ, Klumperman J. Peri-Golgi vesicles contain retrograde but not anterograde proteins consistent with the cisternal progression model of intra-Golgi transport. J Cell Biol 2001;155(7):1213-24.
61. Ostermann J. Stoichiometry and kinetics of transport vesicle fusion with Golgi membranes. EMBO Rep 2001;2(4):324-9.
62. Glick BS, Elston T, Oster G. A cisternal maturation mechanism can explain the asymmetry of the Golgi stack. FEBS Lett 1997;414(2):177-81.
63. Weiss M, Nilsson T. Protein sorting in the Golgi apparatus: a consequence of maturation and triggered sorting. FEBS Lett 2000;486(1):2-9.
64. Losev E, Reinke CA, Jellen J, Strongin DE, Bevis BJ, Glick BS. Golgi maturation visualized in living yeast. Nature 2006;441(7096):1002-6.
65. Matsuura-Tokita K, Takeuchi M, Ichihara A, Mikuriya K, Nakano A. Live imaging of yeast Golgi cisternal maturation. Nature 2006;441(7096):1007-10.
66. Marsh BJ, Volkmann N, McIntosh JR, Howell KE. Direct continuities between cisternae at different levels of the Golgi complex in glucose-

stimulated mouse islet beta cells. Proc Natl Acad Sci U S A 2004;101(15):5565-70.
67. Trucco A, Polishchuk RS, Martella O, Di Pentima A, Fusella A, Di Giandomenico D, San Pietro E, Beznoussenko GV, Polishchuk EV, Baldassarre M and others. Secretory traffic triggers the formation of tubular continuities across Golgi sub-compartments. Nat Cell Biol 2004;6(11):1071-81.
68. Martinez-Alonso E, Egea G, Ballesta J, Martinez-Menarguez JA. Structure and dynamics of the Golgi complex at 15 degrees C: low temperature induces the formation of Golgi-derived tubules. Traffic 2005;6(1):32-44.
69. Clermont Y, Rambourg A, Hermo L. Connections between the various elements of the cis- and mid-compartments of the Golgi apparatus of early rat spermatids. Anat Rec 1994;240(4):469-80.
70. Tanaka K, Mitsushima A, Fukudome H, Kashima Y. Three-dimensional architecture of the Golgi complex observed by high resolution scanning electron microscopy. J Submicrosc Cytol 1986;18(1):1-9.
71. Tanaka K, Fukudome H. Three Dimensional Organisation of the Golgi Complex Observed by Scanning Electron Microscopy. J. Electr. Microsc. Tech. 1991;17:15-23.
72. Orci L, Glick BS, Rothman JE. A new type of coated vesicular carrier that appears not to contain clathrin: its possible role in protein transport within the Golgi stack. Cell 1986;46(2):171-84.
73. Malhotra V, Serafini T, Orci L, Shepherd JC, Rothman JE. Purification of a novel class of coated vesicles mediating biosynthetic protein transport through the Golgi stack. Cell 1989;58(2):329-36.
74. Melancon P, Glick BS, Malhotra V, Weidman PJ, Serafini T, Gleason ML, Orci L, Rothman JE. Involvement of GTP-binding "G" proteins in transport through the Golgi stack. Cell 1987;51(6):1053-62.
75. Waters MG, Serafini T, Rothman JE. 'Coatomer': a cytosolic protein complex containing subunits of non-clathrin-coated Golgi transport vesicles. Nature 1991;349(6306):248-251.
76. Orci L, Palmer DJ, Ravazzola M, Perrelet A, Amherdt M, Rothman JE. Budding from Golgi membranes requires the coatomer complex of non-clathrin coat proteins. Nature 1993;362(6421):648-52.
77. Orci L, Schekman R, Perrelet A. Interleaflet clear space is reduced in the membrane of COP I and COP II-coated buds/vesicles. Proc Natl Acad Sci U S A 1996;93(17):8968-70.
78. Pepperkok R, Scheel J, Horstmann H, Hauri HP, Griffiths G, Kreis TE. Beta-COP is essential for biosynthetic membrane transport from the endoplasmic reticulum to the Golgi complex in vivo. Cell 1993;74(1):71-82.
79. Stenbeck G, Harter C, Brecht A, Herrmann D, Lottspeich F, Orci L, Wieland FT. beta'-COP, a novel subunit of coatomer. Embo J 1993;12(7):2841-5.
80. Stenbeck G, Schreiner R, Herrmann D, Auerbach S, Lottspeich F, Rothman JE, Wieland FT. Gamma-COP, a coat subunit of non-clathrin-coated vesicles with homology to Sec21p. FEBS Lett 1992;314(2):195-8.
81. Harter C. COPI proteins: A model for their role in vesicle budding. Protoplasma 1999;207(3 - 4):125-132.

82. Kahn RA, Gilman AG. The protein cofactor necessary for ADP-ribosylation of Gs by cholera toxin is itself a GTP binding protein. J Biol Chem 1986;261(17):7906-11.
83. Serafini T, Orci L, Amherdt M, Brunner M, Kahn RA, Rothman JE. ADP-ribosylation factor is a subunit of the coat of Golgi-derived COP-coated vesicles: a novel role for a GTP-binding protein. Cell 1991;67(2):239-53.
84. Taylor T, Kahn R, Melancon P. Two distinct members of the ADP-ribosylation factor family of GTP-binding proteins regulate cell-free intra-golgi transport. Cell 1992;70(1):69-79.
85. Donaldson JG, Cassel D, Kahn RA, Klausner RD. ADP-ribosylation factor, a small GTP-binding protein, is required for binding of the coatomer protein beta-COP to Golgi membranes. Proc Natl Acad Sci U S A 1992;89(14):6408-12.
86. Palmer DJ, Helms JB, Beckers CJ, Orci L, Rothman JE. Binding of coatomer to Golgi membranes requires ADP-ribosylation factor. J Biol Chem 1993;268(16):12083-9.
87. Antonny B, Beraud-Dufour S, Chardin P, Chabre M. N-terminal hydrophobic residues of the G-protein ADP-ribosylation factor-1 insert into membrane phospholipids upon GDP to GTP exchange. Biochemistry 1997;36(15):4675-84.
88. Donaldson JG, Finazzi D, Klausner RD. Brefeldin A inhibits Golgi membrane-catalysed exchange of guanine nucleotide onto ARF protein. Nature 1992;360(6402):350-2.
89. Helms JB, Rothman JE. Inhibition by brefeldin A of a Golgi membrane enzyme that catalyses exchange of guanine nucleotide bound to ARF. Nature 1992;360(6402):352-4.
90. Presley JF, Ward TH, Pfeifer AC, Siggia ED, Phair RD, Lippincott-Schwartz J. Dissection of COPI and Arf1 dynamics in vivo and role in Golgi membrane transport. Nature 2002;417(6885):187-93.
91. Elsner M, Hashimoto H, Simpson JC, Cassel D, Nilsson T, Weiss M. Spatiotemporal dynamics of the COPI vesicle machinery. EMBO Rep 2003;4(10):1000-4.
92. Zhang CJ, Rosenwald AG, Willingham MC, Skuntz S, Clark J, Kahn RA. Expression of a dominant allele of human ARF1 inhibits membrane traffic in vivo. J Cell Biol 1994;124(3):289-300.
93. Tanigawa G, Orci L, Amherdt M, Ravazzola M, Helms JB, Rothman JE. Hydrolysis of bound GTP by ARF protein triggers uncoating of Golgi-derived COP-coated vesicles. J Cell Biol 1993;123(6 Pt 1):1365-71.
94. Pepperkok R, Lowe M, Burke B, Kreis TE. Three distinct steps in transport of vesicular stomatitis virus glycoprotein from the ER to the cell surface in vivo with differential sensitivities to GTP gamma S. J Cell Sci 1998;111 (Pt 13):1877-88.
95. Spang A, Matsuoka K, Hamamoto S, Schekman R, Orci L. Coatomer, Arf1p, and nucleotide are required to bud coat protein complex I-coated vesicles from large synthetic liposomes. Proc Natl Acad Sci U S A 1998;95(19):11199-204.
96. Orci L, Palmer DJ, Amherdt M, Rothman JE. Coated vesicle assembly in the Golgi requires only coatomer and ARF proteins from the cytosol. Nature 1993;364(6439):732-734.

97. Reinhard C, Schweikert M, Wieland FT, Nickel W. Functional reconstitution of COPI coat assembly and disassembly using chemically defined components. Proc Natl Acad Sci U S A 2003;100(14):8253-7.
98. Kahn RA, Gilman AG. The protein cofactor necessary for ADP-ribosylation of Gs by cholera toxin is itself a GTP binding protein. J. Biol. Chem. 1986;261(17):7906-7911.
99. Randazzo PA, Yang YC, Rulka C, Kahn RA. Activation of ADP-ribosylation factor by Golgi membranes. Evidence for a brefeldin A- and protease-sensitive activating factor on Golgi membranes. J. Biol. Chem. 1993;268(13):9555-9563.
100. Peyroche A, Paris S, Jackson CL. Nucleotide exchange on ARF mediated by yeast Gea1 protein. Nature 1996;384(6608):479-81.
101. Morinaga N, Tsai SC, Moss J, Vaughan M. Isolation of a brefeldin A-inhibited guanine nucleotide-exchange protein for ADP ribosylation factor (ARF) 1 and ARF3 that contains a Sec7-like domain. Proc Natl Acad Sci U S A 1996;93(23):12856-60.
102. Chardin P, Paris S, Antonny B, Robineau S, Beraud-Dufour S, Jackson CL, Chabre M. A human exchange factor for ARF contains Sec7- and pleckstrin-homology domains. Nature 1996;384(6608):481-4.
103. Barlowe C, Schekman R. SEC12 encodes a guanine-nucleotide-exchange factor essential for transport vesicle budding from the ER. Nature 1993;365(6444):347-9.
104. Cox R, Mason-Gamer RJ, Jackson CL, Segev N. Phylogenetic analysis of Sec7-domain-containing Arf nucleotide exchangers. Mol Biol Cell 2004;15(4):1487-505.
105. Kawamoto K, Yoshida Y, Tamaki H, Torii S, Shinotsuka C, Yamashina S, Nakayama K. GBF1, a Guanine Nucleotide Exchange Factor for ADP-Ribosylation Factors, is Localized to the cis-Golgi and Involved in Membrane Association of the COPI Coat. Traffic 2002;3(7):483-495.
106. Zhao X, Lasell TKR, Melancon P. Localization of Large ADP-Ribosylation Factor-Guanine Nucleotide Exchange Factors to Different Golgi Compartments: Evidence for Distinct Functions in Protein Traffic. Mol. Biol. Cell %R 10.1091/mbc.01-08-0420 2002;13(1):119-133.
107. Shinotsuka C, Yoshida Y, Kawamoto K, Takatsu H, Nakayama K. Overexpression of an ADP-ribosylation factor-guanine nucleotide exchange factor, BIG2, uncouples brefeldin A-induced adaptor protein-1 coat dissociation and membrane tubulation. J Biol Chem 2002;277(11):9468-73.
108. Charych EI, Yu W, Miralles CP, Serwanski DR, Li X, Rubio M, De Blas AL. The brefeldin A-inhibited GDP/GTP exchange factor 2, a protein involved in vesicular trafficking, interacts with the beta subunits of the GABA receptors. J Neurochem 2004;90(1):173-89.
109. Shinotsuka C, Waguri S, Wakasugi M, Uchiyama Y, Nakayama K. Dominant-negative mutant of BIG2, an ARF-guanine nucleotide exchange factor, specifically affects membrane trafficking from the trans-Golgi network through inhibiting membrane association of AP-1 and GGA coat proteins. Biochem Biophys Res Commun 2002;294(2):254-60.
110. Zhao X, Lasell TK, Melancon P. Localization of large ADP-ribosylation factor-guanine nucleotide exchange factors to different Golgi compartments:

evidence for distinct functions in protein traffic. Mol Biol Cell 2002;13(1):119-33.
111. Niu T-K, Pfeifer AC, Lippincott-Schwartz J, Jackson CL. Dynamics of GBF1, a Brefeldin A-Sensitive Arf1 Exchange Factor at the Golgi. Mol. Biol. Cell %R 10.1091/mbc.E04-07-0599 2005;16(3):1213-1222.
112. Cukierman E, Huber I, Rotman M, Cassel D. The ARF1 GTPase-activating protein: zinc finger motif and Golgi complex localization. Science 1995;270(5244):1999-2002.
113. Szafer E, Pick E, Rotman M, Zuck S, Huber I, Cassel D. Role of coatomer and phospholipids in GTPase-activating protein-dependent hydrolysis of GTP by ADP-ribosylation factor-1. J Biol Chem 2000;275(31):23615-9.
114. Weiss M, Nilsson T. A kinetic proof-reading mechanism for protein sorting. Traffic 2003;4(2):65-73.
115. Bigay J, Gounon P, Robineau S, Antonny B. Lipid packing sensed by ArfGAP1 couples COPI coat disassembly to membrane bilayer curvature. Nature 2003;426(6966):563-566.
116. Antonny B, Huber I, Paris S, Chabre M, Cassel D. Activation of ADP-ribosylation factor 1 GTPase-activating protein by phosphatidylcholine-derived diacylglycerols. J Biol Chem 1997;272(49):30848-51.
117. Goldberg J. Structural and functional analysis of the ARF1-ARFGAP complex reveals a role for coatomer in GTP hydrolysis. Cell 1999;96(6):893-902.
118. Liu W, Duden R, Phair RD, Lippincott-Schwartz J. ArfGAP1 dynamics and its role in COPI coat assembly on Golgi membranes of living cells. J Cell Biol 2005;168(7):1053-63.
119. Eugster A, Frigerio G, Dale M, Duden R. COP I domains required for coatomer integrity, and novel interactions with ARF and ARF-GAP. Embo J 2000;19(15):3905-17.
120. Watson PJ, Frigerio G, Collins BM, Duden R, Owen DJ. Gamma-COP appendage domain - structure and function. Traffic 2004;5(2):79-88.
121. Yang JS, Lee SY, Gao M, Bourgoin S, Randazzo PA, Premont RT, Hsu VW. ARFGAP1 promotes the formation of COPI vesicles, suggesting function as a component of the coat. J Cell Biol 2002;159(1):69-78.
122. Eugster A, Frigerio G, Dale M, Duden R. The alpha- and beta'-COP WD40 domains mediate cargo-selective interactions with distinct di-lysine motifs. Mol Biol Cell 2004;15(3):1011-23.
123. Nilsson T, Rabouille C, Hui N, Watson R, Warren G. The role of the membrane-spanning domain and stalk region of N-acetylglucosaminyltransferase I in retention, kin recognition and structural maintenance of the Golgi apparatus in HeLa cells. J Cell Sci 1996;109 (Pt 7):1975-89.
124. Burke J, Pettitt JM, Schachter H, Sarkar M, Gleeson PA. The transmembrane and flanking sequences of beta 1,2-N-acetylglucosaminyltransferase I specify medial-Golgi localization. J Biol Chem 1992;267(34):24433-40.
125. Colley KJ, Lee EU, Paulson JC. The signal anchor and stem regions of the beta-galactoside alpha 2,6-sialyltransferase may each act to localize the enzyme to the Golgi apparatus. J Biol Chem 1992;267(11):7784-93.

126. Teasdale RD, D'Agostaro G, Gleeson PA. The signal for Golgi retention of bovine beta 1,4-galactosyltransferase is in the transmembrane domain. J Biol Chem 1992;267(18):13113.
127. Milland J, Russell SM, Dodson HC, McKenzie IF, Sandrin MS. The cytoplasmic tail of alpha 1,3-galactosyltransferase inhibits Golgi localization of the full-length enzyme. J Biol Chem 2002;277(12):10374-8.
128. Milland J, Taylor SG, Dodson HC, McKenzie IF, Sandrin MS. The cytoplasmic tail of alpha 1,2-fucosyltransferase contains a sequence for golgi localization. J Biol Chem 2001;276(15):12012-8.
129. Bretscher MS, Munro S. Cholesterol and the Golgi apparatus. Science 1993;261(5126):1280-1.
130. Masibay AS, Balaji PV, Boeggeman EE, Qasba PK. Mutational analysis of the Golgi retention signal of bovine beta-1,4-galactosyltransferase. J Biol Chem 1993;268(13):9908-16.
131. Munro S. A comparison of the transmembrane domains of Golgi and plasma membrane proteins. Biochem Soc Trans 1995;23(3):527-30.
132. Yuan Z, Teasdale RD. Prediction of Golgi Type II membrane proteins based on their transmembrane domains. Bioinformatics 2002;18(8):1109-15.
133. Nezil FA, Bloom M. Combined influence of cholesterol and synthetic amphiphillic peptides upon bilayer thickness in model membranes. Biophys J 1992;61(5):1176-83.
134. Mitra K, Ubarretxena-Belandia I, Taguchi T, Warren G, Engelman DM. Modulation of the bilayer thickness of exocytic pathway membranes by membrane proteins rather than cholesterol. Proc Natl Acad Sci U S A 2004;101(12):4083-8.
135. Dahdal RY, Colley KJ. Specific sequences in the signal anchor of the beta-galactoside alpha-2,6-sialyltransferase are not essential for Golgi localization. Membrane flanking sequences may specify Golgi retention. J Biol Chem 1993;268(35):26310-9.
136. Munro S. An investigation of the role of transmembrane domains in Golgi protein retention. Embo J 1995;14(19):4695-704.
137. Brugger B, Sandhoff R, Wegehingel S, Gorgas K, Malsam J, Helms JB, Lehmann WD, Nickel W, Wieland FT. Evidence for segregation of sphingomyelin and cholesterol during formation of COPI-coated vesicles. J Cell Biol 2000;151(3):507-18.
138. Graham TR, Krasnov VA. Sorting of yeast alpha 1,3 mannosyltransferase is mediated by a lumenal domain interaction, and a transmembrane domain signal that can confer clathrin-dependent Golgi localization to a secreted protein. Mol Biol Cell 1995;6(7):809-24.
139. Chen C, Ma J, Lazic A, Backovic M, Colley KJ. Formation of insoluble oligomers correlates with ST6Gal I stable localization in the golgi. J Biol Chem 2000;275(18):13819-26.
140. Ma J, Qian R, Rausa FM, 3rd, Colley KJ. Two naturally occurring alpha2,6-sialyltransferase forms with a single amino acid change in the catalytic domain differ in their catalytic activity and proteolytic processing. J Biol Chem 1997;272(1):672-9.
141. Nilsson T, Slusarewicz P, Hoe MH, Warren G. Kin recognition. A model for the retention of Golgi enzymes. FEBS Lett 1993;330(1):1-4.

142. Fleischer B, McIntyre JO, Kempner ES. Target sizes of galactosyltransferase, sialyltransferase, and uridine diphosphatase in Golgi apparatus of rat liver. Biochemistry 1993;32(8):2076-81.
143. Cole NB, Smith CL, Sciaky N, Terasaki M, Edidin M, Lippincott-Schwartz J. Diffusional mobility of Golgi proteins in membranes of living cells. Science 1996;273(5276):797-801.
144. Weiss M, Hashimoto H, Nilsson T. Anomalous protein diffusion in living cells as seen by fluorescence correlation spectroscopy. Biophys J 2003;84(6):4043-52.
145. Young WW, Jr. Organization of Golgi glycosyltransferases in membranes: complexity via complexes. J Membr Biol 2004;198(1):1-13.
146. de Graffenried CL, Bertozzi CR. The roles of enzyme localisation and complex formation in glycan assembly within the Golgi apparatus. Curr Opin Cell Biol 2004;16(4):356-63.
147. Giraudo CG, Maccioni HJ. Ganglioside glycosyltransferases organize in distinct multienzyme complexes in CHO-K1 cells. J Biol Chem 2003;278(41):40262-71.
148. Sasai K, Ikeda Y, Tsuda T, Ihara H, Korekane H, Shiota K, Taniguchi N. The critical role of the stem region as a functional domain responsible for the oligomerization and Golgi localization of N-acetylglucosaminyltransferase V. The involvement of a domain homophilic interaction. J Biol Chem 2001;276(1):759-65.
149. Einstein A. Über die von der molekulartheoretischen Theorie der Wärme geforderte Bewegung von in ruhenden Flüssigkeiten suspendierte Teilchen. Ann. Phys. (Leipzig) 1905;17:549–560.
150. Brown R. A brief account of microscopical observations made in the months of June, July, and August, 1827, on the particles contained in the pollen of plants; and on the general existence of active molecules in organic and inorganic bodies. Edinb. New Philos. J. 1828;5:358–371.
151. Berg HC. Random Walks in Biology. Princton: Princton University Press; 1983.
152. Murray JD. Mathematical Biology. Berlin: Springer; 1989.
153. Saffman PG, Delbruck M. Brownian motion in biological membranes. Proc Natl Acad Sci U S A 1975;72(8):3111-3.
154. Guigas G, Weiss M. Size-dependent diffusion of membrane inclusions. Biophys J 2006.
155. Peters R, Cherry RJ. Lateral and Rotational Diffusion of Bacteriorhodopsin in Lipid Bilayers: Experimental Test of the Saffman-Delbruck Equations. PNAS %R 10.1073/pnas.79.14.4317 1982;79(14):4317-4321.
156. Vaz WL, Criado M, Madeira VM, Schoellmann G, Jovin TM. Size dependence of the translational diffusion of large integral membrane proteins in liquid-crystalline phase lipid bilayers. A study using fluorescence recovery after photobleaching. Biochemistry 1982;21(22):5608-12.
157. Lee CC, Petersen NO. The Lateral Diffusion of Selectively Aggregated Peptides in Giant Unilamellar Vesicles. Biophys. J. 2003;84(3):1756-1764.
158. Gambin Y, Lopez-Esparza R, Reffay M, Sierecki E, Gov NS, Genest M, Hodges RS, Urbach W. Lateral mobility of proteins in liquid membranes revisited. PNAS 2006;103(7):2098-2102.

159. Saxton MJ. Anomalous subdiffusion in fluorescence photobleaching recovery: a Monte Carlo study. Biophys J 2001;81(4):2226-40.
160. Vaz WL. Diffusion and chemical reactions in phase-separated membranes. Biophys Chem 1994;50(1-2):139-45.
161. Saxton MJ. Anomalous diffusion due to obstacles: a Monte Carlo study. Biophys J 1994;66(2 Pt 1):394-401.
162. Cussler EL. Diffusion. Mass Transfer in Fluid Systems. Cambridge: Cambridge University Press; 1997.
163. Saxton MJ. Anomalous diffusion due to binding: a Monte Carlo study. Biophys J 1996;70(3):1250-62.
164. Metzler R, Klafter J. The random walk's guide to anomalous diffusion: a fractional dynamics approach. Phys. Rep. 2000;339(1):1-77.
165. Nagle JF. Long tail kinetics in biophysics? Biophys J 1992;63(2):366-70.
166. Doi M, Edwards SF. The Theory of Polymer Dynamics. Oxford: Clarendon Press; 1986.
167. Briels WJ. Theory of Polymer Dynamics. Enschede: University of Twente in Enschede
http://cb.tnw.utwente.nl/PolymeerDictaat/polymerdynamics.html; 1998.
168. Smith PR, Morrison IE, Wilson KM, Fernandez N, Cherry RJ. Anomalous diffusion of major histocompatibility complex class I molecules on HeLa cells determined by single particle tracking. Biophys J 1999;76(6):3331-44.
169. Ghosh RN, Webb WW. Automated detection and tracking of individual and clustered cell surface low density lipoprotein receptor molecules. Biophys. J. 1994;66(5):1301-1318.
170. Simson R, Yang B, Moore SE, Doherty P, Walsh FS, Jacobson KA. Structural mosaicism on the submicron scale in the plasma membrane. Biophys. J. 1998;74(1):297-308.
171. Schutz GJ, Schindler H, Schmidt T. Single-molecule microscopy on model membranes reveals anomalous diffusion. Biophys J 1997;73(2):1073-80.
172. Deverall MA, Gindl E, Sinner EK, Besir H, Ruehe J, Saxton MJ, Naumann CA. Membrane lateral mobility obstructed by polymer-tethered lipids studied at the single molecule level. Biophys J 2005;88(3):1875-86.
173. Tolic-Norrelykke IM, Munteanu EL, Thon G, Oddershede L, Berg-Sorensen K. Anomalous diffusion in living yeast cells. Phys Rev Lett 2004;93(7):078102.
174. Golding I, Cox EC. Physical nature of bacterial cytoplasm. Phys Rev Lett 2006;96(9):098102.
175. Wachsmuth M, Waldeck W, Langowski J. Anomalous diffusion of fluorescent probes inside living cell nuclei investigated by spatially-resolved fluorescence correlation spectroscopy. J Mol Biol 2000;298(4):677-89.
176. Schwille P, Haupts U, Maiti S, Webb WW. Molecular dynamics in living cells observed by fluorescence correlation spectroscopy with one- and two-photon excitation. Biophys J 1999;77(4):2251-65.
177. Schwille P, Korlach J, Webb WW. Fluorescence correlation spectroscopy with single-molecule sensitivity on cell and model membranes. Cytometry 1999;36(3):176-82.
178. Lindblom G, Oradd G, Filippov A. Lipid lateral diffusion in bilayers with phosphatidylcholine, sphingomyelin and cholesterol An NMR study of

dynamics and lateral phase separation. Chem Phys Lipids 2006;141(1-2):179-84.
179. Filippov A, Oradd G, Lindblom G. Sphingomyelin structure influences the lateral diffusion and raft formation in lipid bilayers. Biophys J 2006;90(6):2086-92.
180. Edidin M, Zagyansky Y, Lardner TJ. Measurement of membrane protein lateral diffusion in single cells. Science 1976;191(4226):466-8.
181. Zagyansky Y, Edidin M. Lateral diffusion of concanavalin A receptors in the plasma membrane of mouse fibroblasts. Biochim Biophys Acta 1976;433(1):209-14.
182. Brown EB, Wu ES, Zipfel W, Webb WW. Measurement of molecular diffusion in solution by multiphoton fluorescence photobleaching recovery. Biophys J 1999;77(5):2837-49.
183. Soumpasis DM. Theoretical analysis of fluorescence photobleaching recovery experiments. Biophys J 1983;41(1):95-7.
184. Weiss M. Challenges and artifacts in quantitative photobleaching experiments. Traffic 2004;5(9):662-71.
185. Magde D. Thermodynamic Fluctuations in a Reacting System—Measurement by Fluorescence Correlation Spectroscopy. Physical Review Letters 1972;29(11):705.
186. Elson EL, Schlessinger J, Koppel DE, Axelrod D, Webb WW. Measurement of lateral transport on cell surfaces. Prog Clin Biol Res 1976;9:137-47.
187. Magde D, Elson EL, Webb WW. Fluorescence correlation spectroscopy. II. An experimental realization. Biopolymers 1974;13(1):29-61.
188. Ehrenberg M, Rigler R. Fluorescence correlation spectroscopy applied to rotational diffusion of macromolecules. Q Rev Biophys 1976;9(1):69-81.
189. Rigler R, Mets U, Widengren J, Kask P. Fluorescence correlation spectroscopy with high count rates and low background, analysis of translational diffusion. Eur Biophys J 1993;22(169-175).
190. Rigler R, Widengren J. Ultrasensitive detection of single molecules by fluorescence correlation spectroscopy. Bioscience 1990;3:180-183.
191. Schwille P, Haustein E. Fluorescence Correlation Spectroscopy. Resources in biophysics: Biophysical Society http://www.biophysics.org/education/resources.htm.
192. Bacia K, Schwille P. A dynamic view of cellular processes by in vivo fluorescence auto- and cross-correlation spectroscopy. Methods 2003;29(1):74-85.
193. Hall D, Minton AP. Macromolecular crowding: qualitative and semiquantitative successes, quantitative challenges. Biochim Biophys Acta 2003;1649(2):127-39.
194. Zimmerman SB, Minton AP. Macromolecular crowding: biochemical, biophysical, and physiological consequences. Annu Rev Biophys Biomol Struct 1993;22:27-65.
195. Chebotareva NA, Kurganov BI, Livanova NB. Biochemical effects of molecular crowding. Biochemistry (Mosc) 2004;69(11):1239-51.
196. Ross PD, Minton AP. Hard quasispherical model for the viscosity of hemoglobin solutions. Biochem Biophys Res Commun 1977;76(4):971-6.

197. Ross PD, Minton AP. Analysis of non-ideal behavior in concentrated hemoglobin solutions. J Mol Biol 1977;112(3):437-52.
198. Zimmerman SB, Trach SO. Estimation of macromolecule concentrations and excluded volume effects for the cytoplasm of Escherichia coli. J Mol Biol 1991;222(3):599-620.
199. Ellis RJ. Macromolecular crowding: obvious but underappreciated. Trends Biochem Sci 2001;26(10):597-604.
200. Jarvis TC, Ring DM, Daube SS, von Hippel PH. "Macromolecular crowding": thermodynamic consequences for protein- protein interactions within the T4 DNA replication complex. J. Biol. Chem. 1990;265(25):15160-15167.
201. Snoussi K, Halle B. Protein self-association induced by macromolecular crowding: a quantitative analysis by magnetic relaxation dispersion. Biophys J 2005;88(4):2855-66.
202. Drenckhahn D, Pollard TD. Elongation of actin filaments is a diffusion-limited reaction at the barbed end and is accelerated by inert macromolecules. J. Biol. Chem. 1986;261(27):12754-12758.
203. Zimmerman SB, Trach SO. Effects of macromolecular crowding on the association of E. coli ribosomal particles. Nucleic Acids Res 1988;16(14A):6309-26.
204. Zimmerman SB, Trach SO. Macromolecular crowding extends the range of conditions under which DNA polymerase is functional. Biochim Biophys Acta 1988;949(3):297-304.
205. Rivas G, Fernandez JA, Minton AP. Direct observation of the enhancement of noncooperative protein self-assembly by macromolecular crowding: Indefinite linear self-association of bacterial cell division protein FtsZ. PNAS %R 10.1073/pnas.051634398 2001;98(6):3150-3155.
206. Luby-Phelps K, Castle PE, Taylor DL, Lanni F. Hindered diffusion of inert tracer particles in the cytoplasm of mouse 3T3 cells. Proc Natl Acad Sci U S A 1987;84(14):4910-3.
207. Popov S, Poo MM. Diffusional transport of macromolecules in developing nerve processes. J Neurosci 1992;12(1):77-85.
208. Arrio-Dupont M, Cribier S, Foucault G, Devaux PF, d'Albis A. Diffusion of fluorescently labeled macromolecules in cultured muscle cells. Biophys J 1996;70(5):2327-32.
209. Seksek O, Biwersi J, Verkman AS. Translational diffusion of macromolecule-sized solutes in cytoplasm and nucleus. J Cell Biol 1997;138(1):131-42.
210. Luby-Phelps K. Cytoarchitecture and physical properties of cytoplasm: volume, viscosity, diffusion, intracellular surface area. Int Rev Cytol 2000;192:189-221.
211. Verkman AS. Solute and macromolecule diffusion in cellular aqueous compartments. Trends Biochem Sci 2002;27(1):27-33.
212. Saxton MJ. Chemically limited reactions on a percolation cluster. Journal of Chemical Physics 2002;116(1):203-208.
213. Bujan-Nunez MC, Miguel-Fernandez A, Lopez-Quintela MA. Diffusion-influenced controlled reaction in an inhomogeneous medium: Small concentration of reagents. Journal of Chemical Physics 2000;112(19):8495-8501.

214. Berry H. Monte carlo simulations of enzyme reactions in two dimensions: fractal kinetics and spatial segregation. Biophys J 2002;83(4):1891-901.
215. Weiss M. Stabilizing Turing patterns with subdiffusion in systems with low particle numbers. Physical Review E (Statistical, Nonlinear, and Soft Matter Physics) 2003;68(3):036213-5.
216. Turing AM. The Chemical Basis of Morphogenesis. Philosophical Transactions of the Royal Society of London. Series B, Biological Sciences 1952;237(641).
217. Hunding A, Ebersbach G, Gerdes K. A Mechanism for ParB-dependent Waves of ParA, a Protein Related to DNA Segregation during Cell Division in Prokaryotes. Journal of Molecular Biology 2003;329(1):35-43.
218. Nedelec FJ, Surrey T, Maggs AC, Leibler S. Self-organization of microtubules and motors. Nature 1997;389(6648):305-8.
219. Falcke M. Pattern Selection by Gene Expression in Dictyostelium Discoideum. Physical Review Letters 1998;80(17):3875.
220. Sekimura T, Madzvamuse A, Wathen AJ, Maini PK. A model for colour pattern formation in the butterfly wing of Papilio dardanus. Proc Biol Sci 2000;267(1446):851-9.
221. Asai R, Taguchi E, Kume Y, Saito M, Kondo S. Zebrafish Leopard gene as a component of the putative reaction-diffusion system. Mech. Dev. 1999;89(1-2):87-92.
222. Howard M, Kruse K. Cellular organization by self-organization: mechanisms and models for Min protein dynamics. J. Cell Biol. 2005;168(4):533-536.
223. Howard M, Rutenberg AD, de Vet S. Dynamic Compartmentalization of Bacteria: Accurate Division in E. Coli. Physical Review Letters 2001;87(27):278102.
224. Huang KC, Meir Y, Wingreen NS. Dynamic structures in Escherichia coli: Spontaneous formation of MinE rings and MinD polar zones. PNAS 2003;100(22):12724-12728.
225. Kruse K. A Dynamic Model for Determining the Middle of Escherichia coli. Biophys. J. 2002;82(2):618-627.
226. Meinhardt H, de Boer PAJ. Pattern formation in Escherichia coli: A model for the pole-to-pole oscillations of Min proteins and the localization of the division site. PNAS 2001;98(25):14202-14207.
227. von Hippel PH, Berg OG. Facilitated target location in biological systems. J. Biol. Chem. 1989;264(2):675-678.
228. Richter PH, Eigen M. Diffusion controlled reaction rates in spheroidal geometry. Application to repressor--operator association and membrane bound enzymes. Biophys Chem 1974;2(3):255-63.
229. Riggs AD, Bourgeois S, Cohn M. The lac repressor-operator interaction. 3. Kinetic studies. J Mol Biol 1970;53(3):401-17.
230. Halford SE, Marko JF. How do site-specific DNA-binding proteins find their targets? Nucleic Acids Res 2004;32(10):3040-52.
231. Banks DS, Fradin C. Anomalous diffusion of proteins due to molecular crowding. Biophys J 2005;89(5):2960-71.
232. Fiedler K, Veit M, Stamnes MA, Rothman JE. Bimodal interaction of coatomer with the p24 family of putative cargo receptors. Science 1996;273(5280):1396-9.

233. Dominguez M, Dejgaard K, Fullekrug J, Dahan S, Fazel A, Paccaud JP, Thomas DY, Bergeron JJ, Nilsson T. gp25L/emp24/p24 protein family members of the cis-Golgi network bind both COP I and II coatomer. J Cell Biol 1998;140(4):751-65.
234. Sohn K, Orci L, Ravazzola M, Amherdt M, Bremser M, Lottspeich F, Fiedler K, Helms JB, Wieland FT. A major transmembrane protein of Golgi-derived COPI-coated vesicles involved in coatomer binding. J Cell Biol 1996;135(5):1239-48.

Paper I

EMBO reports

scientific report

Spatiotemporal dynamics of the COPI vesicle machinery

Markus Elsner[1], Hitoshi Hashimoto[1], Jeremy C. Simpson[1], Dan Cassel[2], Tommy Nilsson[1] & Matthias Weiss[1,3+]

[1]Cell Biology and Cell Biophysics Programme, EMBL, Heidelberg, Germany, [2]Department of Biology, Technion, Haifa, Israel, and [3]Physics Department, MEMPHYS Center for Biomembrane Physics, University of Southern Denmark, Odense, Denmark

Assembly of the coat protein I (COPI) vesicle coat is controlled by the small GTPase ADP ribosylation factor 1 (ARF1) and its GTPase-activating protein, ARFGAP1. Here, we investigate the diffusional behaviours of coatomer, the main component of the coat, and also those of ARF1 and ARFGAP1. Using fluorescence-correlation spectroscopy, we found that most ARF1 and ARFGAP1 molecules are highly mobile in the cytosol (diffusion constant $D \approx 15\ \mu m^2\ s^{-1}$), whereas coatomer diffuses 5–10 times more slowly than expected ($D \approx 1\ \mu m^2\ s^{-1}$). This slow diffusion causes diffusion-limited binding kinetics to Golgi membranes, which, in FRAP (fluorescence recovery after photobleaching) experiments, translates into a twofold slower binding rate. The addition of aluminium fluoride locks coatomer onto Golgi membranes and also decreases the binding kinetics of both ARF1 and ARFGAP1, suggesting that these proteins function in concert to mediate sorting and vesicle formation.

EMBO reports **4**, 1000–1005 (2003)
doi:10.1038/sj.embor.embor942

INTRODUCTION

Newly synthesized proteins move through the secretory pathway in membrane-bound structures that originate from the endoplasmic reticulum (ER). Forward movement is offset by the recycling of resident proteins. Two recycling mechanisms exist in mammalian cells, one that is mediated by coat protein I (COPI) vesicles, and another that is independent of known coat proteins (for a review, see Storrie & Nilsson, 2002). Whereas COPI-independent recycling is poorly understood, COPI-dependent recycling has been characterized extensively. After nucleotide exchange (GDP to GTP), the small GTPase ADP ribosylation factor 1 (ARF1) becomes firmly attached to Golgi membranes, whereas on GTP hydrolysis ARF1 is released back into the cytoplasm, an event that requires an activating protein, ARF GTPase-activating protein 1 (ARFGAP1). While it is present on membranes, ARF1 is able to recruit coatomer, the main coat component of COPI. Coatomer, as well as ARF1 and ARFGAP1, can also bind individually to cytosolic domains of resident proteins. The formation of vesicles *in vitro* requires only ARF1 and coatomer (Ostermann *et al.*, 1993; Spang *et al.*, 1998) when a non-hydrolysable GTP derivative, GTPγS, is used. However, the incorporation of cargo proteins requires GTP hydrolysis by ARF1 (Lanoix *et al.*, 1999, 2001; Malsam *et al.*, 1999; Pepperkok *et al.*, 2000). How GTP hydrolysis by ARF1, which is known to release coatomer, promotes sorting into COPI buds and vesicles can be explained in terms of a kinetic proofreading mechanism (Weiss & Nilsson, 2003).

Despite many advances in the understanding of the biogenesis of COPI vesicles, the binding and assembly kinetics of the COPI-vesicle machinery are poorly characterized. Recent studies of the binding kinetics of ARF1 and coatomer *in vivo*, using fluorescence recovery after photobleaching (FRAP; Presley *et al.*, 2002), unexpectedly revealed that coatomer shows a twofold slower recovery than ARF1, suggesting that release of coatomer from membranes occurs by mechanisms that do not involve ARF1. This interpretation was supported by the observation that on addition of aluminium fluoride, coatomer was locked onto the membrane, whereas ARF1 detached with unperturbed kinetics.

Here, we have determined the cytosolic mobilities of GFP-tagged COPI components. We find that coatomer is nearly an order of magnitude less mobile in the cytoplasm than would be theoretically expected, whereas ARF1 and ARFGAP1 are highly mobile. However, ARF1 and ARFGAP1 are also found in slow-moving fractions that are likely to represent the formation of complexes with other factors. We also show that the binding kinetics of ARFGAP1 to Golgi membranes are similar to those of ARF1 and confirm the apparent twofold slower binding kinetics of coatomer (Presley *et al.*, 2002). On the basis of computer

[1]Cell Biology and Cell Biophysics Programme, EMBL, Meyerhofstrasse 1, D-69117 Heidelberg, Germany
[2]Department of Biology, Technion, Haifa 32000, Israel
[3]Physics Department, MEMPHYS Center for Biomembrane Physics, University of Southern Denmark, Campusvej 55, DK-5230 Odense M, Denmark
+Corresponding author. Tel: +45 6550 3686; Fax: +45 6615 8760; E-mail: mweiss@memphys.sdu.dk

Received 14 April 2003; revised 19 August 2003; accepted 19 August 2003
Published online 19 September 2003

simulations, however, we suggest that this is due to diffusion-limited kinetics of coatomer.

RESULTS AND DISCUSSION

FRAP can be used to determine the diffusional mobilities of fluorescently labelled molecules: on bleaching an area of interest (typically several square micrometres), the diffusion constant of the molecule can be deduced from the recovery of fluorescence. Alternatively, FRAP can be used to monitor the dynamic exchange of peripheral membrane proteins. The fluorescence recovery rate in this case is a combination of attachment and detachment rates of the peripheral protein. This only holds true, however, if the time needed for the molecules to diffuse through the cytoplasm towards the target is short. This can be tested by assessing the diffusion coefficient with FRAP, in which restricting the bleaching to the focal spot gives high temporal and lateral resolution (for a review, see Elson & Qian, 1989). Alternatively, fluorescence-correlation spectroscopy (FCS) can be used to determine the diffusion constant by monitoring the Brownian movement of individual proteins without bleaching the cell. FCS monitors fluctuations of the fluorescence that arise due to the diffusion of single green fluorescent protein (GFP)-tagged molecules in a confocal volume of ~1 μm^3. Calculating the autocorrelation function $C(\tau)$ of the recorded fluorescence time series $F(t)$, one can determine from the characteristic decay time of $C(\tau)$, the diffusion coefficient D of the protein of interest. FCS provides information more readily about the state of the molecules; that is, if a portion associates with other molecules, this will give both free/fast and bound/slow populations. In this study, we combine FCS and FRAP to analyse the main COPI components: coatomer, ARF1 and ARFGAP1.

Full-length complementary DNAs encoding GFP and GFP-tagged ARF1, ARFGAP1 and ε-COP were expressed in HeLa and Chinese hamster ovary (CHO) cells and monitored by FCS (see Methods). For free GFP in the cytoplasm, the data were best described by a single diffusing component with a diffusion coefficient of $D \approx 25\ \mu m^2\ s^{-1}$, indicating an approximately threefold to fourfold higher viscosity of cytoplasm as compared with buffer (Fig. 1A). For ARF1 (Fig. 1B), we saw two components that contribute to $C(\tau)$: a fast and a slow population, with diffusion coefficients $D \approx 15\ \mu m^2\ s^{-1}$ and $D \approx 0.5\ \mu m^2\ s^{-1}$, respectively, being present in average proportions of 85% and 15%, respectively. The faster component is consistent with the expectations for monomeric ARF1–GFP (see Methods), whereas the slower fraction is probably due to complex formation with other proteins. For ARFGAP1 (Fig. 1C), we saw similar curves: that is, a fast population (70%; $D \approx 13\ \mu m^2\ s^{-1}$; consistent with the theoretical expected value), and a minority of slow molecules (30%; $D \approx 0.5\ \mu m^2\ s^{-1}$). The slow diffusion of the minor ARFGAP1 fraction suggested complex formation of ARFGAP1 with a larger protein complex, such as coatomer. To test this, we increased the level of cytosolic coatomer by applying brefeldin A (BFA), which causes the release of coatomer from Golgi membranes (Helms & Rothman, 1992). In support of our hypothesis, we found that the average fraction of the slow component of ARFGAP1 increased from 30% to about 50% (Fig.1C), whereas $C(\tau)$ for ARF1 was not affected (data not shown).

We then determined the mobility of coatomer using GFP-tagged ε-COP stably expressed in HeLa (Fig. 1D) and CHO (Fig. 1E) cells. As expected, we saw a fast component (HeLa cells, 74%; $D \approx 16\ \mu m^2\ s^{-1}$; CHO cells, 48%; $D \approx 16\ \mu m^2\ s^{-1}$), which was consistent with the theoretical expectations for free, monomeric ε-COP–GFP. The slower component (HeLa cells, 26%; $D \approx 0.5\ \mu m^2\ s^{-1}$; CHO cells, 52%; $D \approx 0.5\ \mu m^2\ s^{-1}$) most probably represents ε-COP–GFP incorporated into the coatomer complex, but its mobility is much slower than expected from the size of coatomer. Consistent with this, the addition of BFA to increase the cytosolic pool of coatomer increased the slow fraction on average from 52% to 70% in CHO cells (Fig. 1E). To confirm that the slower component was indeed coatomer, we removed β-COP by RNA interference (RNAi). This coatomer component is required for the assembly of the coatomer complex (Eugster *et al.*, 2000) and, as expected, its removal resulted in a marked reduction of the slow component (Fig. 1F). We therefore conclude that the slower component of ε-COP–GFP corresponds to coatomer. As the slower fraction of ARFGAP1 has the same diffusion constant as the slower component of coatomer and its levels are increased on BFA treatment, we suggest that ARFGAP1 and coatomer might exist as a complex in the cytosol. Further experiments to test coatomer association with ARFGAP1 and other proteins are underway.

A possible explanation for the unexpectedly slow diffusion of coatomer and a portion of ARFGAP1 is that coatomer is involved in coat formation on peripheral ER exit sites (Stephens *et al.*, 2000). To test this, we microinjected cells with a plasmid encoding a GDP-restricted mutant of Sar1 (0.1 mg ml^{-1}; incubation for 6 h), which leads to the disassembly of ER exit sites (Ward *et al.*, 2001). At most, the mobility of coatomer increased about twofold as determined by FCS (data not shown), which is clearly insufficient to explain the slow diffusion of coatomer. A more likely explanation is provided by the fact that the large coatomer complex is predicted to encounter steric hindrance due to membranes and cytoskeletal structures while diffusing through the cytoplasm. For large complexes, obstructed diffusion could easily account for a slow-down of diffusion by a factor of 5–10 (Saxton, 1993).

To complement the FCS measurements, we also performed FRAP using ε-COP–GFP. We bleached a circular spot (area, 47 μm^2) through the entire thickness of the cell and fitted the resulting recovery curves with the appropriate formula for a single diffusing species (Saxton, 2001). Fitting with a two-component expression was not successful, as the time resolution of the FRAP measurement (154 ms) was insufficient to resolve the recovery of free ε-COP–GFP (recovery time $T \approx 240$ ms, assuming $D \approx 16\ \mu m^2\ s^{-1}$). The diffusion coefficient determined in this way ($D_{COPI} \approx 1.7\ \mu m^2\ s^{-1}$) was higher than that obtained by FCS, which is in part explained by the contribution of the fast but unresolved pool of free ε-COP–GFP. However, the diffusion constant determined by FRAP was still significantly slower (approximately fivefold) than theoretically expected.

We next used FRAP to investigate the binding kinetics of ARF1, ARFGAP1 and coatomer to Golgi membranes. We bleached the entire pool of the GFP-tagged proteins in the Golgi region, then monitored and fitted the recovery. Whereas ARF1 (Fig. 2A) and ARFGAP1 (Fig. 2C) showed similar recovery curves with a characteristic time constant of $T \approx 10$ s, coatomer (Fig. 2E) seemed to recover with a twofold slower rate, in agreement with a previous report on ARF1 and coatomer (Presley *et al.*, 2002).

Applying aluminium fluoride to the cells locked coatomer onto Golgi membranes (Fig. 2F), whereas ARFGAP1 showed a 30% increase in T (Fig. 2D). For ARF1, the recovery time changed even more significantly to $T \approx 20$ s (Fig. 2B), whereas the addition of fluoride did not have any effect (data not shown). In contrast to previous reports (Presley *et al.*, 2002), this provides *in vivo* evidence that the entire COPI vesicle machinery is affected by aluminium fluoride.

Because coatomer diffuses significantly more slowly than the main fraction of ARF1 and ARFGAP1, we next investigated to what extent this could affect binding kinetics determined by FRAP. A simple model was constructed for analysing the FRAP experiment. For simplicity, we assumed the cell to have a square shape and then overlaid a grid in the x–y direction with a lattice of 11 × 11 sites, each having a volume of 3 × 3 × 3 μm^3 (Fig.3A). The area of this 'cell' is therefore 1,089 μm^2, which is comparable to the area of CHO and HeLa cells. The Golgi apparatus was modelled by 12 adjacent lattice points in the middle of the cell (Fig. 3A, grey areas), consistent with fluorescence microscopy pictures of CHO and HeLa cells in which Golgi sites represent about 10% of the cell area. Neighbouring cytosolic sites were coupled to support a diffusive flux of proteins, whereas the attachment and detachment of proteins to and from the Golgi sites could only occur from neighbouring cytosolic lattice points

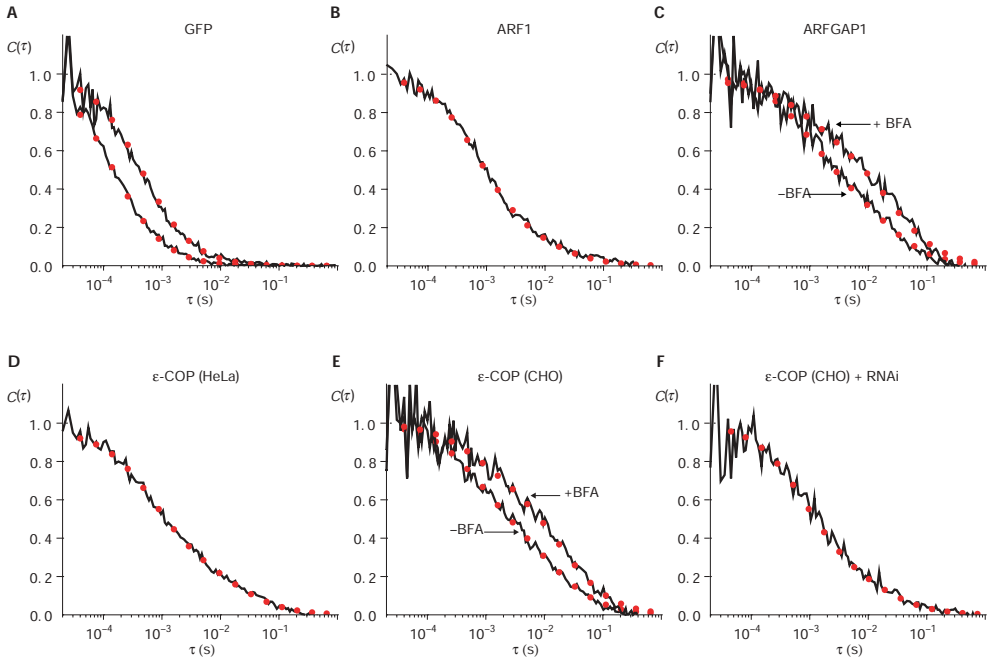

Fig. 1 | Cytoplasmic mobility of COPI proteins. Representative fluorescence-correlation spectroscopy (FCS) curves for (**A**) green fluorescent protein (GFP) in buffer and cytoplasm, (**B**) ADP ribosylation factor 1 (ARF1), (**C**) ARF GTPase-activating protein 1 (ARFGAP1) and (**D**) ε-COP (ε-coat-protein) in HeLa cells (black lines), with best fits according to equation (1) (red symbols; see Methods). The autocorrelation function $C(\tau)$ shown for ARF1 involves a fast (87%; $D \approx 15\ \mu m^2\ s^{-1}$; where D is the diffusion coefficient) and a slow (13%; $D \approx 0.5\ \mu m^2\ s^{-1}$) population, which is probably because of interactions with nucleotide-exchange factors. Similarly, ARFGAP1 shows a large, fast pool (40%; $D \approx 13\ \mu m^2\ s^{-1}$) and a minority of slow molecules (60%; $D \approx 0.5\ \mu m^2\ s^{-1}$), which increased on addition of brefeldin A (BFA). The FCS curve of ε-COP comprises a fast component (73%; $D \approx 16\ \mu m^2\ s^{-1}$), due to monomeric ε -COP, and a slow one (27%; $D \approx 0.5\ \mu m^2\ s^{-1}$), due to ε -COP, which is incorporated into coatomer. (**E**) In untreated Chinese hamster ovary (CHO) cells, the FCS curve also showed two components (left curve, fast, 45%; $D \approx 16\ \mu m^2\ s^{-1}$; slow, 55%; $D \approx 0.5\ \mu m^2\ s^{-1}$), and applying BFA to release coatomer from Golgi membranes increased the slow component (to 68%). (**F**) Knocking out the β-COP subunit of coatomer reduced the slow component to less than 20%. This confirms that the slow component is the coatomer complex. RNAi, RNA intereference.

with rates R and γ, respectively. To account for the height of the cell, we coupled the corresponding sites of a second, identically shaped lattice to the first one to support diffusional flux. Our cell is therefore a box of $11 \times 11 \times 2$ sites. As the Golgi apparatus typically does not fill the entire thickness of the cell, that is, cytosol is present above and below it, we did not specify Golgi sites on the second lattice. The Golgi region therefore consists of 12 Golgi sites and 12 cytosolic sites below them. To be consistent with the FRAP experiments described above, we used $\gamma = 0.05\ s^{-1}$ in the simulations and fixed the ratio $R = 3\gamma$, so that at steady state the Golgi pool of the protein is threefold larger than the cytosolic pool in a corresponding area.

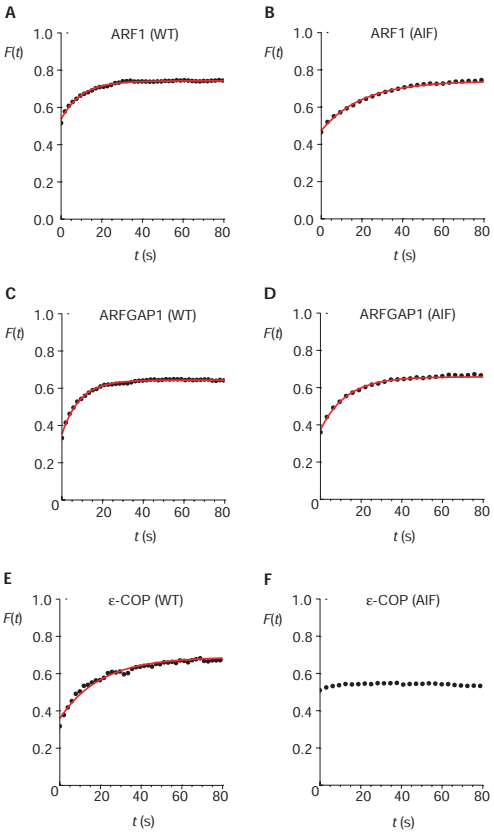

Fig. 2 | Binding kinetics of COPI proteins. Recovery, after bleaching the Golgi pool, of (**A**,**B**) ADP ribosylation factor 1 (ARF1) with and without aluminium fluoride, (**C**,**D**) ARF GTPase-activating protein 1 (ARFGAP1) with and without aluminium fluoride, and (**E**,**F**) ε-COP (ε-coat-protein) with and without aluminium fluoride (black symbols) with best fits (red lines). Whereas in untreated cells the typical recovery times T for ARF1 and ARFGAP1 were quite similar (**A**, $T_{ARF1} \approx 10$ s; **C**, $T_{ARFGAP1} \approx 9$ s), COPI showed a markedly slower recovery (**E**, $T_{COPI} \approx 20$ s). Applying aluminium fluoride approximately doubled the recovery time for ARF1 (**B**, $T \approx 20$ s), whereas ARFGAP1 showed only a 30% slower recovery (**D**, $T \approx 13$ s), and coatomer was locked onto the membrane (**F**). WT, wild type.

Using this model, we investigated the following three situations: first, an instantaneous bleaching of only the Golgi sites (Fig. 3B); second, an instantaneous bleaching of the Golgi region (Fig. 3C); and third, bleaching the Golgi region at $\omega = 500\ s^{-1}$ for 4 s (Fig. 3D), which was the typical bleaching time used in our FRAP experiments. Qualitatively, the three situations all resulted in similar recovery curves: the recovery was fastest for $D = 15\ \mu m^2\ s^{-1}$, with a typical recovery time $T \approx 10$ s, consistent with the experimental observations (Fig. 2A,B). These results were not altered significantly when using $D = 10\ \mu m^2\ s^{-1}$. For $D < 2\ \mu m^2\ s^{-1}$ however, the recovery was significantly slower, an effect which became more pronounced as D decreased. As the rates R and γ were the same in all simulations, this could only occur due to a diffusion-limited recovery. Neither the incorporation of a cytosolic contribution (Fig. 3C) nor the more realistic situation of bleaching for a finite time (Fig. 3D) qualitatively altered this result. Moreover, fitting the curves for $D = 15\ \mu m^2\ s^{-1}$ and $D = 1.5\ \mu m^2\ s^{-1}$ with single exponential kinetics with typical times T_1 and T_2 gave a ratio of $T_2/T_1 \approx 1.9$–2.1 in all three cases, although the rates R and γ had not been altered. These results show how a diffusion-limited recovery curve can result in apparently slower binding kinetics. One might have anticipated that ARFGAP1, if complexed to coatomer, should also show a diffusion-limited recovery. However, the experimental recovery curves for ARFGAP1 only provided some variation in the recovery times from cell to cell ($7\ s < T < 15$ s). This is most readily explained by the excess of ARFGAP1 when expressed as a GFP fusion protein compared with the levels of endogenous coatomer. Unbound ARFGAP1 diffusing more rapidly would mask the more slowly diffusing coatomer–ARFGAP1 complex. Each of the COPI components can also bind to Golgi membranes by themselves, explaining to some extent their fast recovery rates. There are also coatomer-independent processes on Golgi membranes that require the action of ARF1. For example, ARF1 regulates phospholipase D, which catalyses the hydrolysis of phosphatidylcholine (Williger *et al.*, 1999) and recruits PtdIns-4-OH-kinase-β to Golgi membranes (Godi *et al.*, 1999).

In summary, we have presented evidence that ARF1, ARFGAP1 and coatomer have approximately the same kinetics of binding to Golgi membranes when taking into account the observed diffusion-limited behaviour of coatomer. Previously, the apparent discrepancy between ARF1 and coatomer kinetics seen in FRAP experiments was taken as evidence that GTP hydrolysis by ARF1 is not responsible for coatomer dissociation (Presley *et al.*, 2002). Our results do not support this conclusion, and instead suggest that the coat components bind and dissociate in concert. In addition, our data suggest that ARFGAP1 is recruited to membranes alongside ARF1 and coatomer, and is thus likely to have a key function in the regulation of coat dynamics and sorting, for example through a kinetic proofreading scheme (Weiss & Nilsson, 2003).

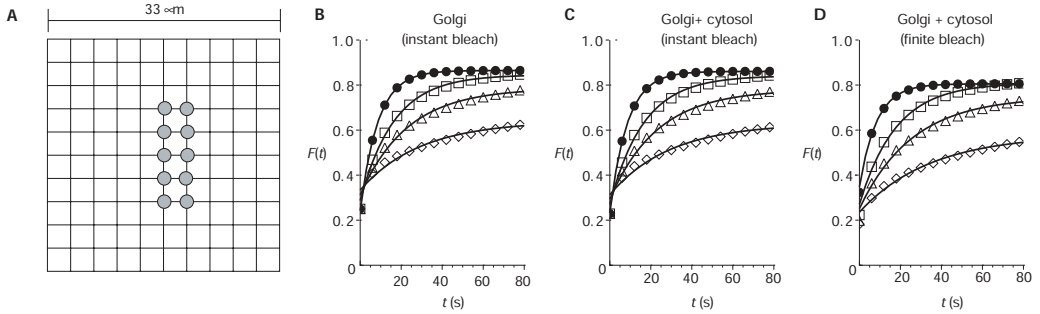

Fig. 3 | Simulation of diffusion-limited reaction kinetics. (**A**) Simulation of fluorescence recovery after photobleaching (FRAP) was performed on a model cell consisting of a square lattice of $11 \times 11 \times 2$ sites with 12 Golgi sites embedded in the first layer (marked in grey; see main text for details). (**B**–**D**) Resulting recovery curves for various diffusion coefficients (filled circles, $D = 15\ \mu m^2\ s^{-1}$; open squares, $D = 1.5\ \mu m^2\ s^{-1}$; open triangles, $D = 0.5\ \mu m^2\ s^{-1}$; open diamonds, $D = 0.1\ \mu m^2\ s^{-1}$), with best fits according to single-exponential kinetics (lines). Bleaching was performed instantaneously on (**B**) Golgi sites only, (**C**) the Golgi region and (**D**) on the Golgi region at a rate of $500\ s^{-1}$ for 4 s. The recovery curves depend strongly on the diffusion coefficient D and the typical recovery time increases about twofold in all cases when comparing $D = 15\ \mu m^2\ s^{-1}$ with $D = 1.5\ \mu m^2\ s^{-1}$. For lower values of D, this effect becomes even more marked. t, time.

METHODS

Cell culture and microscopy. Monolayer HeLa or CHO cells were cultured in DMEM and RPMI, respectively, both supplemented with 10% fetal calf serum, 100 units ml^{-1} penicillin, 100 mg ml^{-1} streptomycin and 10 mM glutamine (Gibco). The ARF1–GFP and ARFGAP1–GFP plasmids will be described elsewhere. The ε-COP–GFP cDNA fragment (a gift from R. Pepperkok) was inserted into pSG-puro and stably expressed in HeLa cells. The ε-COP–GFP CHO cell line was a gift from J. Presley. The concentrations of the chemicals used and the plasmids injected were: ARF1, 25 μg ml^{-1}; BFA, 5 μg ml^{-1}; aluminium fluoride, 30 mM NaF and 50 μM $AlCl_3$.

Oligonucleotides used for RNAi were derived from a cDNA that encodes human β-COP (GenBank accession number NM_016451). The most inhibitory RNA was against nucleotides 161–181 downstream from the ATG (target sequence: 5′-AACU UCCUGGACUUCUGAUGA-3′). Complementary oligonucleotides (5′-CUUCCUGGACUUCUGAUGAdTdT-3′) and (5′-UCAUCA GAAGUCCAGGAAGdTdT-3′) were synthesized, annealed and purified (Dharmacon). Lyophilized oligonucleotide duplexes were resuspended in water at 20 μM.

FCS measurements were carried out with a ConfoCor2 (Carl Zeiss) using an Apochromat 40×/1.2W objective, a 488-nm laser, a 505–550-nm bandpass and a pinhole width of 1 Airy unit. In all cases, 20 fluorescence time series ($F(t)$) of 10 s were recorded (time resolution, 50 ns), correlated according to Wohland *et al.* (2001) and superimposed for fitting. In all cases, multiple cells and different locations (outside the nucleus and the Golgi) were used for FCS. From cell to cell, results were consistent. Reported diffusion coefficients and slow:fast ratios are averages, and the figures shown are representative examples of single cells.

All FRAP experiments were performed with an open pinhole, that is the marked region of interest was bleached throughout the entire thickness of the cell.

Data evaluation and simulation. FCS curves were fitted with a Levenberg–Marquart algorithm (Press *et al.*, 1993) using the expression for three-dimensional diffusion of two components (Schwille *et al.*, 1997):

$$C(\tau) = \frac{Af}{\left(1+\tau/\tau_D^{(1)}\right)\sqrt{\left(1+\tau/\left(S^2\tau_D^{(1)}\right)\right)}} + \frac{A(1-f)}{\left(1+\tau/\tau_D^{(2)}\right)\sqrt{\left(1+\tau/\left(S^2\tau_D^{(2)}\right)\right)}} \quad (1)$$

Here, f is the fraction of particles with diffusion coefficient $D_1 < D_2$, and $\tau_D^{(1,2)} = r_0^2/(4D_{1,2})$ are the characteristic times of the autocorrelation decay, which includes the diffusion coefficient and the radius (r_0) of the confocal volume. The elongation of the optical volume along the optical axis is described by the stretching factor S. From the times $\tau_D^{(1)}$ and $\tau_D^{(2)}$, the diffusion coefficients D_1 and D_2 were extracted by comparison with the calibration using GFP in buffer: that is, $D_{GFP} \approx 87\ \mu m^2\ s^{-1}$ (Wachsmuth *et al.*, 2000) corresponds to $\tau_D \approx 130$ μs, $f = 1$ in equation (1) (Fig. 1A). From this, and knowing the molecular weight of GFP (25 kDa), we were also able to predict the diffusion coefficients of ARF1, ARFGAP1 and coatomer using the Einstein–Stokes relationship for $D = k_BT/(3\pi\eta d)$. Here, k_BT is the thermal energy, η is the viscosity of the fluid and d is the diameter of the protein. Assuming η to be 3–4 times bigger for cytosol than for water (Fig.1A), and relating the protein's diameter to its molecular weight (m; $d^3 \sim m$), the predicted diffusion coefficients were $D_{ARF1} \approx 17\ \mu m^2\ s^{-1}$, $D_{ARFGAP1} \approx 15\ \mu m^2\ s^{-1}$ and $D_{COPI} \approx 8\ \mu m^2\ s^{-1}$.

Recovery curves from FRAP experiments performed to study binding kinetics were fitted with a single exponential kinetics; that is, $F(t) = A\ (1 - \exp(-t/T)) + B$. Here, B is the fluorescence in the Golgi region obtained in the first scan after bleaching, and A determines the saturation level of the recovery.

Diffusion-limited FRAP was studied using a model as described in the main text. On the cytosolic sites, the three-dimensional

diffusion equation was solved with a fourth-order Runge–Kutta algorithm (Press *et al.*, 1993) using reflecting boundary conditions at the edges and the Golgi sites. Diffusion of proteins in the Golgi was considered by solving the diffusion equation on the Golgi sites with reflecting boundary conditions and a diffusion coefficient $D = 1\ \mu m^2\ s^{-1}$, which is typical on membranes (Weiss *et al.*, 2003). During bleaching, the diffusion and binding reactions continued.

ACKNOWLEDGEMENTS

We thank J. Presley and J. Lippincott-Schwartz for providing us with ε-COP–GFP, J. Young for critically reading the manuscript, and R. Pepperkok for helpful comments and advice and for the use of the Advanced Light Microscopy Facility at EMBL. M.W. was supported by an EMBO long-term fellowship.

REFERENCES

Elson, E.L. & Qian, H. (1989) Interpretation of fluorescence correlation spectroscopy and photobleaching recovery in terms of molecular interactions. *Methods Cell Biol.*, **30**, 307–332.

Eugster, A., Frigerio, G., Dale, M. & Duden, R. (2000) COPI domains required for coatomer integrity, and novel interactions with ARF and ARF–GAP. *EMBO J.*, **19**, 3905–3917.

Godi, A., Pertile, P., Meyers, R., Marra, P., Di Tullio, G., Iurisci, C., Luini, A., Corda, D. & De Matteis, M.A. (1999) ARF mediates recruitment of PtdIns-4-OH kinase-β and stimulates synthesis of PtdIns(4,5)P2 on the Golgi complex. *Nature Cell Biol.*, **1**, 280–287.

Helms, J.B. & Rothman, J.E. (1992) Inhibition by brefeldin A of a Golgi membrane enzyme that catalyses exchange of guanine nucleotide bound to ARF. *Nature*, **360**, 352–354.

Lanoix, J., Ouwendijk, J., Lin, C.C., Stark, A., Love, H.D., Ostermann, J. & Nilsson, T. (1999) GTP hydrolysis by ARF1 mediates sorting and concentration of Golgi resident enzymes into functional COP I vesicles. *EMBO J.*, **18**, 4935–4948.

Lanoix, J., Ouwendijk, J., Stark, A., Szafer, E., Cassel, D., Dejgaard, K., Weiss, M. & Nilsson, T. (2001) Sorting of Golgi resident proteins into different subpopulations of COPI vesicles: a role for ArfGAP1. *J. Cell Biol.*, **155**, 1199–1212.

Malsam, J., Gommel, D., Wieland, F.T. & Nickel, W. (1999) A role for ADP ribosylation factor in the control of cargo uptake during COPI-coated vesicle biogenesis. *FEBS Lett.*, **462**, 267–272.

Ostermann, J., Orci, L., Tani, K., Amherdt, M., Ravazzola, M., Elazar, Z. & Rothman, J.E. (1993) Stepwise assembly of functionally active transport vesicles. *Cell*, **75**, 1015–1025.

Pepperkok, R., Whitney, J.A., Gomez, M. & Kreis, T.E. (2000) COPI vesicles accumulating in the presence of a GTP restricted *arf1* mutant are depleted of anterograde and retrograde cargo. *J. Cell Sci.*, **113**, 135–144.

Presley, J.F., Ward, T.H., Pfeifer, A.C., Siggia, E.D., Phair, R.D. & Lippincott-Schwartz, J. (2002) Dissection of COPI and Arf1 dynamics *in vivo* and role in Golgi membrane transport. *Nature*, **417**, 187–193.

Press, W.H., Teukolsky, S.A. & Vetterling, W.T. (1993) *Numerical Recipes in C*. Cambridge Univ. Press, Cambridge, UK.

Saxton, M.J. (1993) Lateral diffusion in archipelago. *Biophys. J.*, **64**, 1053–1062.

Saxton, M.J. (2001) Anomalous subdiffusion in fluorescence photobleaching recovery: a Monte Carlo study. *Biophys. J.*, **81**, 2226–2240.

Schwille, P., Bieschke, J. & Oehlenschläger, F. (1997) Kinetic investigations by fluorescence correlation spectroscopy: the analytical and diagnostic potential of diffusion studies. *Biophys. Chem.*, **66**, 211–228.

Spang, A., Matsuoka, K., Hamamoto, S., Schekman, R. & Orci, L. (1998) Coatomer, Arf1p, and nucleotide are required to bud coat protein complex I-coated vesicles from large synthetic liposomes. *Proc. Natl Acad. Sci. USA*, **95**, 11199–11204.

Stephens, D.J., Lin-Marq, N., Pagano, A., Pepperkok, R. & Paccaud, J.P. (2000) COPI-coated ER-to-Golgi transport complexes segregate from COPII in close proximity to ER exit sites. *J. Cell Sci.*, **113**, 2177–2185.

Storrie, B. & Nilsson, T. (2002) The Golgi apparatus: balancing new with old. *Traffic*, **3**, 521–529.

Wachsmuth, M., Waldeck, W. & Langowski, J. (2000) Anomalous diffusion of fluorescent probes inside living cell nuclei investigated by spatially resolved fluorescence correlation spectroscopy. *J. Mol. Biol.*, **298**, 677–689.

Ward, T.H., Polishchuk, R.S., Caplan, S., Hirschberg, K. & Lippincott-Schwartz, J. (2001) Maintenance of Golgi structure and function depends on the integrity of ER export. *J. Cell Biol.*, **155**, 557–570.

Weiss, M. & Nilsson, T. (2003) A kinetic proof-reading mechanism for protein sorting. *Traffic*, **4**, 65–73.

Weiss, M., Hashimoto, H. & Nilsson, T. (2003) Membrane protein diffusion in living cells as seen by fluorescence correlation spectroscopy. *Biophys. J.*, **84**, 4043–4052.

Williger, B.T., Ostermann, J. & Exton, J.H. (1999) Arfaptin 1, an ARF-binding protein, inhibits phospholipase D and endoplasmic reticulum/Golgi protein transport. *FEBS Lett.*, **443**, 197–200.

Wohland, T., Rigler, R. & Vogel, H. (2001) The standard deviation in fluorescence correlation spectroscopy. *Biophys. J.*, **80**, 2987–2999.

Paper II

Anomalous Subdiffusion Is a Measure for Cytoplasmic Crowding in Living Cells

Matthias Weiss,* Markus Elsner,† Fredrik Kartberg,† and Tommy Nilsson†
*MEMPHYS-Center for Biomembrane Physics, Physics Department, University of Southern Denmark, Campusvej 55, Odense M, Denmark; and †Department of Medical Biochemistry, Göteborg University, Medicinaregatan 9A, Göteborg, Sweden

ABSTRACT Macromolecular crowding dramatically affects cellular processes such as protein folding and assembly, regulation of metabolic pathways, and condensation of DNA. Despite increased attention, we still lack a definition for how crowded a heterogeneous environment is at the molecular scale and how this manifests in basic physical phenomena like diffusion. Here, we show by means of fluorescence correlation spectroscopy and computer simulations that crowding manifests itself through the emergence of anomalous subdiffusion of cytoplasmic macromolecules. In other words, the mean square displacement of a protein will grow less than linear in time and the degree of this anomality depends on the size and conformation of the traced particle and on the total protein concentration of the solution. We therefore propose that the anomality of the diffusion can be used as a quantifiable measure for the crowdedness of the cytoplasm at the molecular scale.

INTRODUCTION

At first glance the cytoplasm of mammalian cells appears to be an unstructured, aqueous liquid in which proteins, sugar molecules, and other solvents are dissolved. Taking a closer look, one realizes that the cytoplasm is in fact structured on many length scales: on the μm-scale we find organelles like the mitochondria, endosomes, and the Golgi apparatus. On a smaller scale ($\sim$100 nm) the endoplasmic reticulum (ER) imposes a random reticular network (Marsh et al., 2001) together with the cytoskeletal elements, such as microtubuli and actin filaments. Together, these yield a higher order structure of the cytoplasm (see, for example, Alberts et al., 1994 for a more detailed introduction). As a consequence, diffusional movement of particles, such as macromolecules, can be obstructed. In fact, it has been reported that the diffusional mobility in the cytoplasm strongly decreases with an increasing radius of the tracked particle, leaving particles with a radius >25–30 nm immobile (Luby-Phelps et al., 1986, 1987; Seksek et al., 1997; Arrio-Dupont et al., 2000). Extensive computer simulations also have shown that the molecular mobility is reduced when a particle diffuses in a maze-like environment (Saxton, 1993): When increasing the concentration c of obstacles in the maze, the tracer particles appeared to diffuse slower and slower until complete immobilization occurred beyond a certain value, c^*. Interestingly, when approaching c^* the characteristics of the diffusional motion changed dramatically. The mean square displacement $v(t)$ of the monitored particles did no longer grow linearly in time but, rather, showed a power law $v(t) \sim t^{\alpha}$ with $\alpha < 1$. This kind of diffusion is known as anomalous subdiffusion and has been found in many different contexts; e.g., for the movement of lipids on model membranes (Schutz et al., 1997), integral membrane proteins on organellar membranes (Weiss et al., 2003) and proteins in the nucleoplasm (Wachsmuth et al., 2000), solute transport in porous media (Drazer and Zanette, 1999), and the translocation of polymers (Metzler and Klafter, 2003; Kantor and Kardar, 2004).

In the case of obstructed diffusion, the emergence of a transitional subdiffusive regime is observed when the concentration of obstacles is increased. This transient subdiffusive behavior collapses back to normal diffusion after a timescale T which diverges in the limit $c \rightarrow c^*$. At $c = c^*$ (the so-called percolation threshold), subdiffusion is observed on all timescales. Whereas T grows with increasing obstacle concentration, the (transient) anomality parameter α decreases concomitantly from unity to a finite value α^* at c^*, which is given by $\alpha^* \approx 0.697$ and $\alpha^* \approx 0.526$ for two- and three-dimensional environments, respectively (Havlin and Ben-Avraham, 1987; Bouchaud and Georges, 1990). These values were obtained for continuum percolation in a ''Swiss-cheese'' model (see Havlin and Ben-Avraham, 1987 for details) and presumably represent the best approximation to the actual values in nature. However, other mechanisms can also lead to anomalous subdiffusion where the entire range $0 < \alpha < 1$ may be observed (see, for example, Bouchaud and Georges, 1990; Metzler and Klafter, 2000). Regardless of its microscopic origin, anomalous subdiffusion has been shown to strongly influence the formation of spatiotemporal patterns (Weiss, 2003) as well as kinetic rates (Saxton, 2002) and the time course of enzymatic reactions (Berry, 2002).

When neglecting the higher-order structuring of the cytoplasm by cytoskeletal elements and membranes, one could anticipate from the above that one deals with an unstructured aqueous solution in which normal diffusion

Submitted April 9, 2004, and accepted for publication August 16, 2004.

Matthias Weiss and Markus Elsner contributed equally to this work.

Address reprint requests to Matthias Weiss, MEMPHYS-Center for Biomembrane Physics, Physics Department, University of Southern Denmark, Campusvej 55, DK-5230 Odense M, Denmark. Tel.: 45-6550-3686; E-mail: mweiss@memphys.sdu.dk.

0006-3495/04/11/3518/07 $2.00

doi: 10.1529/biophysj.104.044263

should be observed. Yet, the assumption of the cytoplasm as being a homogenous viscous solution is somewhat misleading as differently sized proteins, lipids, and sugars constitute up to 40% of the cytoplasmic volume (Fulton, 1982). This phenomenon is commonly referred to as *molecular crowding* and has recently received increased attention (Ellis and Minton, 2003; Rivas et al., 2004) since, for example, enzymatic reactions and protein folding appear to be strongly affected by the crowdedness (for reviews see Ellis, 2001; Hall and Minton, 2003). Also, crowding seems to contribute significantly to the high viscosity of the cytoplasm which has been determined to be three- to fourfold higher than that of water (Verkman, 2002; Elsner et al., 2003). Despite the increased interest in the phenomena associated with molecular crowding, the term ''crowdedness'' so far has been used without a quantitative definition of what it actually means. In other words, we lack a definition of a quantity which summarizes *how* crowded an environment really is and also states in which primary physical property of the heterogeneous fluid the crowdedness is manifested. As basic criterion, a quantitative measure of crowdedness should be independent of influences imposed by the cytoskeletal and membrane obstacles discussed above. Rather, it should reflect a basic and unambiguous physical quantity which can be assigned to the highly, yet heterogeneous, concentrated protein/sugar solution called cytoplasm.

Here we utilize fluorescence correlation spectroscopy (FCS) to show that inert tracer particles show anomalous subdiffusion in the cytoplasm of living cells over a wide range of particle sizes. This behavior is found to occur irrespective of the stage of the cell cycle or the presence of ER membrane structures and cytoskeletal scaffolds. Using computer simulations, we demonstrate that this effect most likely arises due to molecular crowding, e.g., diffusing particles are scattered by nearby particles due to excluded-volume interactions. We verify our hypothesis in vitro by determining the degree of anomalous diffusion of tracer particles in highly concentrated dextran solutions.

MATERIALS AND METHODS

Cell culture

HeLa cell lines were grown in DMEM supplemented with 10% fetal calf serum, 100 μg/ml penicillin, 100 mg/ml streptomycin, and 10 mM glutamine (Gibco, Eggenstein, Germany). FITC-labeled dextrans of different molecular masses (10, 40, 500, 2000 kDa: Molecular Probes, Eugene, OR; 150 kDa: Sigma, Germany) were either injected with an Eppendorf microinjection system (Eppendorf, Hamburg, Germany) or incorporated by electroporation. Microtubules were disrupted by incubating cells with 20 μM nocodazole at 37°C for one hour. To disrupt the ER network, cells were treated with 5 μg/ml Filipin III (Sigma, Germany) for 30 min at 37°C and 45 min at 30°C. The efficiency of the treatment was confirmed by examining the change of the fluorescence pattern of HeLa cells expressing the ER marker Sec61 fused to CFP (see Axelsson and Warren, 2004 for details). Experiments using mitotic cells were accomplished by arresting HeLa cells in the metaphase of mitosis by incubating them for 16 h in the presence of 100 nM nocodazole (Sigma Chemical, St. Louis, MO) (Zieve et al., 1980).

For subcellular fractionation, HeLa cells were scraped off the culture dish and collected by centrifugation (500g, 5 min.). Cells were washed with phosphate-buffered saline (PBS) twice and once with homogenization buffer. The homogenization buffer consisted of 20 mM HEPES-KOH (pH 7.4), 1 mM DTT (both Biomol, Hamburg, Germany), 250 mM sucrose (USB, Cleveland, OH), 1 mM EDTA (Merck, Hamburg, Germany), plus protease inhibitors (1 μg/ml aprotinin, 1 μg/ml leupeptin, 1 μg/ml pepstatin, 1 μg/ml antipain, 1 mM Benzamidine-HCl, 40 μg/ml phenylmethylsulfonyl fluoride). Cell pellets were resuspended in 4 volumes of homogenization buffer in the presence of protease inhibitors and homogenized using a ball-bearing homogenizer (10 passages with a 16 μm clearing). The homogenate was then centrifuged sequentially at $10^3 g$ (P1), $10^4 g$ (P10), and at $10^5 g$ (P100), retaining the supernatant at each subsequent centrifugation step. The final $10^5 g$ supernatant (S100) was boiled in equal volume sample buffer and various amounts (0.1–10 μg) of protein were resolved on a 12.5% SDS-polyacrylamide gel. Protein bands were visualized by Coomassie Brilliant blue G250 (Merck, Darmstadt, Germany).

Fluorescence microscopy and FCS

FCS measurements were carried out on a LSM510/ConfoCor 2 (Carl Zeiss, Jena, Germany) using a 488-nm laser line for illumination. The fluorescence was detected with a bandpass filter (505–550 nm) and the objective (Apochromat 40×/1.2 W) was heated to 37°C using an objective heater (Bioptechs, Butler, PA). The pinhole for all shown measurements was 1 Airy unit. We verified that for free diffusion in water, the autocorrelation function of the fluorescence was well fitted by Eq. 1 with $\alpha = 1$. Thus, our analysis does not suffer from deviations of the confocal volume from a three-dimensional Gaussian point-spread function (see also discussions in Hess and Webb, 2002; Weiss et al., 2003). For each cell and condition, at least 30 fluorescence time series of 10 s duration were recorded, autocorrelated, and superimposed for fitting with XMGRACE (see http://plasma-gate.weizmann.ac.il/Grace/).

Autocorrelation times τ_D were translated into apparent hydrodynamic radii by comparison with green fluorescent protein (EGFP, Molecular Probes) in PBS: From the diffusion coefficient $D \approx 85\ \mu m^2/s$ of GFP in buffer (Terry et al., 1995) and the determined diffusive time $\tau_D = 130\ \mu s$, we obtained via the Einstein-Stokes equation $D = k_B T/(6\pi\eta r)$ a mean radius $r = 2.6$ nm for GFP ($k_B T \approx 4.3 \times 10^{-21}$ J is the thermal energy and $\eta \approx 10^{-3}$ kg/(m × s) is the viscosity of water). This value agrees well with the dimensions derived from the crystal structure of GFP (Yang et al., 1996).

Fitting anomalous diffusion

To determine if the experimentally observed autocorrelation function $C(\tau)$ is governed by anomalous subdiffusion one has to generalize the well-known expression for the autocorrelation decay due to normal diffusion. Knowing the illumination profile (which is usually approximated by a three-dimensional Gaussian), this task is essentially done when the propagator $G(\vec{r}_1, \vec{r}_2, \tau)$ of the density of the (sub)diffusing particles is known. This function simply tells the probability to find a particle at position $\vec{r}_2$ after a time τ when it was initially at position $\vec{r}_1$. For normal diffusion $G(\vec{r}_1, \vec{r}_2, \tau)$ is simply a Gaussian which satisfies the diffusion equation and it is easy to derive the appropriate expression for $C(\tau)$ (for details see, for example, Hess and Webb, 2002; Weiss et al., 2003). In contrast, the propagator for subdiffusion is somewhat more difficult to obtain. Bearing in mind that subdiffusion is commonly defined via the asymptotic power-law increase of the mean square displacement $v(t) \sim t^\alpha$ ($\alpha < 1$), a straight-forward (yet approximative) approach to determine $G(\vec{r}_1, \vec{r}_2, \tau)$ is to assume a time-dependent diffusion coefficient $D(t) = \Gamma t^{\alpha-1}$ so that $v(t) = D(t) \times t$. Clearly, this interpretation is problematic for small times as $D(t)$ diverges for $t \to 0$. Yet, assuming that one still can use this approximation for all times, one obtains the propagator

$$G(\vec{r}_1,\vec{r}_2,\tau)=\frac{\exp(-|\vec{r}_1-\vec{r}_2|^2/(\Gamma\tau^\alpha))}{\sqrt{\pi\Gamma\tau^\alpha}},$$

which satisfies the modified diffusion equation

$$\frac{\partial G(\vec{r}_1,\vec{r}_2,t)}{\partial t}=D(t)\Delta G(\vec{r}_1,\vec{r}_2,t).$$

Using this expression in conjunction with a Gaussian illumination profile, we obtain

$$C(\tau)=\frac{1+fe^{-\tau/\tau_T}}{(1+(\tau/\tau_D)^\alpha)\sqrt{1+(\tau/(S^2\tau_D))^\alpha}}. \qquad (1)$$

Here, α is the degree of the anomalous subdiffusion, and τ_D is the diffusive time which is related to the diffusion coefficient D and the width r_0 of the focus as $\tau_D=r_0^2/(4D)$ for $\alpha=1$. The parameter S considers the unavoidable extension of the confocal volume along the optical axis, whereas f, τ_T are the triplet fraction and time, respectively, which take care of the photophysics on short timescales.

The fitting function Eq. 1 has been used previously to determine anomalous subdiffusion in FCS experiments (Schwille et al., 1999; Wachsmuth et al., 2000; Weiss et al., 2003) and the very same approach served as a starting point to derive fitting functions for quantitative photobleaching experiments (Feder et al., 1996; Saxton, 2001). However, the outlined strategy appears somewhat questionable due to the divergence of the time-dependent diffusion coefficient on short timescales. A mathematically correct treatment of the problem therefore has to employ a fractional Fokker-Planck equation (FFPE), i.e., a sophisticated extension of the normal diffusion equation. For the FFPE one can analytically calculate the propagator in terms of Fox functions for all $\alpha<1$ (see Metzler and Klafter, 2000). From this, one could derive $C(\tau)$ analytically. However, the emerging function only has a limited value for a later fitting procedure as its complexity severely hampers the fitting to experimental data. We therefore have chosen a different approach: Using the series expansions of the propagator (cf. Metzler and Klafter, 2000), we calculated numerically the propagator and the resulting correlation function. We then fitted these curves with Eq. 1 (fixing the triplet fraction to $f=0$) to test if the obtained value α_{fit} corresponds to the value α_{FPE} imposed in the FFPE. In all cases, Eq. 1 yielded a good fit to the $C(\tau)$ as obtained from the FFPE (see Fig. 1 for a representative example). The anomality degrees α_{fit} and α_{FPE} on the other hand were slightly different (Fig. 1, *inset*) and a linear regression yielded $\alpha_{fit}=1.1\times\alpha_{FPE}-0.12$. In the range $0.5\le\alpha\le1$ the deviations between Eq. 1 and the FFPE is therefore $<10\%$ which is within the accuracy of the experimental data. In view of this and due to its much simpler use in the fitting procedure, we have chosen to always use Eq. 1 for fitting.

Computer simulations

To investigate the effect of crowdedness by means of computer simulations, we considered a cubic probe volume with linear extension L and periodic boundary conditions. In total, $N=5000$ spherical particles/proteins having molecular masses in the range 50 kD–1 MDa were positioned at random locations in the probe volume. By changing L we were able to change the apparent concentration of particles. To consider excluded volume effects, we imposed a soft-core potential between the particles, which is common for mesoscopic simulations (Nikunen et al., 2003): Each particle k experienced a (repulsive) force $\vec{f}_{ik}=A(1-d/r_c)\vec{e}_{ik}$ from a neighboring molecule i along the vector $\vec{e}_{ik}$ pointing from particle k to particle i. Here, d measures the distance between the particles i, k, minus the radii r_i, r_k of the two particles. For $d>r_c$ the particles do not meet and thus $\vec{f}_{ik}=\vec{f}_{ki}=0$. Besides this excluded volume interaction, all particles were also subject to thermal noise,

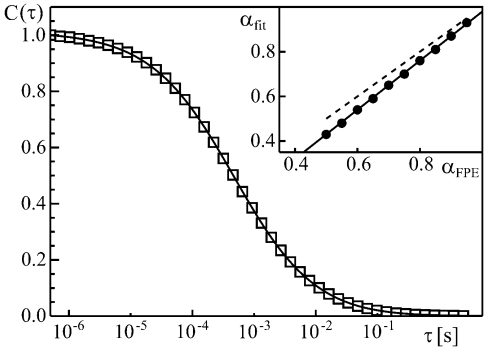

FIGURE 1 The autocorrelation curve $C(\tau)$ obtained for subdiffusive motion in the framework of a FFPE ($\alpha_{FPE}=0.65$, *open symbols*) is well described by a fit with Eq. 1 ($\alpha_{fit}=0.59$, *full line*). (*Inset*) The actual value α_{fit} for the anomality obtained by this fitting (*closed symbols*) slightly deviates from the value α_{FPE} imposed in the FFPE (*dashed line*). The dependence is best described by $\alpha_{fit}=1.1\alpha_{FPE}-0.12$ (*full line*).

i.e., for each time step Δt the new position emerged from the old one via the (overdamped) Langevin equation $\vec{x}_i(t+\Delta t)=\vec{\xi}+\Delta t\sum_k\vec{f}_{ik}/\gamma_i$. Here, ξ is Gaussian random number with variance $2D_i\Delta t$ and the friction of the particle is assumed to be given by Stoke's formula ($\gamma_i=6\pi\eta r_i$) from which one also obtains the diffusion coefficient via $D_i=k_BT/\gamma_i$. The radii were calculated from the imposed molecular mass m_i via the empiric formula $r_i=(8m_i/50)^{1/3}$ nm. This relation has been derived by considering that BSA ($m=66$ kDa) is approximately globular and has an apparent radius of 2 nm. The distribution $p(m)$ of molecular weights m was taken to be either a Poissonian or uniform (see main text), and a upper cutoff at $m=1$ MDa was imposed. Before monitoring the diffusional motion, the particles were allowed to equilibrate for 5000 time steps. The remaining parameters were $\Delta t=10^{-9}$ s, $r_c=2$ nm, $A/(6\pi\eta)=10^3$ μm^2/s.

RESULTS

We first monitored with FCS the diffusional motion of fluorescently labeled dextrans in PBS to verify that we observe normal diffusion under these conditions. Indeed, fitting the experimental data with Eq. 1 yielded $\alpha=1\pm0.05$ which indicates that finding anomalous subdiffusion with our setup is not an artifact of a distorted confocal volume (Hess and Webb, 2002; see also discussion in Weiss et al., 2003). Representative autocorrelation curves $C(\tau)$ for dextrans of different molecular weight are shown in Fig. 2. The measurements in PBS also allowed us to determine the apparent hydrodynamic radius r_H of the particles (see Methods). In the inset of Fig. 2 we show the increase of the radii for increasing molecular weight m ($r_H\sim m^{0.4}$). In fact, the radii increase slower than anticipated for a simple random-coil polymer for which a description as a linear Gaussian chain yields $r_H\sim m^{0.5}$ (Doi, 1996). This deviation is in agreement with previous reports (Cheng et al., 2002) and may be explained by the fact that dextrans become strongly branched polymers when their mass increases (Nordmeier, 1993).

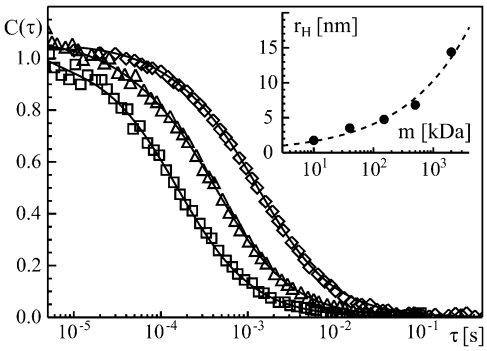

FIGURE 2 Representative autocorrelation curves for dextran in PBS (*squares, triangles, diamonds*: molecular masses $m = 10$ kDa, 150 kDa, 2 MDa, respectively). Best fits according to Eq. 1 (*full lines*) always resulted in $\alpha \approx 1$, indicating normal diffusion. (*Inset*) The hydrodynamic radius r_H as extracted from the diffusive time τ_D of the autocorrelation decay increases approximately as $r_H \sim m^{0.4}$ (*dashed line*).

We next investigated the motion of labeled dextrans in the cytoplasm of HeLa cells in interphase. Representative examples for the obtained autocorrelation curves $C(\tau)$ are shown in Fig. 3. In strong contrast to the behavior in PBS, all dextrans showed subdiffusive motion in cytoplasm albeit with varying degrees of the anomality parameter α. Moreover, the characteristic timescales τ_D of the autocorrelation decays were increased with respect to the ones found for PBS which indicates an overall decrease of the diffusional mobility. Surprisingly, the determined degrees of anomality α did not correlate linearly with the hydrodynamic sizes of the

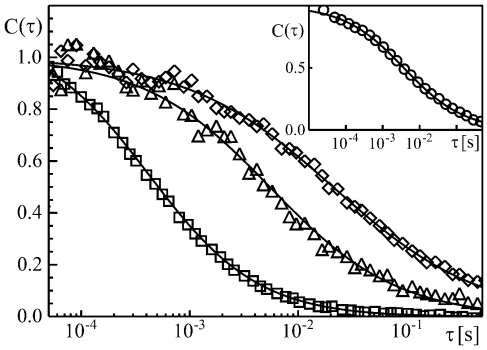

FIGURE 3 Representative autocorrelation curves for dextran in the cytoplasm of living cells in interphase (*squares, triangles, diamonds*: molecular masses 10 kDa, 150 kDa, 2 MDa, respectively). Best fits according to Eq. 1 (*full lines*) revealed that all dextrans moved subdiffusively ($\alpha = 0.86$, 0.74, 0.64; *from left*). (*Inset*) A FITC-labeled IgG antibody ($m = 150$ kDa, $r_H \approx 5.5$ nm) also showed strong subdiffusion ($\alpha \approx 0.55$).

dextran particles (see Table 1). Rather, we observed a very strong subdiffusive motion for small dextrans (40 kDa) which relaxed for increasing mass (500 kDa) and then became stronger again (2 MDa). We next verified that the observed subdiffusion in cytoplasm was not a particular feature of dextran by monitoring the diffusion of a FITC-labeled IgG antibody ($m \approx 150$ kDa) in cytoplasm. Having an apparent hydrodynamic radius $r_H \approx 5.5$ nm (cf. also Arrio-Dupont et al., 2000), we expected IgG to show a similar degree of subdiffusion as seen with 150 kDa dextran ($r_H \approx 5$ nm). In fact, we observed a stronger anomality ($\alpha \approx 0.55$, see also Fig. 3, *inset*), which may be explained by the fact that an IgG has a different shape than a 150 kDa dextran in solution.

We hypothesized that molecular crowding may have caused the observed anomalous subdiffusion rather than obstruction by cytoskeletal elements or membrane structures. To test for the validity of this assumption, we monitored the diffusional properties of a selection of dextrans in i), nocodazole-treated; ii), latrunculin-treated; iii), Filipin-treated; and iv), mitotic cells. In cases i and ii the microtubules and actin filaments are depolymerized, respectively, whereas in case iii the ER membrane is broken down and other membrane structures like the Golgi apparatus are not affected (Axelsson and Warren, 2004). In case iv the interior of the cell has undergone major changes due to the impending cell division, e.g., the microtubules form a spindle rather than an astral array. In agreement with our hypothesis, the subdiffusion persisted in all cases with similar values for α (see summary in Table 2). This provides strong evidence that obstruction by higher-order structures is not the major cause of the observed subdiffusion. Rather, the observed subdiffusion is caused by molecular crowding.

To obtain further evidence for if and when molecular crowding can cause the emergence of subdiffusion, we used computer simulations of spherical soft-core molecules subject to thermal noise and excluded volume effects (see Methods). To be able to model the cytoplasmic environment, we had to first get an idea about the distribution of protein masses/sizes in the cytoplasm of mammalian cells. We therefore analyzed purified HeLa cytosol by SDS page and Coomassie staining (see Methods). The resulting distribution of molecular weights $p(m)$ is shown in Fig. 4 *a* and is most consistent with a Poisson distribution with a mean $\langle m \rangle = 80$ kDa. Bearing in mind that the used approach actually overestimates the fraction of small proteins due to the denaturing conditions in the gel (protein

TABLE 1 Summary of masses *m*, hydrodynamic radii r_H (in PBS), and anomalities α and diffusive times τ_D of dextrans in the cytoplasm of living cells

m	r_H	α	τ_D
10 kDa	1.8 nm	0.84 ± 0.04	0.39 ± 0.05 ms
40 kDa	3.5 nm	0.59 ± 0.04	2.9 ± 1.3 ms
150 kDa	4.8 nm	0.73 ± 0.03	6.1 ± 1.9 ms
500 kDa	6.8 nm	0.82 ± 0.05	3.1 ± 1 ms
2 MDa	14.4 nm	0.71 ± 0.04	15.9 ± 4.5 ms

TABLE 2 Summary of the found degrees of anomality α and diffusive times τ_D in the cytoplasm of living cells under various treatments

m	Interphase α, τ_D	Mitotic α, τ_D	Filipin α, τ_D	Nocodazole α, τ_D	Latrunculin α, τ_D
10 kDa	0.87 ± 0.03	0.74 ± 0.02	0.74 ± 0.06	0.76 ± 0.07	0.74 ± 0.05
	0.39 ± 0.05 ms	0.39 ± 0.06 ms	0.55 ± 0.26 ms	0.34 ± 0.03 ms	1.8 ± 0.06 ms
150 kDa	0.73 ± 0.03	0.75 ± 0.04	0.83 ± 0.04	0.76 ± 0.06	0.76 ± 0.05
	6.1 ± 1.9 ms	1.7 ± 0.6 ms	2.2 ± 0.8 ms	7.8 ± 4.3 ms	1.9 ± 0.3 ms
500 kDa	0.82 ± 0.05	0.75 ± 0.06	0.76 ± 0.05	0.79 ± 0.04	0.76 ± 0.03
	3.1 ± 0.9 ms	5.6 ± 1.3 ms	3.2 ± 0.7 ms	2.7 ± 0.5 ms	3.3 ± 0.2 ms

complexes are disrupted), we tested two distributions in the simulations which were inspired by the experimental distribution $p(m)$ (see Fig. 4 *a*): i), a Poisson distribution with $\langle m \rangle = 350$ kDa, and ii), a uniform distribution. In both cases we only considered proteins with masses up to 1 MDa and, for simplicity, assumed the proteins to be globular. In both simulation settings, we observed a size-dependent emergence of anomalous subdiffusion which also clearly depended on the fractional volume occupied by the globular proteins (''excluded volume''). In Fig. 4 *b* we show representative curves for the mean square displacement obtained for scenario i, i.e., a Poissonian distribution of molecular masses, at an excluded volume of 13%. Although small proteins were still diffusing more or less normally, the big particles clearly moved subdiffusively. This size-dependence is further highlighted in Fig. 4 *c*, where one can observe the decrease of the anomality parameter α with increasing effective particle size. This result was only slightly altered in scenario ii, i.e., for a uniform size distribution. The decrease of α with increasing radii persisted (Fig. 4 *d*) albeit occurring at bigger radii and at lower values for the excluded volume (7% instead of 13%). As both settings yielded the same gross features, we conclude that an excluded volume interaction (= molecular crowding) likely explains the subdiffusion observed in the cytoplasm of living cells. The successful simulations of course only represent the simplest possible configuration due to the use of globular particles. To quantitatively explain the experimentally observed α-values, a more detailed approach may be necessary which includes, for example, the polymeric nature of the probe (see also Discussion).

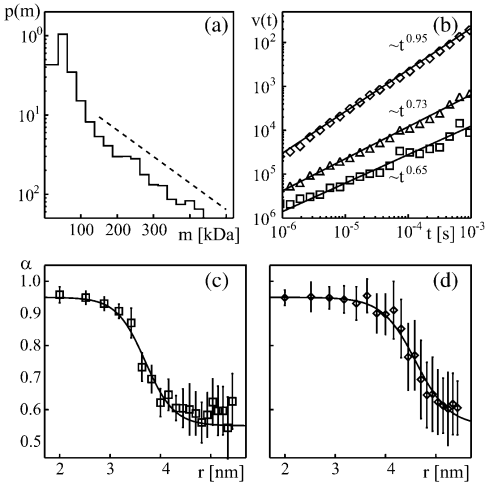

FIGURE 4 (*a*) The distribution $p(m)$ of protein masses m in the cytoplasm of HeLa cells (see Methods) is well described by a Poissonian (*dashed line*, mean $\langle m \rangle = 80$ kDa). Due to the denaturing conditions of the gel, the fraction of low protein masses is overestimated and can be expected to be significantly higher in reality. (*b*) Average mean square displacement $v(t)$ for globular proteins with radii 2 nm, 3.6 nm, and 5.4 nm (from top) as obtained by simulations using a Poissonian weight distribution (mean $\langle m \rangle = 350$ kDa to soften the overestimation of low masses). The proteins occupied a fractional volume of 13%. Dashed lines highlight the power-law increase $v(t) \sim t^{\alpha}$. (*c*) Using the same parameters, the anomality parameter α is seen to decrease for increasing particle radii r. The full line is a guide to the eye. (*d*) Same as in (*c*) for a uniform distribution of molecular weights (50 kDa $\leq m \leq$ 1MDa). Here, a similar decrease of α is observed, yet it occurs for higher values of r and a lower fractional volume occupied by the proteins (7%).

To verify the simulation results and consistently test if the mere effect of crowding can cause anomalous subdiffusion, we also studied the diffusional properties of some labeled dextrans (10 kDa, 40 kDa, 500 kDa) in aqueous solution when varying the molar percentages of macromolecules (unlabeled dextran in the range 60–90 kDa; from Acros Organics, Geel, Belgium) to hinder diffusion. As these artificially created crowded fluids were intended to mimic the cytoplasm of living cells, we expected to observe an overall correlation of the α-values between in vitro and in vivo experiments using a particular probe. Consistent with our findings in vivo (the cytoplasm), we observed an increase of the diffusional time τ_D and a concomitant decrease of the anomality parameter α for the tested dextrans when the concentration C of unlabeled dextran (i.e., the crowding) in the solution was increased (Fig. 5). These experiments also confirmed the simulation results, i.e., the interaction via excluded volume can cause subdiffusion. In accordance with the results in living cells, we again observed that 40 kDa dextran appeared to be much more subdiffusive than its 500 kDa counterpart. We speculate that in both cases this may be caused by a partial reptational movement of the fairly short 40 kDa polymer whereas the more heavy dextrans may be more globular and are thus less prone to reptation (see also Discussion). Nevertheless, we

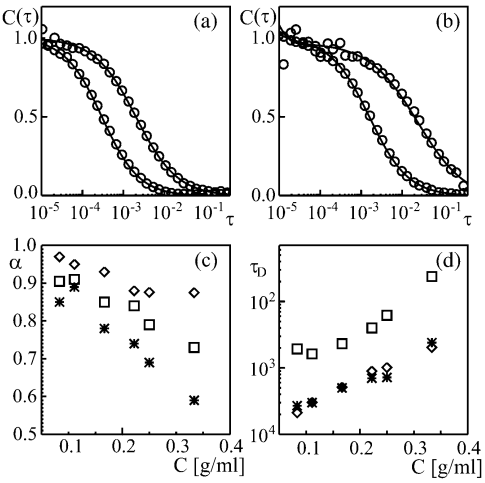

FIGURE 5 (*a*) Representative autocorrelation curves for 10 kDa dextran in solutions with different crowdedness due to dissolved unlabeled dextran (0.08 and 0.25 g/ml, from left). A shift and stretching of $C(\tau)$ is visible for increasing crowdedness. (*b*) Same as in *a* but for 500 kDa dextran. (*c*) The anomality parameter α decreases with increasing crowdedness as measured by the macromolecular concentration (*diamonds*, 10 kDa; *asterisks*, 40 kDa; *squares*, 500 kDa). (*d*) The diffusive time τ_D concomitantly increases with increasing macromolecular concentration, indicating an increase of the effective viscosity. For better visibility error bars have been omitted.

conclude that the degree of anomalous diffusion (α) is a direct reflection of molecular crowding. By comparing in vivo measurements with those in vitro, one can therefore use the determined α-values as a measure for molecular crowding.

DISCUSSION

In summary, we have determined with FCS that inert tracer particles show anomalous subdiffusion in the cytoplasm of mammalian cells. As the occurrence of subdiffusion was not altered in cells where cytoskeletal or organellar membrane architecture have been disrupted, we conclude that the observed subdiffusion is due to molecular crowding. In support of this view, we showed with simulations that subdiffusion naturally arises in a concentration-dependent manner in a system where particles are subject to Brownian motion and only interact via excluded volumes. We further verified these simulation results by monitoring the emergence of subdiffusion in highly concentrated dextran solutions. Thus, we have provided strong evidence that molecular crowding causes anomalous subdiffusion in the cytoplasm of living cells.

It is likely that the observed subdiffusion only persists for intermediate times and that normal diffusion is reencountered for asymptotically large times. For example, in our simulations we observed via the growth of the mean square displacement $v(t)$ that even for a fairly low excluded volume subdiffusion transiently emerged on scales $t < 1$ μs and then collapsed back to normal diffusion. For increasing particle concentration this subdiffusive regime eventually extended beyond the 1 ms-scale (cf. Fig. 4). Similar phenomena are, for example, also found for obstructed diffusion with immobile obstacles near to the percolation threshold (Saxton, 2001) or for reptating polymers (Doi, 1996). Bearing this in mind, our results do not contradict but rather complement previous studies on cytoplasmic diffusion by means of photobleaching techniques (Seksek et al., 1997; Arrio-Dupont et al., 2000) which employ larger spatial and temporal scales than in FCS and therefore potentially miss the regime of subdiffusion.

In regards to the nature of the used probe, we observed that small dextran molecules can exhibit a much stronger anomalous subdiffusion than their more heavy counterparts (cf. Table 1 and Fig. 5). The most likely explanation for this phenomenon is a (partially) reptational movement of small dextrans. In the ideal case, reptation yields $\alpha = 0.5$ (Doi, 1996) whereas obstructed diffusion of globular particles typically yields a higher value for α (see Introduction). For our case, we propose that small dextrans adopt a ''snake-like'' conformation whereas the more heavy dextrans are more globular and thus are rather subject to obstructed diffusion than reptation. This reasoning is supported by the fact that fructan, a close relative to dextran, was shown to behave like a random-coil polymer for masses $m \ll 100$kDa, whereas above 100 kDa it appeared more like a globule (Kitamura et al., 1994). This reasoning appears even more plausible when bearing in mind that the conformation of (bio)polymers can depend critically on the solvent and that dextrans show strong branching when their mass increases (Nordmeier, 1993). Of course, for reptational movement the simple picture used in the simulations becomes invalid and has to be replaced by a more elaborate polymer model in a heterogeneous environment. It will be interesting to study the crossover from reptation to obstructed diffusion in more detail (M. Weiss et al., unpublished results).

Despite the caveat that the observed subdiffusion may be a transient feature, it is still likely to play a major role in cytoplasmic processes. In our approach with FCS, we observed subdiffusion on a scale of ~500 nm (the diameter of the confocal volume), a scale which is ~100-fold bigger than the typical radius of a globular protein and almost corresponds to the typical size of an *Escherichia coli* bacterium. At least on this scale, anomalous diffusion can greatly modulate the interaction of proteins, e.g., in reaction networks (Berry, 2002; Saxton, 2002) and maybe in protein folding (Ellis, 2001; Hall and Minton, 2003).

Most importantly, the described emergence of subdiffusion provides a means to define a quantitative measure to what crowdedness actually means. In fact, the term ''crowdedness'' by its mere literal sense signals that the

size and conformation of a test particle dictates if it feels an environment as being crowded. Being a water molecule, the cytoplasm does not appear to be any more crowded than any other solution. However, for a macromolecule, and even more for a polymer-like dextran, the cytoplasm with all its embedded proteins provides an obstacle-rich environment. We therefore propose that the degree of anomality α can serve as a size- and conformation-dependent quantity to characterize the concentration/composition of a heterogeneous solution like the cytoplasm. In other words, by using a defined and standardized set of in vitro solutions (where the composition is varied), it should be feasible to use the degree of anomality α as a quantitative measure to probe molecular crowding in vivo, be it in the cytoplasm, the nucleus, or other cellular or extracellular environments.

M.W. acknowledges helpful discussions with P. L. Hansen, J. H. Ipsen, and B. Klösgen.

The MEMPHYS-Center for Biomembrane Physics is supported by the Danish National Research Foundation. We also thank the Advanced Light Microscopy Facility (European Molecular Biology Laboratory, Heidelberg) and the SWEGENE Centre for Cellular Imaging at Göteborg University, Gothenburg, Sweden.

REFERENCES

Alberts, B., D. Bray, J. Lewis, M. Raff, K. Roberts, and J. D. Watson. 1994. Molecular Biology of the Cell, 3rd ed. Garland Publishing, New York.

Arrio-Dupont, M., G. Foucault, M. Vacher, P. F. Devaux, and S. Cribier. 2000. Translational diffusion of globular proteins in the cytoplasm of cultured muscle cells. *Biophys. J.* 78:901–907.

Axelsson, M. A., and G. Warren. 2004. Rapid, ER-independent diffusion of the mitotic Golgi haze. *Mol. Biol. Cell.* 15:1843–1852.

Berry, H. 2002. Monte Carlo simulations of enzyme reactions in two dimensions: fractal kinetics and spatial segregation. *Biophys. J.* 83:1891–1901.

Bouchaud, J. P., and A. Georges. 1990. Anomalous diffusion in disordered media—statistical mechanisms, models, and physical applications. *Physics Rep.* 195:127–293.

Cheng, Y., R. K. Prud'homme, and J. L. Thomas. 2002. Diffusion of mesoscopic probes in aqueous polymer solutions measured by fluorescence recovery after photobleaching. *Macromolecules.* 35:8111–8121.

Doi, M. 1996. Introduction to Polymer Physics. Clarendon Press, Oxford.

Drazer, G., and D. H. Zanette. 1999. Experimental evidence of power-law trapping-time distributions in porous media. *Phys. Rev. E.* 60:5858–5864.

Ellis, R. J. 2001. Macromolecular crowding: obvious but underappreciated. *Trends Biochem. Sci.* 26:597–604.

Ellis, R. J., and A. P. Minton. 2003. Cell biology: join the crowd. *Nature.* 425:27–28.

Elsner, M., H. Hashimoto, J. C. Simpson, D. Cassel, T. Nilsson, and M. Weiss. 2003. Spatiotemporal dynamics of the copi vesicle machinery. *EMBO Rep.* 4:1000–1004.

Feder, T. J., I. Brust-Mascher, J. P. Slattery, B. Baird, and W. W. Webb. 1996. Constrained diffusion or immobile fraction on cell surfaces: a new interpretation. *Biophys. J.* 70:2767–2773.

Fulton, A. B. 1982. How crowded is the cytoplasm? *Cell.* 30:345–347.

Hall, D., and A. P. Minton. 2003. Macromolecular crowding: qualitative and semiquantitative successes, quantitative challenges. *Biochim. Biophys. Acta.* 1649:127–139.

Havlin, S., and D. Ben-Avraham. 1987. Diffusion in disordered media. *Adv. Phys.* 36:695–798.

Hess, S. T., and W. W. Webb. 2002. Focal volume optics and experimental artifacts in confocal fluorescence correlation spectroscopy. *Biophys. J.* 83:2300–2317.

Kantor, Y., and M. Kardar. 2004. Anomalous dynamics of forced translocation. *Phys. Rev. E.* 69:021806.

Kitamura, S., T. Hirano, K. Takeo, M. Mimura, K. Kajiwara, T. Stokke, and T. Harada. 1994. Conformation of $(2 \rightarrow 1)$-β-d-fructan in aqueous solution. *Int. J. Biol. Macromol.* 16:313–317.

Luby-Phelps, K., P. E. Castle, D. L. Taylor, and F. Lanni. 1987. Hindered diffusion of inert tracer particles in the cytoplasm of mouse 3t3 cells. *Proc. Natl. Acad. Sci. USA.* 84:4910–4913.

Luby-Phelps, K., D. L. Taylor, and F. Lanni. 1986. Probing the structure of cytoplasm. *J. Cell Biol.* 102:2015–2022.

Marsh, B. J., D. N. Mastronarde, K. F. Buttle, K. E. Howell, and J. R. McIntosh. 2001. Organellar relationships in the Golgi region of the pancreatic beta cell line, hit-t15, visualized by high resolution electron tomography. *Proc. Natl. Acad. Sci. USA.* 98:2399–2406.

Metzler, R., and J. Klafter. 2000. The random walk's guide to anomalous diffusion: a fractional dynamics approach. *Physics Rep.* 339:1–77.

Metzler, R., and J. Klafter. 2003. When translocation dynamics becomes anomalous. *Biophys. J.* 85:2776–2779.

Nikunen, P., M. Karttunen, and I. Vattulainen. 2003. How would you integrate the equations of motion in dissipative particle dynamics simulations? *Comp. Phys. Comm.* 153:407–423.

Nordmeier, E. 1993. Static and dynamic light-scattering solution behavior of pullulan and dextran in comparison. *J. Phys. Chem.* 97:5770–5785.

Rivas, G., F. Ferrone, and J. Herzfeld. 2004. Life in a crowded world. *EMBO Rep.* 5:23–27.

Saxton, M. J. 1993. Lateral diffusion in an archipelago. Dependence on tracer size. *Biophys. J.* 64:1053–1062.

Saxton, M. J. 2001. Anomalous subdiffusion in fluorescence photobleaching recovery: a Monte Carlo study. *Biophys. J.* 81:2226–2240.

Saxton, M. J. 2002. Chemically limited reactions on a percolation cluster. *J. Chem. Phys.* 116:203–208.

Schutz, G. J., H. Schindler, and T. Schmidt. 1997. Single-molecule microscopy on model membranes reveals anomalous diffusion. *Biophys. J.* 73:1073–1080.

Schwille, P., J. Korlach, and W. W. Webb. 1999. Fluorescence correlation spectroscopy with single-molecule sensitivity on cell and model membranes. *Cytometry.* 36:176–182.

Seksek, O., J. Biwersi, and A. S. Verkman. 1997. Translational diffusion of macromolecule-sized solutes in cytoplasm and nucleus. *J. Cell Biol.* 138:131–142.

Terry, B. R., E. K. Matthews, and J. Haseloff. 1995. Molecular characterization of recombinant green fluorescent protein by fluorescence correlation microscopy. *Biochem. Biophys. Res. Commun.* 217:21–27.

Verkman, A. S. 2002. Solute and macromolecule diffusion in cellular aqueous compartments. *Trends Biochem. Sci.* 27:27–33.

Wachsmuth, M., W. Waldeck, and J. Langowski. 2000. Anomalous diffusion of fluorescent probes inside living cell nuclei investigated by spatially-resolved fluorescence correlation spectroscopy. *J. Mol. Biol.* 298:677–689.

Weiss, M. 2003. Stabilizing turing patterns with subdiffusion in systems with low particle numbers. *Phys. Rev. E.* 68:036213.

Weiss, M., H. Hashimoto, and T. Nilsson. 2003. Anomalous protein diffusion in living cells as seen by fluorescence correlation spectroscopy. *Biophys. J.* 84:4043–4052.

Yang, F., L. G. Moss, and G. N. Phillips. 1996. The molecular structure of green fluorescent protein. *Nat. Biotechnol.* 14:1246–1251.

Zieve, G. W., D. Turnbull, J. M. Mullins, and J. R. McIntosh. 1980. Production of large numbers of mitotic mammalian cells by use of the reversible microtubule inhibitor nocodazole. Nocodazole accumulated mitotic cells. *Exp. Cell Res.* 126:397–405.

Paper III

Evidence for Golgi localization by oligomerization - kin recognition revisited

M. Elsner[1], T. Nilsson[1*] and M. Weiss[2*]

[1] Dept. of Medical and Clinical Genetics, Inst. of BioMedicine, Sahlgrenska Academy, Göteborg University, Medicinaregatan 9A, 41390 Gothenburg, Sweden

[2] Cellular Biophysics Group (BIOMS), German Cancer Research Center, Im Neuenheimer Feld 580, D-69120 Heidelberg

[*] These authors contributed equally to this work

Contact information for corresponding authors:
Dr. Matthias Weiss
Cellular Biophysics Group (BIOMS), B085
German Cancer Research Center
Im Neuenheimer Feld 580
D-69120 Heidelberg
Phone: +49 6221 421930
Fax: +49 6221 421931
email: m.weiss@dkfz.de

Prof. Dr. Tommy Nilsson
Dept. of Medical and Clinical Genetics
Inst. of BioMedicine, Sahlgrenska Academy
Göteborg University
Medicinaregatan 9A
S-41390 Gothenburg, Sweden
Phone: +46 31 773 3606
Fax: +46 31 41 61 08
email: tommy.nilsson@medkem.gu.se

Short title: Kin recognition revisited

Keywords: Golgi apparatus, anomalous diffusion, simulation

Abbreviations used:

Ms Length: words, characters (incl. space).
Abstract: words

Abstract

The mechanism for localization of Golgi resident transmembrane proteins has not been elucidated in detail yet. Both lipid phase separation and oligomerisation have been discussed as not mutually exclusive means to ensure correct sorting. We have previously described the diffusional behavior of Golgi resident proteins. All proteins studied so far show strong anomalous subdiffusion. Here we provide evidence that the observed subdiffusion is an indication for the formation of large oligomers in the membrane. Using computer simulations, we investigate the diffusion properties of dynamically formed oligomers in two dimensions. We show that for the short times, relevant to FCS experiments, the diffusion of the monomers of an oligomer is subdiffusive (i.e. the mean square displacement of a protein will grow less than linear in time) and that the degree of subdiffusion depends on the equilibrium constant of the binding process and on the kinetics of the binding reaction. Furthermore, we show that the experimentally observed subdiffusion is not an artifact of the labeling with EGFP.

Introduction

The Golgi apparatus is one of the dominant organelles in the secretory pathway of mammalian cells. Elucidating its complex dynamics has been a challenge since the first reports on its existence. Phenotypically, the Golgi appears as a ribbon of interconnected stacks of flattened membrane cisternae (1-3), each of which comprise a unique chemical milieu, e.g. in terms of pH(4). Functionally, the Golgi is the main site of lipid metabolism and (protein and lipid) glycosylation. Due to its pronounced role in sorting and sequential modification of nascent proteins, the organelle may be regarded as a cellular post office. Individual Golgi stacks typically consist of 4-6 cisternae whose polar organization is reminiscent of a distillation tower: the *cis* face serves as an entry for cargo that is delivered from the endoplasmic reticulum (ER) while modified cargo leaves the Golgi at the opposing *trans* face. The mode of transport within the Golgi is still a matter of debate. While some experimental evidence supports the view of static cisternae that exchange proteins by means of distinct anterograde and retrograde vesicles, several lines of evidence support the view that the entire stack is subject to a maturation scheme (for review see (5, 6)). Here, the oldest (*trans*-most) cisterna gradually disappears by sending out vesicles with modified cargo while the remnant is finally consumed by the ER. During these processes, a new *cis* cisterna is built *de novo* by newly arriving membrane structures from the ER and retrograde Golgi vesicles. In essence, this scheme predicts that each cisterna will mature from *cis* to *trans* thereby creating an assembly line with a

default anterograde flux of material. While the cisternal maturation has been visualized in yeast very recently(7, 8), the driving force behind the actual physical movement of cisternae in the maturation process (which also seems to work in the absence of microtubules as functional mini-Golgis have been reported in cells treated with microtubule disrupting reagents (9, 10)) has not been elucidated so far.

Irrespective of the aforementioned modes of transport a large family of transmembrane proteins has been identified that preferentially is (dynamically) localized to the Golgi apparatus. Glycosyltransfereases form the largest and most abundant family of Golgi resident proteins. All family members studied so far are type II membrane proteins, with a large catalytic domain on the luminal (i.e. C-terminal) side, a single transmembrane domain and a very short cytoplasmic domain (11, 12). Virtually all Golgi resident proteins show a gradient-like distribution across the Golgi stack with a preference for one or two cisternae (2, 13). The precise localization of the individual glycosyltransferases depends on their retrograde transport by COPI vesicles implicating a dynamical positioning of the resident proteins that is consistent with the cisternal maturation model (14, 15). COPI vesicles are formed exclusively at the Golgi apparatus and the ER-to-Golgi-Intermediate- Compartment by the small GTPase ARF-1 and the heptameric coatomer complex (for review see (5, 16). How Golgi resident enzymes are sorted into COPI vesicles is largely unknown. So far only one characteristic retrieval signal has been identified for transmembrane proteins, the cytoplasmic K(X)KXX sequence which for example mediates the sorting of the p24 protein family into COPI vesicles (17-19). It was found that some proteins, e.g. p24β1, have the ability to reduce the hydrolysis rate of ARF1 by sequestering ARF-GAP1. This led to the formulation of a kinetic-proofreading mechanism, where the cargo increases the residence time of coatomer on the membrane by modulating the ARF1 activity (20, 21).

While the mode of interaction with COPI has remained elusive for glycosyltransferases, the transmembrane domain and a short luminal domain (called stem region) have been shown to be necessary and sufficient for correct Golgi localization(5, 11, 22). Based on this finding, essentially two (not mutually exclusive) mechanisms have been proposed to rationalize the localization of Golgi resident proteins: (1) the transmembrane domain could test the thickness of the cisternal membrane and trigger a localization to the cisterna with the lowest hydrophobic mismatch (23), or (2) the two mentioned domains induce a milieu-dependend, lateral attraction between similar, co-

localizing proteins and the formed 'kin oligomers' are dynamically positioned within the maturing stack by means of COPI-dependend transport ('kin recognition')(24). In agreement with the latter model, the formation of dimers and small oligomers has been shown biochemically for some glycosyltransferases (for review see (12) and (25)). A recent electron microscopy study suggested that the Golgi enzyme GalNacT2 does not distribute equally over the membrane of individual cisterane, but forms clusters(2).

An obvious method to determine the size of (kin) oligomers is to study their diffusional behavior and to determine the size of the complex via the Saffman-Delbruck relation(26). However, since the radius *R* of the transmembrane domain changes the diffusion coefficient *D* only logarithmically (in contrast to bulk diffusion, where *D* and *R* are inversely proportional), even a tenfold change in radius, i.e. the formation of a 100mer, may not be detectable. Using fluorescence correlation spectroscopy (FCS) we have previously investigated the diffusional properties of different Golgi resident proteins(27). While the uncertainty in the diffusional mobility prevented a determination of the oligomeric state of the studied Golgi resident proteins via the Saffman-Delbrück relation, strikingly all of the tested proteins showed a strong anomalous subdiffusion. Anomalous subdiffusion is characterized by a mean square displacement (MSD) $\langle r^2 \rangle \sim t^{\alpha}$ with $\alpha<1$, i.e. the MSD grows *qualitatively* slower than for normal diffusion. Interestingly, the degree of anomality (α) deviated stronger from unity for resident proteins that localized towards the *trans* face of the Golgi. Basically, two mechanisms can explain the occurrence of anomalous subdiffusion in general. On one hand, a diffusing particle may take rests of duration τ between periods of free Brownian motion, e.g. due to (cooperative) binding to more immobile structures. If the probability distribution $p(\tau)$ of the resting periods follows a power law of the form $p(\tau) \sim 1/\tau^{1+\alpha}$, then also very long resting periods are quite probable as the mean resting time diverges. The emerging continuous time random walk (CTRW) shows anomalous subdiffusion with $0<\alpha<1$. We would like to emphasize that a binding event with a single rate constant (which may be the typical for most biochemical reactions) does not lead to a CTRW as $p(\tau)$ is given by a Poisson process (28). An alternative explanation for the observation of anomalous subdiffusion is strongly obstructed diffusion. If the Brownian motion is hindered by obstacles, for example, anomalous diffusion may arise with a degree of anomality that depends on the concentration of obstacles and on the dimension of the environment (diffusion in two/three dimensions yields $\alpha>0.69/0.55$)(29-31). Indeed, early computational studies have confirmed the emergence of subdiffusion due to

obstruction(32) and recent experiments have highlighted the connection between cytoplasmatic crowding and obstructed diffusion (31, 33). A particularly interesting example of anomalous diffusion in the biological context is the motion of monomers inside a polymer/oligomer. Here, the obstruction is due to the bonds to the next neighbors in the polymer, i.e. if a monomer wants to move it will have to drag other monomers with it. A classical result of polymer physics states that the MSD of a monomer inside a very long, linear self avoiding polymer chain moving in two dimensions shows anomalous diffusion with $\alpha=3/5$ (34).

In this study we investigate how the transient formation of oligomers influences the diffusional behavior of individual proteins in a membrane. Using computer simulations, we show that the monomers in the dynamically formed oligomers show anomalous diffusion on the time scales relevant to FCS experiments. The degree of anomality (α) depends on the binding and dissociation rates as well as on the valency of the monomers. In light of this finding, we argue that the previously observed anomalous diffusion of Golgi resident proteins is a fingerprint of the dynamic formation of (kin) oligomers. We finally discuss how this finding can be used to obtain a refined model of the dynamical positioning of Golgi resident proteins.

Results

We have previously studied the diffusional behavior of a number of Golgi of resident transmembrane proteins by means of fluorescence correlation spectroscopy (FCS) (27). In all cases, we observed a strongly anomalous diffusion with a protein-specific value for the degree of anomality α. The anomalous diffusion was strongest for β-Galatosyltransferase, (GalT, $\alpha\approx0.55$) which dominantly localizes to the *trans* cisternae of the Golgi. In fact, the values obtained for α correlated with the dominant localization of the investigated proteins, i.e. the more proteins localized to the *trans* face of the Golgi stack, the stronger was the anomalous diffusion. In that study all proteins had been labeled with the enhanced Green Fluorescent Protein (EGFP) variant (35). Since EGFP has been shown to have a weak tendency to dimerize (36), we first tested if this dimerization alters the previously observed diffusional properties. We therefore constructed a GalT tagged with the monomeric GFP (GalT-mGFP) (37), and analyzed the diffusional behavior again with FCS. Comparing the diffusional properties of the two constructs, we did not observe a significant difference between the correlation curves for GalT-EGFP and GalT-mGFP beyond the

usual cell-to-cell variations (a representative example is shown in Fig.1). Fitting the experimental data with the appropriate fitting function(27) (Eq.1, Materials and Methods) yielded almost identical fits. In good agreement with the previously published data (27), we determined the degree of anomality α for GalT-EGFP from the fitting procedure as $\alpha=0.58\pm0.14$ (n=14). For mGFP we obtained $\alpha=0.57\pm0.13$ (n=18). Thus, the weak dimerization of EGFP hardly affects the diffusional behavior of GalT.

Having confirmed the anomalous diffusion of GalT, the question arises as to why there is such a strange behavior at all. In Ref. (27) a continuous time random walk (CTRW), i.e. power-law distributed resting periods due to cooperative binding events between periods of free diffusion, has been used to rationalize the observed anomalous diffusion. Yet, this explanation requires the cooperative binding to be driven out of equilibrium, e.g. via GTPases, on short time scales (28, 38, 39), which appears somewhat unphysiological. Inspired by the kin recognition theory (12, 25) and the analysis of diffusion of static polymers (40), we hypothesized that the dynamic formation of oligomers can lead to the observed anomalous subdiffusion.

To test this hypothesis, we used computer simulations in which we monitored the mean square displacement of individual monomers (=proteins) that participated in the dynamic oligomerization processes on a membrane. Diffusion was simulated by solving the overdamped Langevin equation numerically (see Methods for details), an approach that is known as Brownian Dynamics.
Besides the thermal random forces that drive the Brownian motion, two additional conservative forces were considered: (i) non-bound particles interacted via a softcore potential when their distance was lower than a critical distance r_s (thus preventing particle penetration), and (ii) particles that did bind to each other were subject to a linear restoring force imposed by a harmonic spring when deviating from an equilibrium distance r_s. For the binding and unbinding reactions a simple on/off kinetics was assumed and each particle was assigned k possible binding sites (valency k); when particles with free binding sites were at a distance less then a critical distance r_c, they could form a new bond with a rate k_{on}. Existing bonds were destroyed with rate k_{off}.

We first focused on valency k=2, i.e. the formation of linear polymers. The time course of the MSD $v(t)$ for different ratios k_{off}/k_{on} is shown in Fig. 2. While the MSD increases proportional to time ($v(t)\sim t$) for $k_{off}/k_{on}>0.1$, a clear two-phase behavior is observed for smaller ratios where one

observes an increase in the average size of steady state oligomers. While for large times normal diffusion is observed ($v(t)\sim t$) the MSD shows a marked deviation from the linear behavior for short times: it increase like $v(t)\sim t^{\alpha}$ with $\alpha<1$ and a minimum value of $\alpha=3/5$. This anomalous scaling of the MSD is the hallmark (and actually one possible definition) of anomalous subdiffusion. In fact, for decreasing ratios k_{off}/k_{on} the anomalous diffusion persists over longer and longer times, eventually overriding completely the normal diffusive behavior for large times (cf. Fig.2). A similar result is observed for valency *k=3* (Fig.3), i.e. again a two-phase behavior is observed in the MSD in general. Most strikingly, the MSD turns even more subdiffusive for small times, i.e. α can be as low as 0.4.

To thoroughly quantify the dependence of the anomalous diffusion (i.e. α) on the ratio k_{off}/k_{on}, we fixed $k_{on}=0.5/s$ while changing k_{off} over several orders of magnitude. From fitting the MSD for valency *k=2, 3*, we obtained a sigmoidal dependence of the anomality on the kinetics of oligomerization (Fig. 4). At valency *k=2*, α asymptotically approaches the value 3/5 for low k_{off}/k_{on} ratios, the value expected theoretically for long linear self avoiding polymers (34). For valency *k=3*, much lower values for α, as low as 0.25, are measured when decreasing the ratio k_{off}/k_{on}. In fact, for all ratios k_{off}/k_{on} the MSD for valency *k=3* polymers is significantly more subdiffusive than for their counterparts with valency *k=2*. To investigate the dependence of α on the individual rates of polymer formation we fixed the $k_{off}/k_{on} = 5\cdot10^{-3}$ and varied k_{on} at valency *k=3*. Fitting the obtained MSD for short times resulted in a quasi-logarithmic dependence of α on k_{on} (Fig. 5). In fact, the transition from anomalous to normal diffusion for increasing k_{on} extends over more than two orders of magnitude and the less dynamic the polymers are (low k_{on}) the stronger is the anomalous diffusion.

Discussion

In summary, we have shown that the dynamic formation of oligomers is a likely explanation for the observed anomalous subdiffusion of membrane proteins. Albeit we have shown that the anomalous subdiffusion is a transient phenomenon, its emergence is well within the timescales relevant for FCS measurements. It therefore is likely to explain the experimentally observed subdiffusion of Golgi resident membrane proteins. The anomality (α) of the diffusion depends on the kinetics of oligomer formation, i.e. on the mean residence time of the monomers inside a steady-state

oligomer, on the affinity of the monomers to each other, i.e. the k_{off}/k_{on} ratio, and on the valency of the monomers. Especially the latter has a surprisingly strong influence on the observed α: while $\alpha \geq 0.6$ linear polymers (valency *k=2*), branched polymers (valency *k=3*) can reach values for α as low as 0.25. This is important since we observe α-values around and below 0.6 for GalT which indicates that the oligomerization may be carried by more than two binding sites. For valency *k=2* and large stable oligomers (low ratio k_{off}/k_{on}) we also reproduce the theoretical value ($\alpha=3/5$) which validates our simulation method and shows that additional effects like molecular crowding do not play an important role in our simulations. As discussed earlier (27) an interpretation of the observed anomalous diffusion in terms of obstructed diffusion due to the heterogeneous lipid environment is impossible as obstructed diffusion on a membrane is limited by the percolation threshold which predicts $\alpha > 0.69$.

Given this constraint and the conceptual problems with a continuous time random walk (see Introduction), the explanation of the observed subdiffusion as a consequence of oligomerization appears compelling. As we were also able to rule out with FCS experiments that the weak dimerization of EGFP plays a major role in the observed anomalous diffusion, our results give strong evidence that Golgi enzymes form oligomers in the membranes of living cells *in vivo*.

Perspective

Taking the above as a strong indication for the existence of kin oligomers in the Golgi of living cells, the question arises as to how these data relate to the original kin recognition hypothesis (24) and the dynamic sorting process within the Golgi. We shall therefore formulate an updated version of the kin recognition hypthesis.

In brief, the original kin recognition hypothesis states that ‘alike’ Golgi resident proteins form large hetero-oligomers via their transmembrane domains and that these oligomers are too big to enter COPI vesicles and leave the cisternae. While our above results are supportive for this idea, the original kin recognition model is, in part, inconsistent with other results that have been found after its formulation in the early 1990s. Several lines of evidence now suggest that COPI vesicles mediate retrograde transport of Golgi resident proteins(21, 43-45) and strong evidence has been given that the preferential incorporation of Golgi residents depends on the ability of ARF1 to hydrolyze GTP (20, 43, 46). Indeed, some proteins (e.g. p24β1) have the ability to influence the activity of ARF1 by sequestering ARFGAP1, i.e. a cargo-associated coat becomes more stable. Based on this, a kinetic proofreading scheme has been proposed that can explain the highly

efficient sorting of cargo into COPI (20). As of yet, glycosyltransferases have not been shown to interact with the COPI machinery in any way which is supportive of the idea that kin-oligomers consist of both, glycoyltransferases and proteins that have the ability to interact with the COPI machinery, e.g. by influencing the hydrolysis rate of ARF1.

From the data presented here and in Ref. (27), we suspect that oligomers formed by *trans*-localizing Golgi proteins are larger than those of *cis*-localizing proteins. If this is true, the large *trans*-localizing oligomers should be most competitive for making COPI vesicles, i.e. they should rather hook up at the *cis* face of the Golgi. How can we resolve this contradiction?

Rather than trying to formulate a detailed model let us make a Gedankenexperiment. Let's assume we have three kin populations K_1, K_2, K_3 that build oligomers of sizes $R_1<R_2<R_3$ on ER and Golgi membranes. Initially, the ER and the three cisternae (*cis*, *medial*, *trans*) of the Golgi may contain each kin in the same amount. Now two counteracting processes compete with each other: while larger oligomers have a strong capacity to reduce the hydrolysis of GTP by ARF-1(20, 43) and therefore are potent in creating a well-filled COPI vesicle, the size of the oligomer imposes an elastic constraint. The oligomer tries to resist the membrane bending which takes place while budding a COPI vesicle. This increases the time needed for the formation of a vesicle and reduces the probability of a successful budding event. In addition, its stiffness reduces the likelihood of finding a large oligomer at the strongly curved cisternal rims where COPI vesicles budding takes place. Therefore, kin K_1 with the smallest (=softest), but still hydrolysis-modulating oligomers will undergo retrograde transport faster than K_2 and K_3, i.e. K_1 will concentrate at the *cis* face and cycle between ER and Golgi. The less competitive kin K_2 will have a chance to also form 'its' COPI vesicles when the mean residence time of the (meanwhile diluted) kin K_1 at the rims is lower than the mean residence time of K_2 at the rims. Now K_2 will start its retrograde transport and compete out K_3, which will eventually also be able to undergo retrograde transport. Since production and loading of vesicles is linked here, the scheme should not be sensitive to overexpression of a particular kin. In other words, a more dynamic view of the kin recognition hypothesis is consistent with available experimental and theoretical data.

Acknowledgement

This work was supported by the Institute for Modeling and Simulation in the Biosciences (BIOMS) initiative in Heidelberg.

Materials and Methods

Modeling and Simulations

We employed computer simulations to investigate if the dynamic formation of oligomers leads to the anomalous diffusion of individual monomers on the timescales relevant for FCS. We considered a square area (390nm x 390nm) with periodic boundary conditions into which particles were initially distributed randomly (density of 10^4 particles/μm^2). The protein density is consistent with studies from (47, 48). Each particle/monomer had a radius r_c=7.8nm and was given a valency *k* (i.e. *k* binding sites). Diffusion of each monomer *i* was simulated by numerically solving the overdamped Langevin equation $x_i^{(j)}(t+\Delta t) = \xi^{(j)} + \Delta t F_i^{(j)}$, where the superscript *j*=1,2 stands for the *x* and *y* direction, respectively. Here, $\xi^{(j)}$ is a Gaussian random number with variance $2 \cdot D_0 \cdot \Delta t$ (D_0 denoting the diffusion coefficient) and $F_i^{(j)} = \sum_k f_{ik}$ is the total force that neighboring particles *k* exert on particle *i*. With the choice $\Delta t = 5 \cdot 10^{-4}$s each monomer had a diffusion coefficient D_0=1 μm^2/s which is a typical value for protein diffusion on membranes.

A simple on/off kinetics with rates k_{on}, k_{off} was assumed for the dynamic oligomer formation. When the distance between two particles with at least one free binding site per monomer was less then a critical distance r_c, binding occurred with a probability $p_{on}=k_{on} \cdot \Delta t$. At each time step each bond between two monomers was destroyed with probability $p_{off} = k_{off} \cdot \Delta t$. Between any two bound particles (*i*,*j*) within a distance d_{ij} a harmonic potential with the equilibrium distance $r_s=r_c/2$ was applied; this lead to a linear restoring force of the form $f_{ij}=\kappa(1-d_{ij}/rs)e_{ij}$, where eij is the corresponding unit vector between the particles. Between any two nonbonded particles within a distance $d_{ij} < r_c/2$ a force of the form $F_{ij}(r) = -\phi(1-d_{ij}/x_r)e_{ij}$ was applied to mimic hard-core repulsion.

Cell Culture and Flurecence correlation spectroscopy

Hela cells were cultured in Dulbecco's Modified Eagle Medium supplemented with 10% fetal calf serum 100 units ml–1 penicillin, 100 mg ml–1 streptomycin and 10 mM glutamine (Gibco). FCS measurements were performed on a Leica TCS SP2 AOBS confocal system with FCS extension and a 63x (NA 1.2) water immersion objective. Cells were grown on standard cover slides with a thickness of 0.08-0.13mm (#0 thickness). Variations in cover glass thickness thickness were corrected using the correction ring of the objective. All experiments were done at 37°C in Dulbecco's Modified Eagle Medium supplemented with 20 mM Hepes. All measurements were performed in the endoplasmic reticulum. Fitting of the normalized data was performed using FCS curves were fitted with a Levenberg–Marquart algorithm using the expression for 2D dimensional diffusion anomalous diffusion(31, 49)

$$c(\tau) = \frac{1}{1+\left(\tau / \tau_D\right)^{\alpha}} \quad (1)$$

Here α is the degree of anomalous diffusion and τ_D the diffusion time of particles.

Figure 1

Representative autocorrelation curves for GalT-mGFP (blue) and GalT-GFP (red). Fitting both data sets with the standard expression for anomalous diffusion in two dimensions (Eq.1, Methods) yields almost identical results: α=0.52, τ_D=48ms for GalT-EGFP; α=0.53, τ_D=50ms for GalT-mGFP.

Figure 2

(A) The mean square displacement *v(t)* for $k_{off}/k_{on}=2\cdot10^{-3}$, $8\cdot10^{-3}$, $2.5\cdot10^{-4}$, $3.9\cdot10^{-6}$ (from top) for valency *k=2*. For comparison, dashed lines show *v(t)~t* (behaviour for large times) and the subdiffusive part $v(t)\sim t^{0.6}$ (for small times). The crossover from anomalous diffusion to normal diffusion shifts to longer time with decreasing k_{off}/k_{on} while the anomality degree α decreases.
(B) Snapshot of the simulation for a low k_{off}/k_{on} ratio. Note the large oligomers formed, and the low number of free monomers. (C) Snapshot of the simulation for a high k_{off}/k_{on} ratio. The size of the oligomers is decreased and a few of free monomers is visible

Figure 3

(A) The mean square displacement *v(t)* for $k_{off}/k_{on}=2.5\cdot10^{-4}$, $2\cdot10^{-3}$, $8\cdot10^{-3}$, $3.2\cdot10^{-2}$ (from top) for valency *k=3*. For comparison, dashed lines show *v(t)~t* (behaviour for large times) and the subdiffusive part $v(t)\sim t^{0.4}$ (for small times). The crossover from anomalous diffusion to normal diffusion shifts to longer time with decreasing k_{off}/k_{on} while the anomality degree α decreases even stronger than for valency *k=2*.
(B) Snapshot of the simulation for a low k_{off}/k_{on} ratio. Note increased oligomer size compared to the valency 2 case , and the absence number of free monomers. (C) Snapshot of the simulation for a high k_{off}/k_{on} ratio. The size of the oligomers is decreased and free monomers exist now.

Figure 4

The degree of anomality α decrease for decreasing values of the ratio k_{off}/k_{on}. While for valency *k=2* (squares) the minimum is well captured by theoretical predictions from polymer theory (α=3/5), the values for α can decrease well down to 0.25 for valency *k=3* (circles). The transition from anomalous to normal diffusion happens at roughly the same ratio k_{off}/k_{on}. Since the actual value for α not only depends on the ratio k_{off}/k_{on}, but also on the actual value of either k_{off} or k_{on} (see Fig.5), the entire curve can be shifted along the x-axis depending on the actual value of k_{off} and k_{on}.

Figure 5

The degree of anomality α (at valency k=3) increases roughly logarithmically with the rate k_{on} while keeping the ratio $k_{off}/k_{on}=5\cdot10^{-3}$. This reflects the fact that a more dynamic formation of oligomers results in a more diffusive ($\alpha\rightarrow1$) motion of the individual proteins.

References

1. **Marsh, B. J. (2005) *Biochim Biophys Acta* 1744, 273-92.**

2. **Grabenbauer, M., Geerts, W. J. C., Fernadez-Rodriguez, J., Hoenger, A., Koster, A. J. & Nilsson, T. (2005) 2, 857-862.**

3. **Marsh, B. J., Mastronarde, D. N., Buttle, K. F., Howell, K. E. & McIntosh, J. R. (2001) *Proc Natl Acad Sci U S A* 98, 2399-406.**

4. **Paroutis, P., Touret, N. & Grinstein, S. (2004) *Physiology (Bethesda)* 19, 207-15.**

5. **Kartberg, F., Elsner, M., Froderberg, L., Asp, L. & Nilsson, T. (2005) *Biochimica et Biophysica Acta (BBA) - Molecular Cell Research* 1744, 351-363.**

6. **Elsner, M., Hashimoto, H. & Nilsson, T. (2003) *Mol Membr Biol* 20, 221-9.**

7. **Losev, E., Reinke, C. A., Jellen, J., Strongin, D. E., Bevis, B. J. & Glick, B. S. (2006) *Nature*.**

8. **Matsuura-Tokita, K., Takeuchi, M., Ichihara, A., Mikuriya, K. & Nakano, A. (2006) *Nature*.**

9. **Stults, N. L., Fechheimer, M. & Cummings, R. D. (1989) *J. Biol. Chem.* 264, 19956-19966.**

10. **Van De Moortele, S., Picart, R., Tixier-Vidal, A. & Tougard, C. (1993) *Eur J Cell Biol.* 60, 217–227.**

11. **Gleeson, P. A. (1998) *Histochem Cell Biol* 109, 517-32.**

12. **Young, W. W., Jr. (2004) *J Membr Biol* 198, 1-13.**

13. **Rabouille, C., Hui, N., Hunte, F., Kieckbusch, R., Berger, E. G., Warren, G. & Nilsson, T. (1995) *J Cell Sci* 108 (Pt 4), 1617-27.**

14. **Storrie, B., White, J., Rottger, S., Stelzer, E. H., Suganuma, T. & Nilsson, T. (1998) *J Cell Biol* 143, 1505-21.**

15. **Cole, N. B., Ellenberg, J., Song, J., DiEuliis, D. & Lippincott-Schwartz, J. (1998) *J Cell Biol* 140, 1-15.**

16. **Bonifacino, J. S. & Glick, B. S. (2004) *Cell* 116, 153-66.**

17. **Dominguez, M., Dejgaard, K., Fullekrug, J., Dahan, S., Fazel, A., Paccaud, J. P., Thomas, D. Y., Bergeron, J. J. & Nilsson, T. (1998) *J Cell Biol* 140, 751-65.**

18. **Fiedler, K., Veit, M., Stamnes, M. A. & Rothman, J. E. (1996) *Science* 273, 1396-9.**

19. **Sohn, K., Orci, L., Ravazzola, M., Amherdt, M., Bremser, M., Lottspeich, F., Fiedler, K., Helms, J. B. & Wieland, F. T. (1996) *J Cell Biol* 135, 1239-48.**

20. **Weiss, M. & Nilsson, T. (2003) *Traffic* 4, 65-73.**

21. **Lanoix, J., Ouwendijk, J., Stark, A., Szafer, E., Cassel, D., Dejgaard, K., Weiss, M. & Nilsson, T. (2001) *J Cell Biol* 155, 1199-212.**

22. **Opat, A. S., van Vliet, C. & Gleeson, P. A. (2001) *Biochimie* 83, 763-73.**

23. **Bretscher, M. S. & Munro, S. (1993) *Science* 261, 1280-1.**

24. **Nilsson, T., Slusarewicz, P., Hoe, M. H. & Warren, G. (1993) *FEBS Lett* 330, 1-4.**

25. **de Graffenried, C. L. & Bertozzi, C. R. (2004) *Curr Opin Cell Biol* 16, 356-63.**

26. **Saffman, P. G. & Delbruck, M. (1975) *Proc Natl Acad Sci U S A* 72, 3111-3.**

27. **Weiss, M., Hashimoto, H. & Nilsson, T. (2003) *Biophys J* 84, 4043-52.**

28. **Metzler, R. & Klafter, J. (2000) *Phys. Rep.* 339, 1-77.**

29. **Bouchaud, J. P. & Georges, A. (1990) *Phys. Rep.* 195, 127-293.**

30. **Saxton, M. J. (2001) *Biophys J* 81, 2226-40.**

31. **Weiss, M., Elsner, M., Kartberg, F. & Nilsson, T. (2004) *Biophys J* 87, 3518-24.**

32. **Saxton, M. J. (1994) *Biophys J* 66, 394-401.**

33. **Banks, D. S. & Fradin, C. (2005) *Biophys J* 89, 2960-71.**

34. **Azuma, R. & Takayama, H. (1999) *Journal of Chemical Physics* 111, 8666-8671.**

35. **Zhang, G., Gurtu, V. & Kain, S. R. (1996) *Biochem Biophys Res Commun.* 227, 707-711.**

36. **Phillips, G. N. (1998) *Green Fluorescent Protein: Properties, Applications, and Protocols.* (Wiley-Liss, New York).**

37. **Zacharias, D. A., Violin, J. D., Newton, A. C. & Tsien, R. Y. (2002) *Science* 296, 913-6.**

38. **Saxton, M. J. (2002) *Molecular Biology of the Cell* 13, 275A-275A.**

39. **Saxton, M. J. (1996) *Biophys J* 70, 1250-62.**

40. **Doi, M. & Edwards, S. F. (1986) *The Theory of Polymer Dynamics* (Clarendon Press, Oxford).**

41. **Fleischer, B., McIntyre, J. O. & Kempner, E. S. (1993) *Biochemistry* 32, 2076-81.**

42. **Giraudo, C. G. & Maccioni, H. J. (2003) *J Biol Chem* 278, 40262-71.**

43. **Lanoix, J., Ouwendijk, J., Lin, C. C., Stark, A., Love, H. D., Ostermann, J. & Nilsson, T. (1999) *Embo J* 18, 4935-48.**

44. **Martinez-Menarguez, J. A., Prekeris, R., Oorschot, V. M., Scheller, R., Slot, J. W., Geuze, H. J. & Klumperman, J. (2001) *J Cell Biol* 155, 1213-24.**

45. **Love, H. D., Lin, C. C., Short, C. S. & Ostermann, J. (1998) *J Cell Biol* 140, 541-51.**

46. **Pepperkok, R., Whitney, J. A., Gomez, M. & Kreis, T. E. (2000) *J Cell Sci* 113, 135-144.**

47. **Griffiths, G., Warren, G., Quinn, P., Mathieu-Costello, O. & Hoppeler, H. (1984) *J Cell Biol* 98, 2133-41.**

48. **Quinn, P., Griffiths, G. & Warren, G. (1984) *J Cell Biol* 98, 2142-7.**

49. **Schwille, P., Haupts, U., Maiti, S. & Webb, W. W. (1999) *Biophys J* 77, 2251-65.**

Figure 1

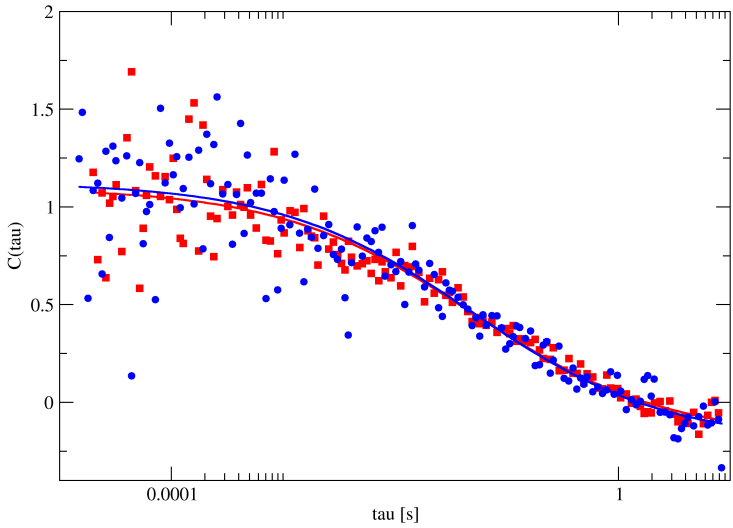

Figure 2

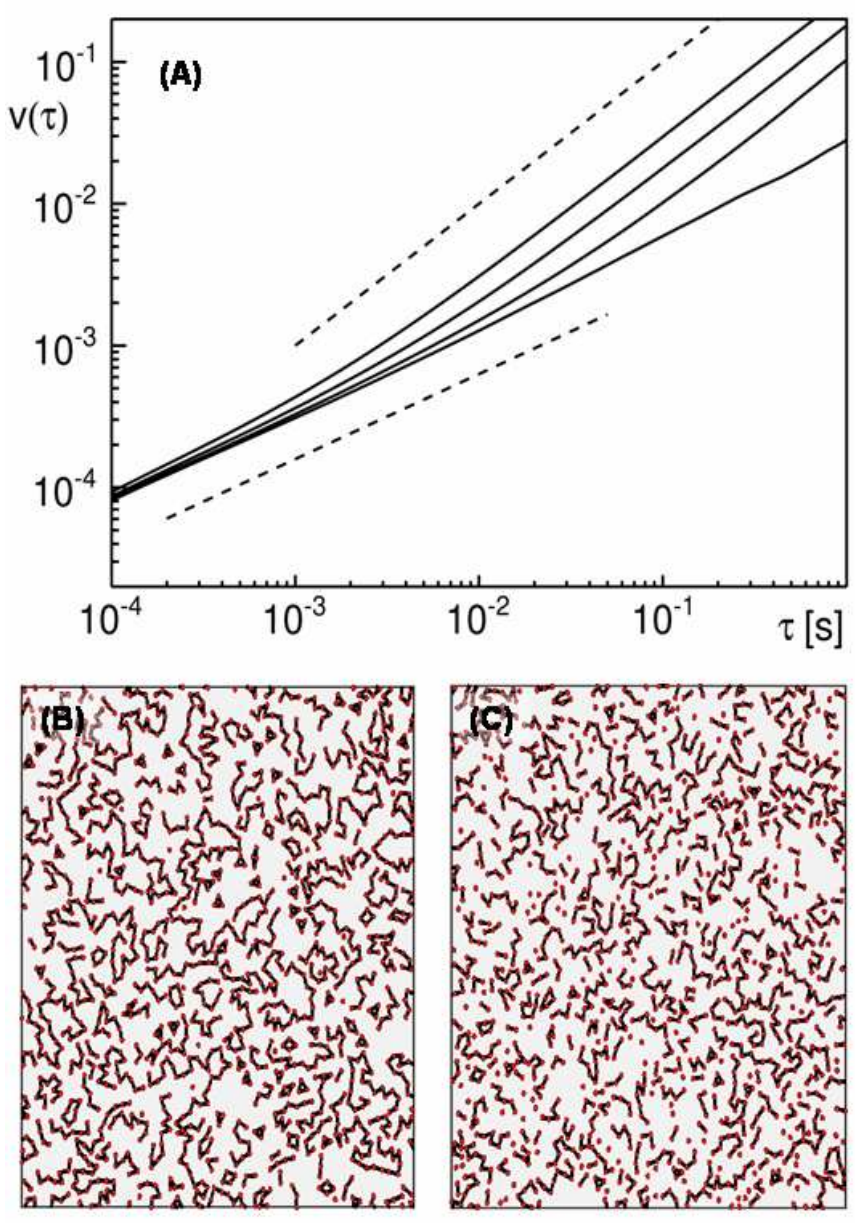

Figure 3

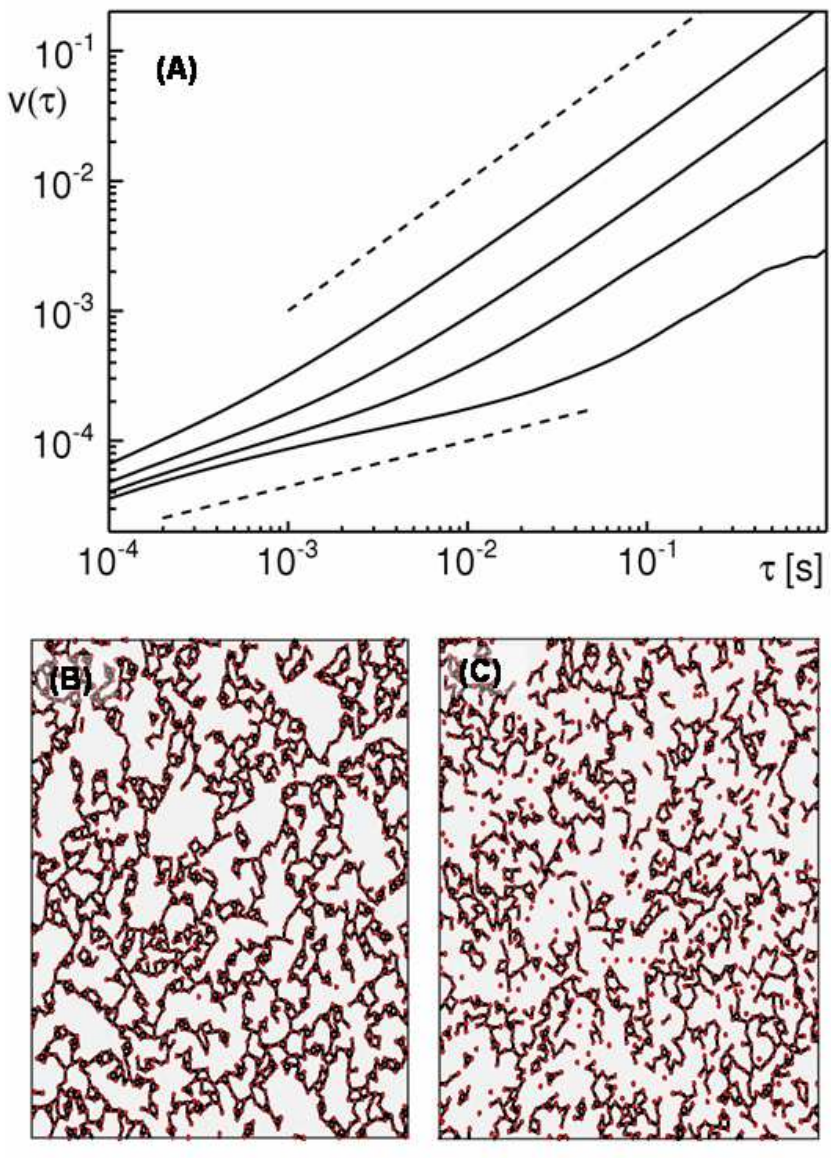

Figure 4

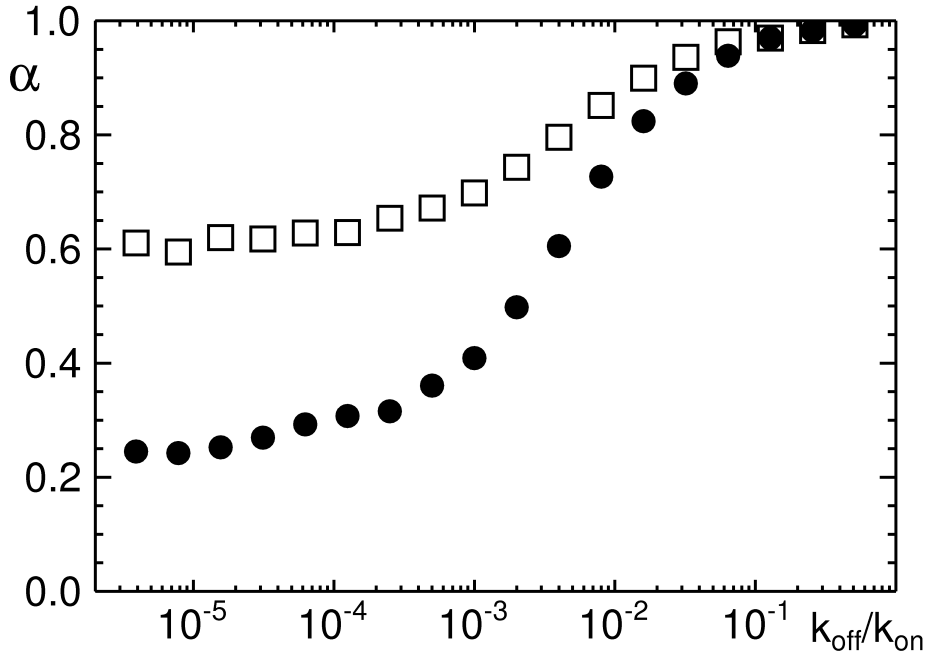

Figure 5